REVIEW

of the

RICAL COMMUNICATION LABORATORY

TELEGRAPH AND TELEPHONE PUBLIC CORPORATION

rmer, Reports of the Electrical Communication Laboratory
Nippon Telegraph and Telephone Public Corporation
from Vol.1, No.1, Sept. 1953 to Vol.7, No.12, Dec. 1959

Published Bimonthly by
ELECTRICAL COMMUNICATION LABORATORY
PON TELEGRAPH AND TELEPHONE PUBLIC CORPORATION
1551, Kitizyôzi, Musasino-si, Tôkyô, Japan

VOLUME 9
NUMBERS 11-12

November - December
1961

Review of the Electrical Communication Laboratory

EDITORIAL COMMITTEE

Susumu OKAMURA *Chairman*

Giichi ITO
Hideo KAWASAKI
Yukio NAKAMURA
Tatsuya SHIMBORI
Takuzo SHINDO
Toyotaro SHIRAMATSU
Takakichi UZAWA
Ginsaku YASAKI

Nobukazu NIIZEKI

EDITORIAL STAFF

Takaaki MIWA *Editor*
Tutomu SAITO *Assistant Editor*
Masao HIROSE 〃

The Review of the Electrical Communication Laboratory is published six times a year (bimonthly) by the Electrical Communication Laboratory, Nippon Telegraph and Telephone Public Corporation, 1551, Kitizyôzi, Musasino-si, Tôkyô, Japan. Telephone: Tôkyô (391) 2261 and 2271.

All rights of republication, including translation into foreign languages, are reserved by the Electrical Communication Laboratory, NTT.

Subscriptions are accepted at ¥1,200 per year. Single copy ¥300 each. Foreign postage is ¥400 per year or ¥65 per copy. Remittance should be made in check payable to the Electrical Communication Laboratory and sent to the Director.

Printed by Aoyama Printing Co., Tokyo, Japan

REVIEW
of the
ELECTRICAL COMMUNICATION LABORATORY

NIPPON TELEGRAPH AND TELEPHONE PUBLIC CORPORATION

Volume 9, Numbers 11-12 November-December 1961

U.D.C. 621.382.333.33.029.6:546.289]:621.317.616

Equivalent Circuits and Four-Terminal Parameters of High Frequency Transistor*

Seiichi KAWAGUCHI† and *Minoru HIRAI*†

The frequency dependent characteristics of the elements of the small signal equivalent circuits of high frequency transistors have been calculated theoretically, and practical approximate circuits of them made. Furthermore, the four-terminal parameters are represented by the approximate circuit elements, and their frequency characteristics examined theoretically. Next, a method of obtaining the equivalent circuit from the grounded-base "h" parameters is described, and a method of measuring the "h" parameters is given. Finally, examples of measured data of four-terminal parameters and equivalent circuits of various types of high frequency transistors are recorded.

1. Introduction

An equivalent circuit commonly adaptable to almost all types of present high frequency transistors is constructed, and frequency characteristics of four terminal parameters are explained using this equivalent circuit. These studies are made to aid in understanding the characteristics of transistors as high frequency amplifiers.

2. Structure of High Frequency Transistors and Composition of Equivalent Circuit(4)

Fig. 1 to Fig. 4(6)(8) show the structures of three typical kinds of high frequency transistors. First the equivalent circuit of the inner region (Base region into which minority carriers are injected from the emitter, and related junction portions of emitter and collector) of transistors having these structures will be considered.

For instance, in Fig. 5 (1) (ring base type) and Fig. 6 (1) (mesa type) the portion surrounded by the dotted line represents the inner region. Fig. 7 shows various equivalent circuits of the inner region. The circuit of Fig. 7 (1) is theoretically the most fundamental, i.e., the grounded base four-terminal y parameters $[y^i]$, $(y_{11}^i, y_{21}^i, y_{12}^i$, and $y_{22}^i)$ of the intrinsic transistor inner region have been calculated from one dimensional theories,(1)(2) transition capacitances of emitter and inner region of collector are added, and inner region base impedance is obtained from two-dimensional theory.(3) Converting the one dimensional grounded-base y parameters of this circuit into h parameters, we obtain the

---

* MS in Japanese received by the Electrical Communication Laboratory, on July 7, 1960. Originally published in the *Kenkyû Zituyôka Hôkoku* (*Electrical Communication Laboratory Technical Journal*), N.T.T., Vol. 10, No. 6, pp. 1015–1041, 1961.

† Semiconductor Research Section.

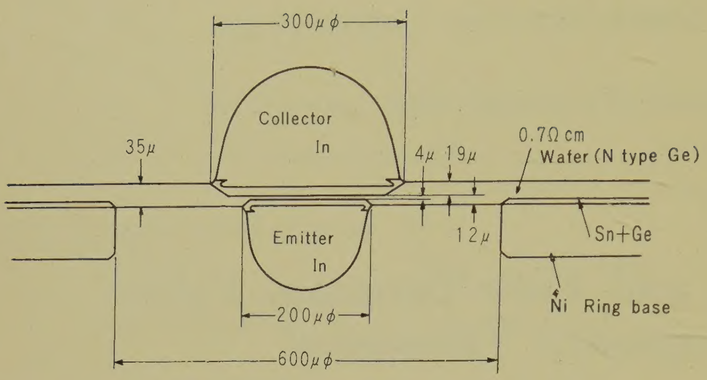

Fig. 1—Element cross section of ECL 1205 (Ge Alloy Type).

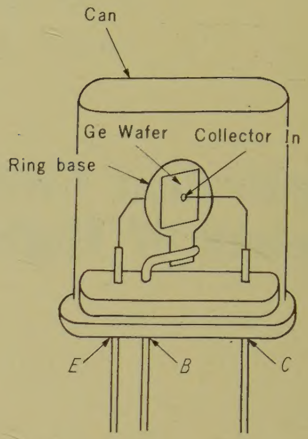

Fig. 2—Structure of ECL-1205 and its stray immittances.

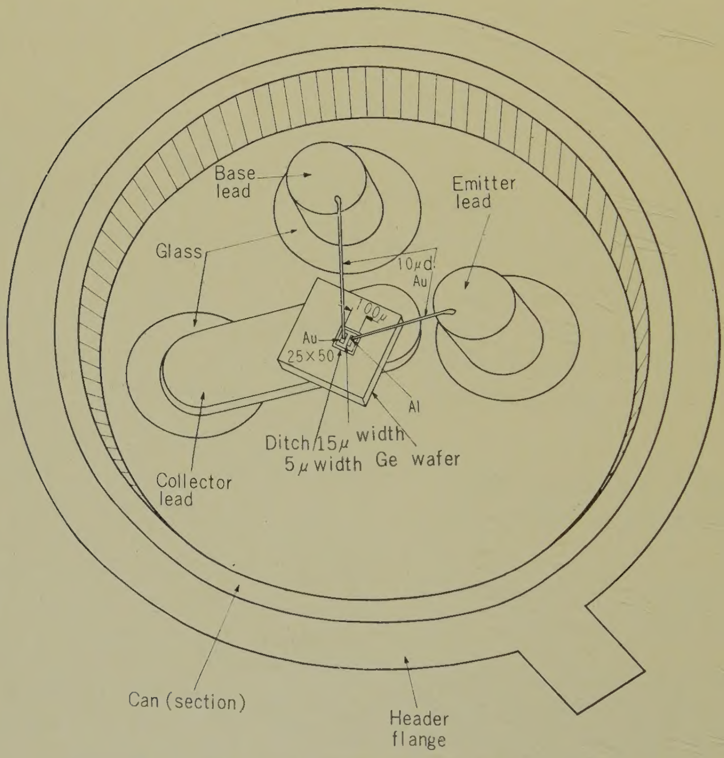

Fig. 3—Inner view of 2N700 (Ge Mesa Type).

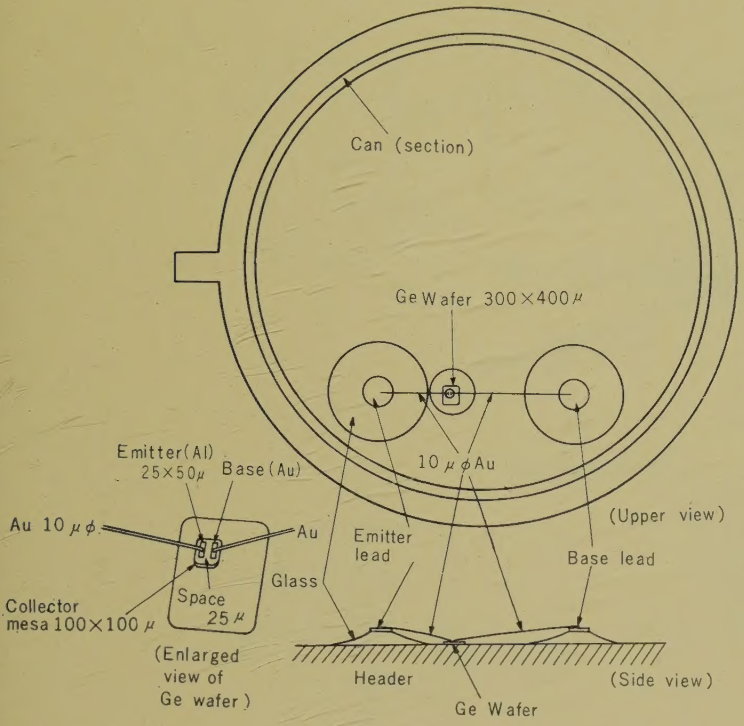

Fig. 4—Structure of 2N1143 (Ge Mesa Type).

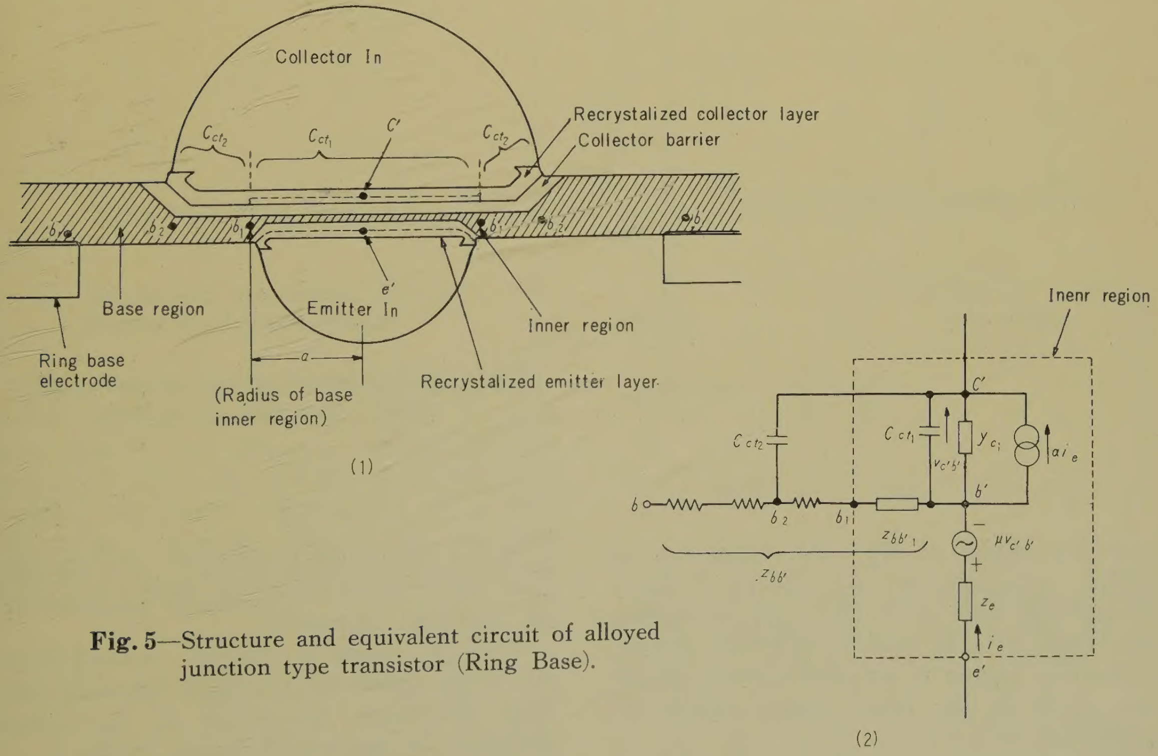

Fig. 5—Structure and equivalent circuit of alloyed junction type transistor (Ring Base).

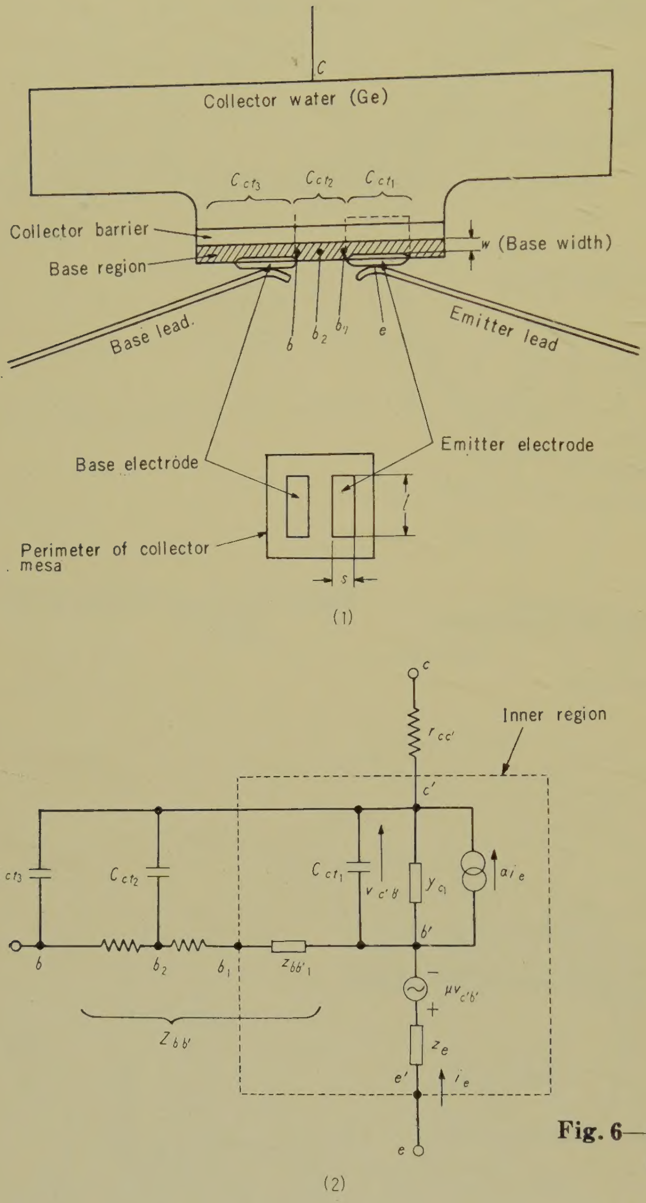

Fig. 6—Structure and equivalent circuit of diffused base type (Line Base).

equivalent circuit of Fig. 7 (2); which can be further converted into the circuits of Fig. 7 (3) and Fig. 7(4). Then, the complete equivalent circuit of each type of transistor is constructed by adding an external passive equivalent circuit to the inner region circuit described above.

For instance, the inner region of the equivalents for alloy type (ring base) and diffused base type (mesa type) are shown in Figs. 5 (2) and 6(2) respectively.

From the point of view of measurements, the entire equivalent circuit of vasious present high frequency transistors is represented generally by the circuit shown in Fig. 8.

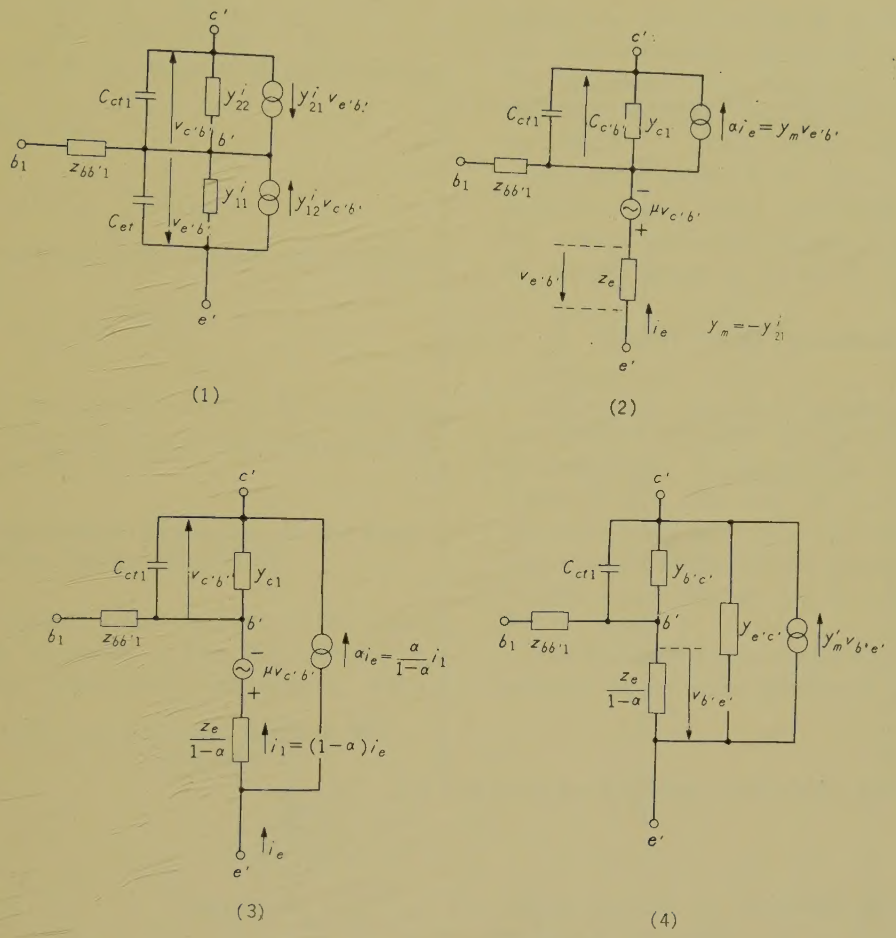

Fig. 7—Various types of equivalent circuit representing inner region of transistor.

3. Theoretical Calculation of Inner Region Equivalent Circuit

Using base width w, minority carrier diffusion constant D, diffusion length L, base inner field F, low frequency emitter junction resistance $r_e \doteqdot kT/qI_E$ (where I_E=emitter bias current) transistion capacitances of emitter and inner region of collector, C_{et}, C_{ct1} and equivalent base specific resistivity ρ_B we define the following constants.

$$\omega_0=\frac{D}{w^2},\quad \epsilon=\frac{eFw}{2kT},\quad \epsilon'^2=\epsilon^2+\frac{w^2}{L^2}$$

$$P=-\frac{I_c^{(p)}}{w}\cdot\frac{dw}{dV_c}\quad\left(I_c^{(p)}:\ \text{Minority carrier bias current}\right)$$

$$\left(V_c:\ \text{Collector junction voltage}\right)$$

$$Q=r_cP\doteqdot-\frac{kT}{qw}\cdot\frac{dw}{dV_c},$$

$$K_e=\omega_0C_{et}r_e,\quad K_{c1}=\omega_0C_{ct1}r_e,\quad R_\square=\frac{\rho_B}{w}. \tag{1}$$

First of all, with the fundamental value (function of frequency) derived from one dimensional theory⁽²⁾

$$\epsilon'\Omega=\sqrt{\epsilon'^2+j\frac{\omega}{\omega_0}}\quad(\omega:\ \text{Angular frequency})$$

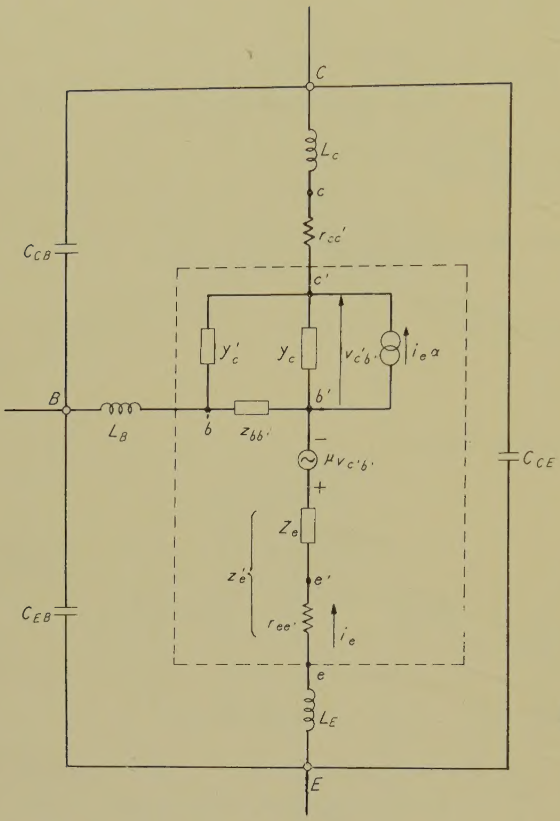

Fig. 8—High frequency equivalent circuit of transistor.

emitter injection efficiency ν_0, surface recombination velocity β_{s0}, the following equations related to $[y_i]$ in Fig. 7(1) can be derived.

$$\left.\begin{aligned} y_{11}{}^i &= \frac{1}{r_e}\cdot\frac{\epsilon+\epsilon'\Omega\coth\epsilon'\Omega}{\epsilon+\epsilon'\coth\epsilon'}, \\ y_{12}{}^i &= -P\frac{\epsilon'\Omega\cdot\exp(-\epsilon)}{\sinh\epsilon'\Omega}, \\ y_{21}{}^i &= -\frac{\gamma_0\beta_{s0}}{r_e}\cdot\frac{\epsilon'\Omega\exp(\epsilon)}{\sinh(\epsilon'\Omega)[\epsilon+\epsilon'\coth\epsilon']}, \\ y_{22}{}^i &= P\left(\frac{\epsilon'\Omega}{\tanh\epsilon'\Omega}-\epsilon\right). \end{aligned}\right\} \tag{2}$$

Next, the theoretical equations related to the one dimensional parameters, with the exception of $Z_{bb'}$ shown in Fig. 7(2), and the following equations are combined to give:

$$\left.\begin{aligned} y_m &= -y_{21}{}^i, \\ \frac{1}{Z_e} &= y_{11}{}^i\left(1+j\frac{k_e}{r_e y_{11}{}^i}\cdot\frac{\omega}{\omega_0}\right), \\ \alpha &= y_m\cdot Z_e \\ \mu &= -Z_e y_{12}{}^i, \\ y_{c1} &= y_{22}{}^i+y_{12}{}^i\cdot\alpha. \end{aligned}\right\} \tag{3}$$

Then, for $Z_{bb'1}$, shown in Fig. 7 two dimensional theory(3) leads to the following relations with

$$y_\Sigma = y_{11}{}^i+y_{21}{}^i+y_{12}{}^i+y_{22}{}^i+j\omega(C_{et}+C_{ct1})$$

where $R_\square$ is expressed in Eq. (1)

(1) Ring base

put, $(\Gamma a)^2 = \dfrac{R_\square y_\Sigma}{\pi}$

(a: Radius of inner region base, refer to Fig. 5)

$$Z_{bb'1} = \frac{R_\square}{2\pi}\cdot\frac{1}{\Gamma a}\cdot\frac{I_0(\Gamma a)}{I_1(\Gamma a)} - \frac{1}{y_\Sigma}$$

(I_0, I_1: 0th & 1st Order of Bessel Function)

(2) Line base

put, $(\Gamma h)^2 = \frac{s}{l} R_\square y_\Sigma$

(l, s=Length and width of base, refer to Fig. 6)

$$Z_{bb'1} = \frac{s}{l} R_\square \frac{\coth \Gamma h}{\Gamma h} - \frac{1}{y_\Sigma}.$$

Frequency characteristics of y_m, Z_e, α, and $Z_{bb'1}$ calculated from the above equations are shown in Fig. 9 to Fig. 13.

4. Approximate Expression of the Inner region Equivalent Circuit

The frequency characteristics of the equivalent circuit elements of Fig. 7(2) obtained by the strictly theoretical calculations shown above are given in Fig. 10 to Fig. 13. These are approximately as shown in Table 1 for the frequency range from low frequencies to the inner current amplification factor cutoff frequency f_α. The values of the various constants expressed in these approximate equations have been calculated theoretically for eleven different design conditions, and the results given in Table 2.

5. Four-Terminal Parameters

Conversion equations between "h" and "y" parameters of the grounded-emitter and grounded-base configurations are listed in Table 3. The "h" and "y" parameters of the grounded-base and grounded-emitter equivalent circuits indicated the portion surrounded by the dotted line in Fig. 8 are recorded in Tables 4 and 5.

Theoretically approximate frequency characteristics of the most important of these para-

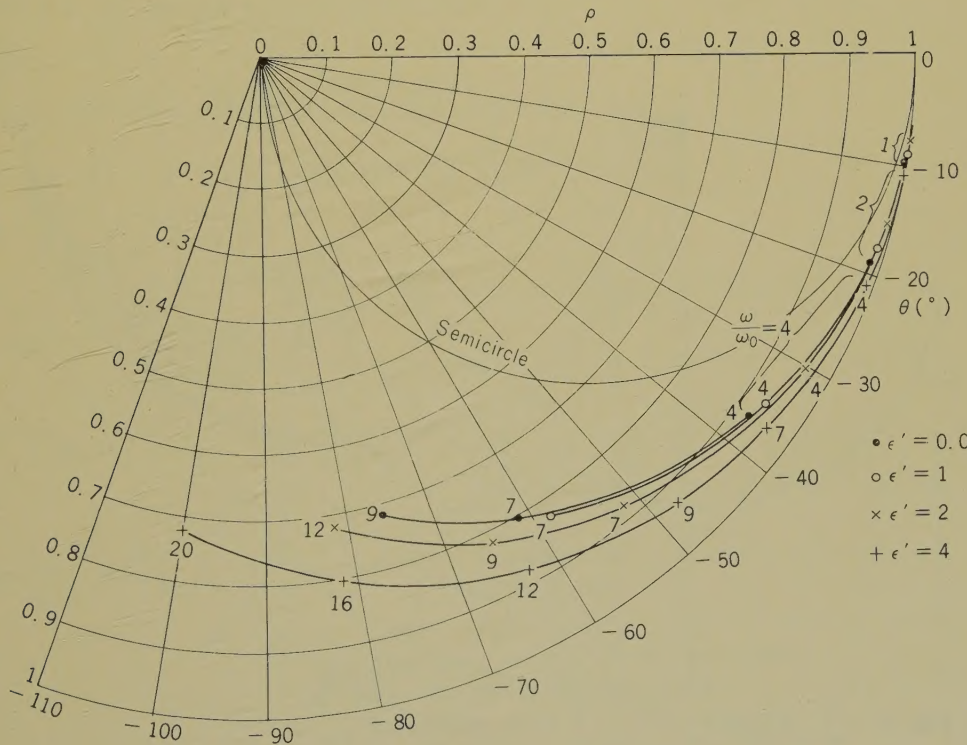

Fig. 9— $\frac{y_m}{y_{m10}} = \rho\angle\theta$.

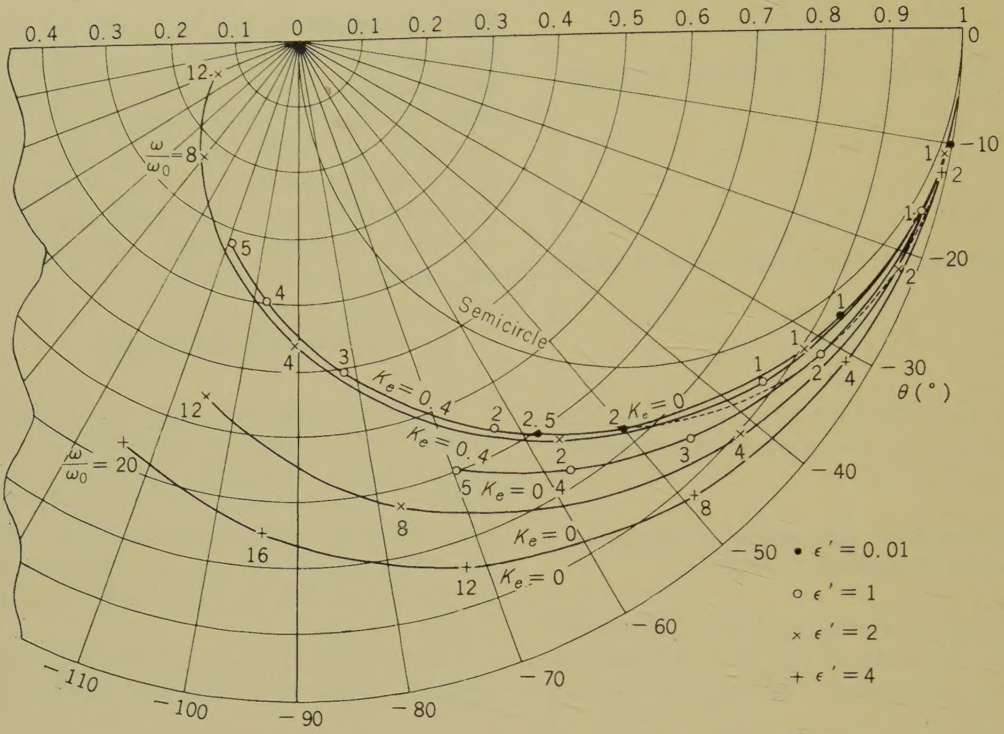

Fig. 10—$\frac{\alpha}{\alpha_0}=\rho\angle\theta$.

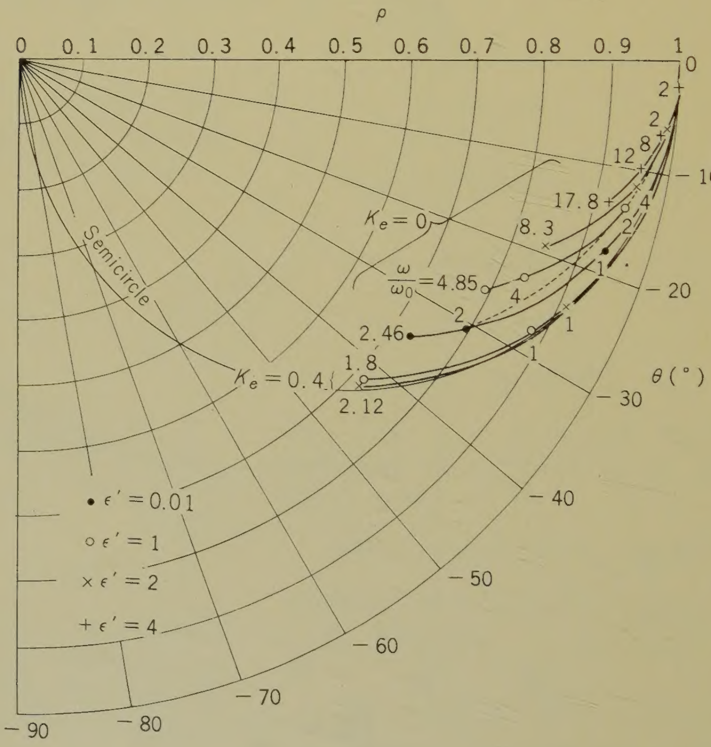

Fig. 11—$\frac{z_e}{r_e}=\rho\angle\theta$.

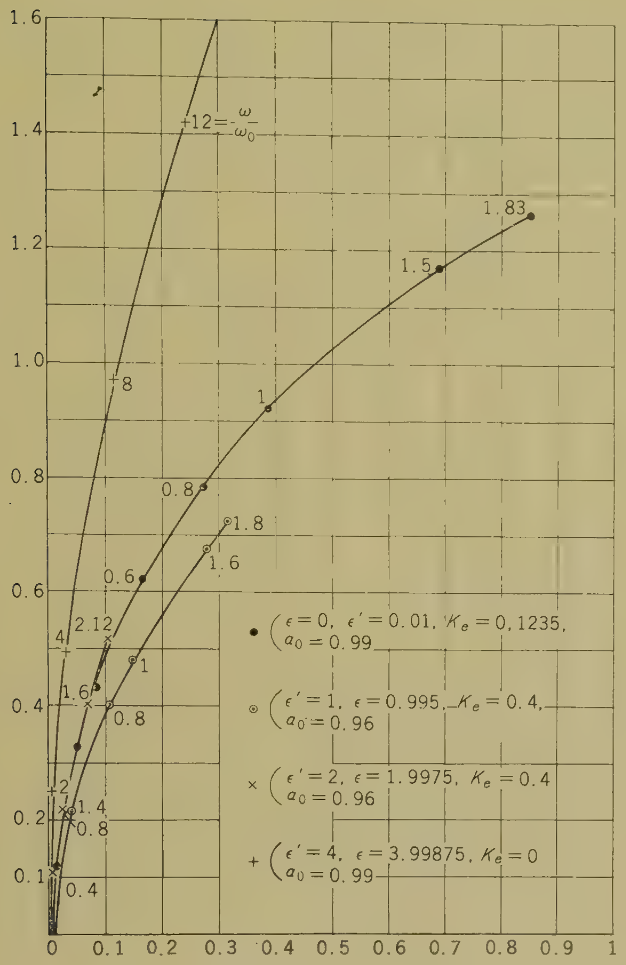

Fig. 12—$\frac{y_{c1}}{P} = r+jx.$

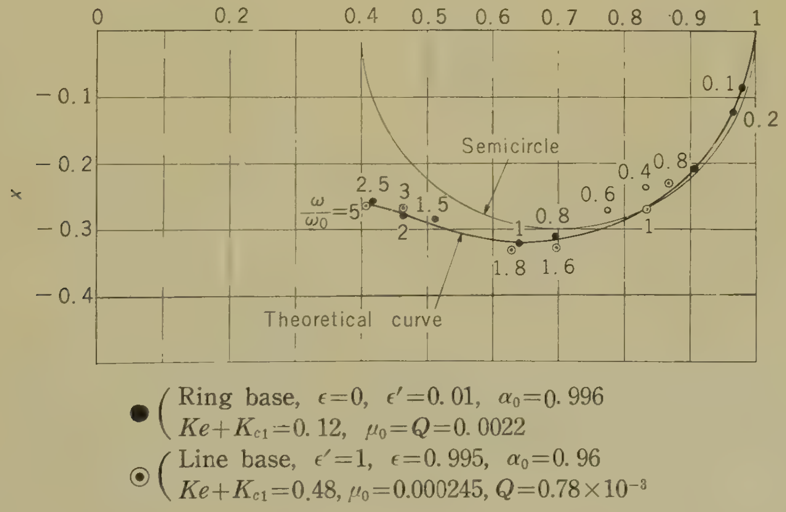

Fig. 13—$\frac{z_{bb'1}}{r_{bb'1}} = r+jx,$

Table 1

APPROXIMATION OF INNER REGION EQUIVALENT CIRCUIT APPROXIMATE EQUATIONS

	Approximate equations	Equivalent circuit	Approximate curves
α μ	$\alpha_0 \frac{e^{-jm\frac{f}{f_a}}}{(\mu_0)\,1+j\frac{f}{f_a}} = \alpha_0 \frac{1-j\,m'\,n'\frac{f}{f_a}}{(\mu_0)\;1+j\,n'\frac{f}{f_a}}$ $m' \doteqdot \frac{(1+m)^2-1}{(1+m)^2+1}$	$n' = \frac{1}{\sqrt{1-(1+\frac{f^2}{f_1^2})\,m'^2}}$	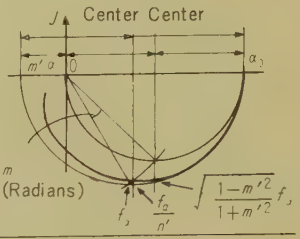 J Center Center $m'\alpha$ 0 α_0 m (Radians) f_a $\frac{f_a}{n'}$ $\sqrt{\frac{1-m'^2}{1+m'^2}}\,f_a$
Z_e	$r_e \frac{1+j\,m_1 n_1 \frac{f}{f_a}}{1+jn_1\frac{f}{f_a}}$ $= r_e \left[m_1 + \frac{1-m_1}{1+jn_1\frac{f}{f_a}} \right]$	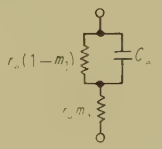 $C_e = \frac{n_1}{2\pi f_a r_e(1-m_1)}$	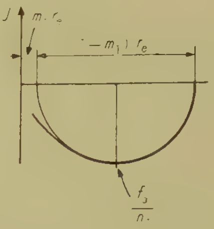
$Z_{bb'1}$	$r_{bb'1} \frac{1+j\,m_2 n_2 \frac{f}{f_a}}{1+jn_2\frac{f}{f_a}}$ $= r_{bb'1} \left[m_2 + \frac{1-m_2}{1+jn_2\frac{f}{f_a}} \right]$	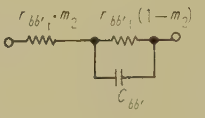 $C_{bb'} = \frac{n_2}{2\pi f_a r_{bb'1}(1-m_2)}$	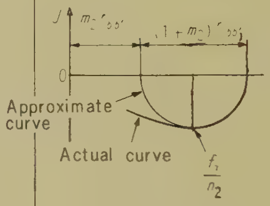 J $m_2 r_{bb'}$ $(1+m_2)\,r_{bb'1}$ 0 Approximate curve Actual curve $\frac{f_a}{n_2}$
y_{c1}	$g_{c0} + \frac{j\,\omega_a C_{c1}\frac{f}{f_a}}{1+j\,n_3\frac{f}{f_a}}$	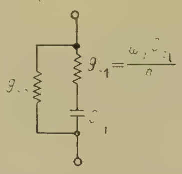 g_{c0} $g_{c1} = \frac{\omega_a C_{c1}}{n_3}$ C_{c1}	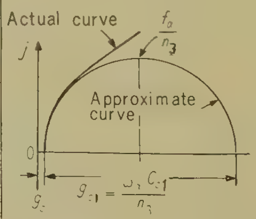 Actual curve $\frac{f_a}{n_3}$ j Approximate curve 0 g_{c0} $g_{c1} = \frac{\omega_a C_{c1}}{n_3}$

Table 2 THEORITICALLY CALCULATED CONSTANTS FOR VARIOUS DESIGN CONDITIONS

ε'	0.01			1			2			4	
ε	0			0.995			1.9975			3.99875	
w/L	0.01			0.1			0.1			0.1	
$K_e=\omega_0 C_{et} r_e$	0	0.1235	0.1645	0	0.2	0.4	0	0.2	0.4	0	0.03125
ω_a/ω_0	2.43	1.9	1.8	4.85	2.7	1.8	8.4	3.55	2.12	18.5	14
m	0.22	0.2	0.2	0.4	0.32	0.23	0.6	0.4	0.25	1.05	1.0
m' at $f=0.3f_\alpha$	0.18	0.18	0.18	0.32	0.268	0.202	0.43	0.32	0.22	0.595	0.58
n' at $f=0.3f_b$	1.018	1.018	1.018	1.06	1.041	1.022	1.12	1.06	1.027	1.275	1.257
m_1	0.10	0.1	0.08	0.32	0.075	0.04	0.42	0.035	0.012	0.5	0.1
n_1	1.02	0.961	0.976	0.898	0.947	0.989	0.8	0.944	0.064	0.5605	0.718
$1-m_1$	0.83	0.9	0.92	0.68	0.925	0.96	0.58	0.965	0.988	0.5	0.9
$n_1/(1-m_1)$	1.23	1.0675	1.06	1.32	1.024	1.03	1.379	0.973	0.976	1.12	0.798
$^*n_1(1-m_1)$	0.8466	0.865	0.893	0.6106	0.876	0.95	0.464	0.9112	0.9525	0.28	0.646
$^*n''=1-\{n_1(1-m_1)\}/n'$	0.166	0.15	0.118	6.424	0.159	0.071	0.586	0.14	0.073	0.78	0.486

* Appears in $Z_e'/(1-\alpha)$ term on Table 7.

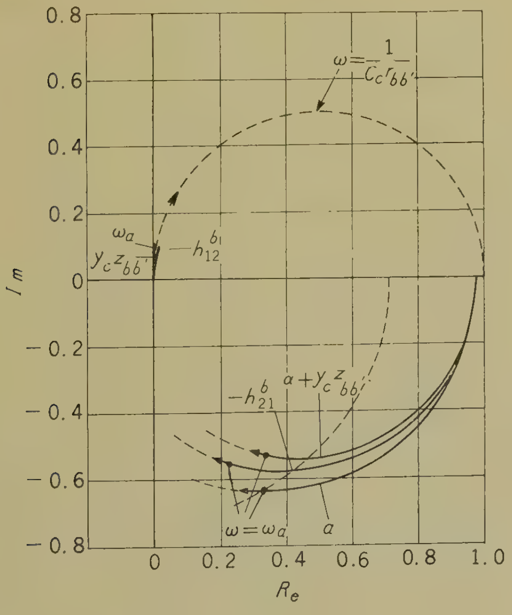

Fig. 14-1—Estimated approximate curve of frequency characteristics of each parameter.

Table 3 CONVERSION EQUATIONS BETWEEN 4 TERMINAL PARAMETERS

	h^b	h^e	y^b	y^e
h^b	$h_{11}^b \quad h_{12}^b$ $h_{21}^b \quad h_{22}^b$	$h_{11}^b=\frac{h_{11}^e}{(1+h_{21}^e)(1-h_{12}^e)+h_{11}^e h_{22}^e}$ $h_{12}^b=\frac{h_{11}^e h_{22}^e-h_{12}^e(1+h_{21}^e)}{(1+h_{21}^e)(1-h_{12}^e)+h_{11}^e h_{22}^e}$ $h_{21}^b=-\frac{h_{11}^e h_{22}^e+h_{21}^e(1-h_{12}^e)}{(1+h_{21}^e)(1-h_{12}^e)+h_{11}^e h_{22}^e}$ $h_{22}^b=\frac{h_{22}^e}{(1+h_{21}^e)(1-h_{12}^e)+h_{11}^e h_{22}^e}$	$h_{11}^b=\frac{1}{y_{11}^b} \quad h_{12}^b=-\frac{y_{12}^b}{y_{11}^b}$ $h_{21}^b=\frac{y_{21}^b}{y_{11}^b} \quad h_{22}^b=\frac{y_{11}^b y_{22}^b-y_{12}^b y_{21}^b}{y_{11}^b}$	$h_{11}^b=\frac{1}{y_{11}^e+y_{12}^e+y_{21}^e+y_{22}^e}$ $h_{12}^b=\frac{y_{12}^e+y_{22}^e}{y_{11}^e+y_{12}^e+y_{21}^e+y_{22}^e}$ $h_{21}^b=-\frac{y_{21}^e+y_{22}^e}{y_{11}^e+y_{12}^e+y_{21}^e+y_{22}^e}$ $h_{22}^b=\frac{y_{11}^e y_{22}^e-y_{12}^e y_{21}^e}{y_{11}^e+y_{12}^e+y_{21}^e+y_{22}^e}$
h^e	$h_{11}^e=\frac{h_{11}^b}{(1+h_{21}^b)(1-h_{12}^b)+h_{11}^b h_{22}^b}$ $h_{12}^e=\frac{h_{11}^b h_{22}^b-h_{12}^b(1+h_{21}^b)}{(1+h_{21}^b)(1-h_{21}^b)+h_{11}^b h_{22}^b}$ $h_{21}^e=-\frac{h_{11}^b h_{22}^b+h_{21}^b(1-h_{12}^b)}{(1+h_{21}^b)(1-h_{12}^b)+h_{11}^b h_{22}^b}$ $h_{22}^e=\frac{h_{22}^b}{(1+h_{21}^b)(1-h_{12}^b)+h_{11}^b h_{22}^b}$	$h_{11}^e \quad h_{12}^e$ $h_{21}^e \quad h_{22}^e$	$h_{11}^e=\frac{1}{y_{11}^b+y_{12}^b+y_{21}^b+y_{22}^b}$ $h_{12}^e=\frac{y_{12}^b+y_{22}^b}{y_{11}^b+y_{12}^b+y_{21}^b+y_{22}^b}$ $h_{21}^e=-\frac{y_{21}^b+y_{22}^b}{y_{11}^b+y_{12}^b+y_{21}^b+y_{22}^b}$ $h_{22}^e=\frac{y_{11}^b y_{22}^b-y_{12}^b y_{21}^b}{y_{11}^b+y_{12}^b+y_{21}^b+y_{22}^b}$	$h_{11}^e=\frac{1}{y_{11}^e} \quad h_{12}^e=-\frac{y_{12}^e}{y_{11}^e}$ $h_{21}^e=\frac{y_{21}^e}{y_{11}^e} \quad h_{22}^e=\frac{y_{11}^e y_{22}^e-y_{12}^e y_{21}^e}{y_{11}^e}$
y^b	$y_{11}^b=\frac{1}{h_{11}^b} \quad y_{12}^b=-\frac{h_{12}^b}{h_{11}^b}$ $y_{21}^b=\frac{h_{21}^b}{h_{11}^b} \quad y_{22}^b=\frac{h_{11}^b h_{22}^b-h_{12}^b h_{21}^b}{h_{11}^b}$	$y_{11}^b=\frac{(1+h_{21}^e)(1-h_{12}^e)+h_{11}^e h_{22}^e}{h_{11}^e}$ $y_{12}^b=-\frac{h_{11}^e h_{22}^e-h_{12}^e(1+h_{21}^e)}{h_{11}^e}$ $y_{21}^b=-\frac{h_{11}^e h_{22}^e+h_{21}^e(1-h_{12}^e)}{h_{11}^e}$ $y_{22}^b=\frac{h_{11}^e h_{22}^e-h_{12}^e h_{21}^e}{h_{11}^e}$	$y_{11}^b \quad y_{12}^b$ $y_{21}^b \quad y_{22}^b$	$y_{11}^b=y_{11}^e+y_{12}^e+y_{21}^e+y_{22}^e$ $y_{12}^b=-(y_{12}^e+y_{22}^e)$ $y_{21}^b=-(y_{21}^e+y_{22}^e)$ $y_{22}^b=y_{22}^e$
y^e	$y_{11}^e=\frac{(1+h_{21}^b)(1-h_{12}^b)+h_{11}^b h_{22}^b}{h_{11}^b}$ $y_{12}^e=-\frac{h_{11}^b h_{12}^b-h_{12}^b(1+h_{21}^b)}{h_{11}^b}$ $y_{21}^e=-\frac{h_{11}^b h_{22}^b+h_{21}^b(1-h_{12}^b)}{h_{11}^b}$ $y_{22}^e=\frac{h_{11}^b h_{22}^b-h_{12}^b h_{21}^b}{h_{11}^b}$	$y_{11}^e=\frac{1}{h_{11}^e} \quad y_{12}^e=-\frac{h_{12}^e}{h_{11}^e}$ $y_{21}^e=\frac{h_{21}^e}{h_{11}^e} \quad y_{22}^e=\frac{h_{11}^e h_{22}^e-h_{12}^e h_{21}^e}{h_{11}^e}$	$y_{11}^e=y_{11}^b+y_{12}^b+y_{21}^b+y_{22}^b$ $y_{12}^e=-(y_{12}^b+y_{22}^b)$ $y_{21}^e=-(y_{21}^b+y_{22}^b)$ $y_{22}^e=y_{22}^b$	$y_{11}^e \quad y_{12}^e$ $y_{21}^e \quad y_{22}^e$

Table 4 “*h*” AND “*y*” PARAMETERS OF GROUNDED-BASE CONFIGURATION

	Middle freq.*	High freq.**
$h_{11}{}^b=\frac{1}{y_{11}{}^b}$	$z_e'+z_{bb}'(1-\alpha)$	$z_e'+\frac{z_{bb}'(1-\alpha)}{1+y_cz_{bb}'}$
$h_{21}{}^b$	$-\alpha$	$-\frac{\alpha+y_cz_{bb}'}{1+y_cz_{bb}'}$
$h_{12}{}^b$	$\mu+y_cz_{bb}'$	$\frac{y_cz_{bb}'}{1+y_cz_{bb}'}$
$h_{22}{}^b$	y_c+y_c'	$\frac{y_c}{1+y_cz_{bb}'}+y_c'$
$y_{21}{}^b=\frac{h_{21}{}^b}{h_{11}{}^b}$	$-\frac{\alpha}{z_e'+z_{bb}'(1-\alpha)}$	$-\frac{\alpha+y_cz_{bb}'}{z_e'(1+y_cz_{bb}')+z_{bb}'(1-\alpha)}$
$y_{12}{}^b=\frac{-h_{12}{}^b}{h_{11}{}^b}$	$-\frac{\mu+y_cz_{bb}'}{z_e'+z_{bb}'(1-\alpha)}$	$-\frac{\mu+y_cz_{bb}'}{z_e'(1+y_cz_{bb}')+z_{bb}'(1-\alpha)}$
$y_{22}{}^b=y_{22}{}^e$	$\frac{(z_e'+z_{bb}')y_c+\alpha\mu}{z_e'+z_{bb}'(1-\alpha)}+y_c'$	$\frac{(z_e'+z_{bb}')y_c}{z_e'(1+y_cz_{bb}')+z_{bb}'(1-\alpha)}+y_c'$

* $y_c\frac{z_e'}{1-\alpha},\quad y_cz_{bb}',\quad y_c'z_{bb}'\ll 1 \qquad \frac{1}{z_{bb}'}\cdot\frac{z_e'}{1-\alpha},\quad 1\gg\mu.$

** $1,\quad y_cz_{bb}',\quad y_c\frac{z_e'}{1-\alpha},\quad \frac{z_e'}{z_{bb}'(1-\alpha)}\gg\mu.$

Table 5 “*h*” AND “*y*” PARAMETERS OF GROUNDED-EMMITTER CONFIGURATION

	Middle freq.*	High freq.**
$h_{11}{}^e=\frac{1}{y_{11}{}^e}$	$\frac{z_e'}{1-\alpha}+z_{bb}'$	$\dfrac{\frac{z_e'}{1-\alpha}+z_{bb}'\left(1+y_c\frac{z_e'}{1-\alpha}\right)}{1+y_c\frac{z_e'}{1-\alpha}+y_c'\left\{\frac{z_e'}{1-\alpha}+z_{bb}'\left(1+y_c\frac{z_e'}{1-\alpha}\right)\right\}}$
$h_{21}{}^e$	$\frac{\alpha}{1-\alpha}$	$\dfrac{\frac{\alpha}{1-\alpha}-\left[y_c\frac{z_e'}{1-\alpha}+y_c'\left\{\frac{z_e'}{1-\alpha}+z_{bb}'\left(1+y_c\frac{z_e'}{1-\alpha}\right)\right\}\right]}{1+y_c\frac{z_e'}{1-\alpha}+y_c'\left\{\frac{z_e'}{1-\alpha}+z_{bb}'\left(1+y_c\frac{z_e'}{1-\alpha}\right)\right\}}$
$h_{12}{}^e$	$y_c\frac{z_e'}{1-\alpha}+y_c'\left(\frac{z_e'}{1-\alpha}+z_{bb}'\right)-\mu$	$\dfrac{y_c\frac{z_e'}{1-\alpha}+y_c'\left\{\frac{z_e'}{1-\alpha}+z_{bb}'\left(1+y_c\frac{z_e'}{1-\alpha}\right)\right\}}{1+y_c\frac{z_e'}{1-\alpha}+y_c'\left\{\frac{z_e'}{1-\alpha}+z_{bb}'\left(1+y_c\frac{z_e'}{1-\alpha}\right)\right\}}$
$h_{22}{}^e$	$\frac{y_c+y_c'}{1-\alpha}$	$\frac{1}{1-\alpha}\cdot\dfrac{y_c+y_c'(1+y_cz_{bb}')}{1+y_c\frac{z_e'}{1-\alpha}+y_c'\left\{\frac{z_e'}{1-\alpha}+z_{bb}'\left(1+y_c\frac{z_e'}{1-\alpha}\right)\right\}}$
$y_{21}{}^e=\frac{h_{21}{}^e}{h_{11}{}^e}$	$\frac{\alpha}{z_e'+z_{bb}'(1-\alpha)}=-y_{21}{}^b$	$\dfrac{\frac{\alpha}{1-\alpha}-y_c\frac{z_e'}{1-\alpha}}{\frac{z_e'}{1-\alpha}+z_{bb}'\left(1+y_c\frac{z_e'}{1-\alpha}\right)}-y_c'$
$y_{12}{}^e=\frac{-h_{12}{}^e}{h_{11}{}^e}$	$-\frac{z_e'y_c-(1-\alpha)\mu}{z_e'+z_{bb}'(1-\alpha)}-y_c'$	$-\frac{z_e'y_c}{z_e'(1+y_cz_{bb}')+z_{bb}'(1-\alpha)}-y_c'$

*, ** Same as Table 4.

Table 6 THEORETICALLY APPROXIMATED FREQUENCY CHARACTERISTICS OF EACH PARAMETERS

	Approximate equations	Approximate curves
$1-\alpha$	$\dfrac{1-\alpha_0+j\,n'(1+\alpha_0 m')\frac{f}{f_a}}{1+j\,n'\frac{f}{f_a}}$ $=1+\alpha_0 m'-\dfrac{\alpha_0(1+m')}{1+j\,n'\frac{f}{f_a}}$	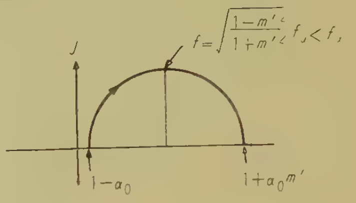 j $f=\sqrt{\frac{1-m'^2}{1+m'^2}}f_a<f_1$ $1-\alpha_0$ $1+\alpha_0 m'$
$\dfrac{1}{1-\alpha}$	$\dfrac{1}{1+\alpha_0 m'}+\dfrac{\frac{1}{1-\alpha_0}-\frac{1}{1+\alpha_0 m'}}{1+j\frac{1+\alpha_0 m'}{1-\alpha_0}n'\frac{f}{f_a}}$	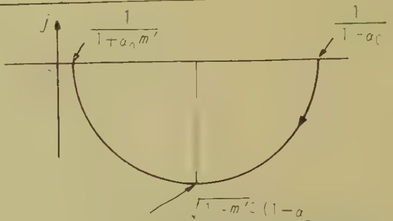 $f'_b=\dfrac{\sqrt{1-m'^2}(1-\alpha_0)}{\sqrt{(1+\alpha_0 m')^2+(1-\alpha_0)^2 m'^2}}f_a$
$b=\dfrac{\alpha}{1-\alpha}$	$b_0\left[-\dfrac{(1-\alpha_0)m'}{1+\alpha_0 m'}+\dfrac{\frac{1+m'}{1+\alpha_0 m'}}{1+j\frac{1+\alpha_0 m'}{1-\alpha_0}n'\frac{f}{f_a}}\right]$ $b_0=\dfrac{\alpha_0}{1-\alpha_0}$	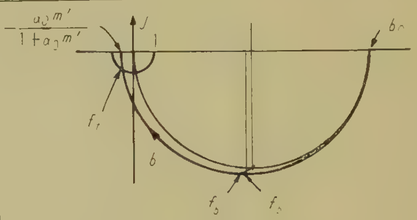 $-\frac{\alpha_0 m'}{1+\alpha_0 m'}$ j 1 b_0 f_1 b f_b f_b' $f_b\doteqdot\dfrac{f_1}{b_0}\doteqdot\dfrac{\sqrt{1-m'^2}(1-\alpha_0)}{\sqrt{(1+\alpha_0 m')^2-(1-\alpha_0)^2 m'^2}}f_a$ $\doteqdot\dfrac{\sqrt{1-m'^2}}{1+\alpha_0 m'}(1-\alpha_0)f_a\doteqdot\dfrac{1-\alpha_0}{1+\alpha_0 m}f_a$

meters and grounded-base and grounded-emitter "h" parameters are listed in Tables 6, 7, and Fig. 14.

6. Method of Obtaining Equivalent Circuit

(1) First of all, the grounded-base "H" parameters, of the equivalent circuit shown in Fig. 8, in the high frequency range in which μ is ignored, are obtained as seen from measuring point. From these, external stray immittances and $r_{cc'}$ are eliminated and $[h^b]$ which is the grounded base "h" parameters of the inner region within the dotted line in Fig. 8 are calculated. Next,

$$y_c Z_{bb'}=\frac{h_{12}{}^b}{1-h_{12}{}^b},\quad\text{and}\quad \alpha=\frac{-h_{12}{}^b-h_{21}{}^b}{1-h_{12}{}^b}$$

are calculated.

Then f_a, m, m', and n' are obtained when we approximate the following equations

Table 7 THEORETICALLY APPROXIMATED FREQUENCY CHARACTERISTICS OF EACH PARAMETER

	Approximate equations and equivalent circuits		Approximate curves
$\frac{Ze'}{1-\alpha}$	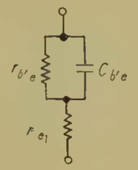 $r_{e_1}=\frac{n'' r_e+r_{ee'}}{1+\alpha_0 m'}$ $n''=1-\frac{n_1(1-m_1)}{n'}$ $r_{b'e}=\frac{r_e+r_{ee'}}{1-\alpha_0}-r_{e_1}$ $C_{b'e}=\frac{n'(1+\alpha_0 m')}{2\pi f_a(1-\alpha_0)r_{b'e}}\doteqdot C_e\frac{n'(1+\alpha_0 m')(1-m_1)r_e}{n_1\{r_e+r_{ee'}-r_{e_1}(1-\alpha_0)\}}$ $\doteqdot\frac{1}{2\pi f_b r_{b'e}}$		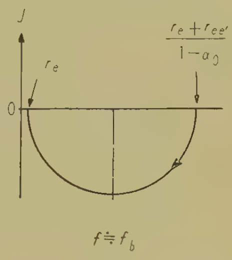
y_c	$y_c=j\omega C_{ct}+\frac{j\omega C_{c1}}{1+jn_3\frac{\omega}{\omega_a}}$ $\doteqdot\frac{\omega_a C_{c_1}}{n_3}\left(\frac{\omega}{\omega_a/n_3}\right)^2+j\omega(C_{ct}+C_{c_1})$	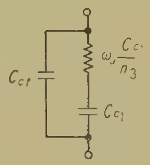	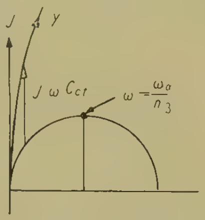
$Z_{bb'}$	$Z_{bb'}=r_{bb'}\frac{1+jl_2n_2\frac{\omega}{\omega_a}}{1+jn_2\frac{\omega}{\omega_a}}$	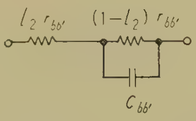	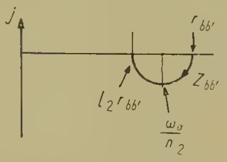
$y_c Z_{bb'}$	at $\omega<0.2\omega_a$ $y_c Z_{bb'}\doteqdot j\omega_a C_{ct} r_{bb'} l_2\frac{\omega}{\omega_a}+j\frac{\omega_a^2 C_{ct} r_{bb'}(1-l_2)+\omega_a C_{c1} r_{bb'}}{1+j(n_2+n_3)\frac{\omega}{\omega_a}}\times\frac{\omega}{\omega_a}$		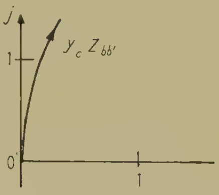

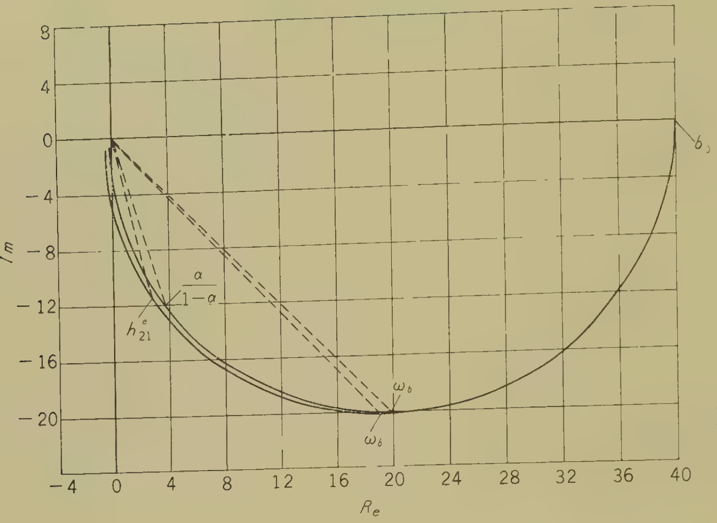

Fig. 14-2—h_{21}^e.

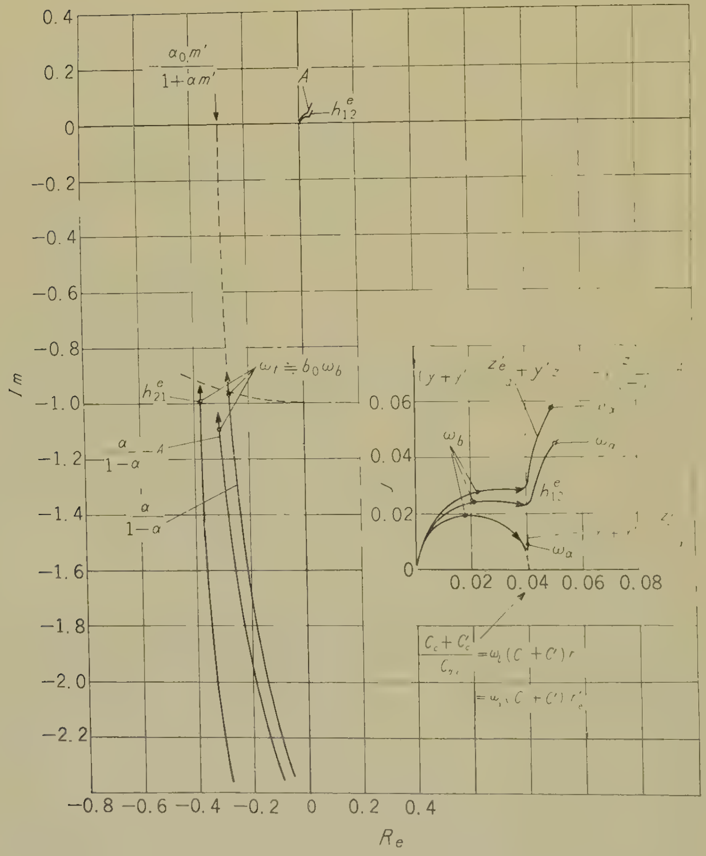

Fig. 14-3—h_{21}^e (enlarge) and h_{12}^e.

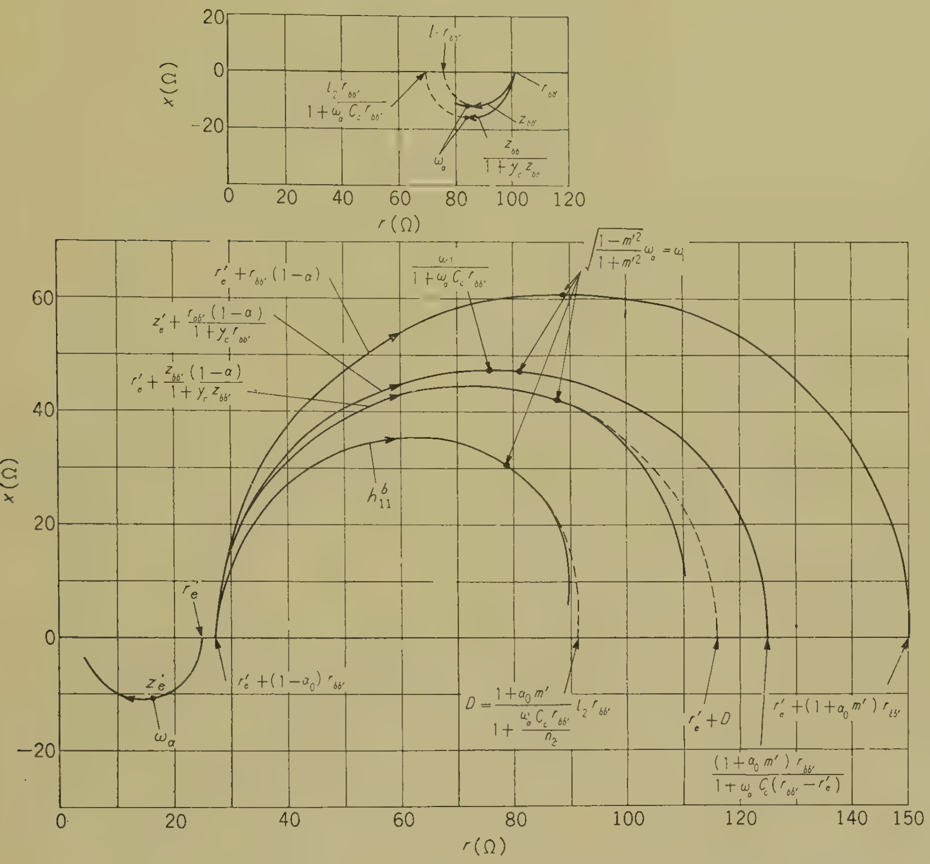

Fig. 14-4—$\frac{z_{bb'}}{1+y_c z_{bb'}}$ and h_{11}^b.

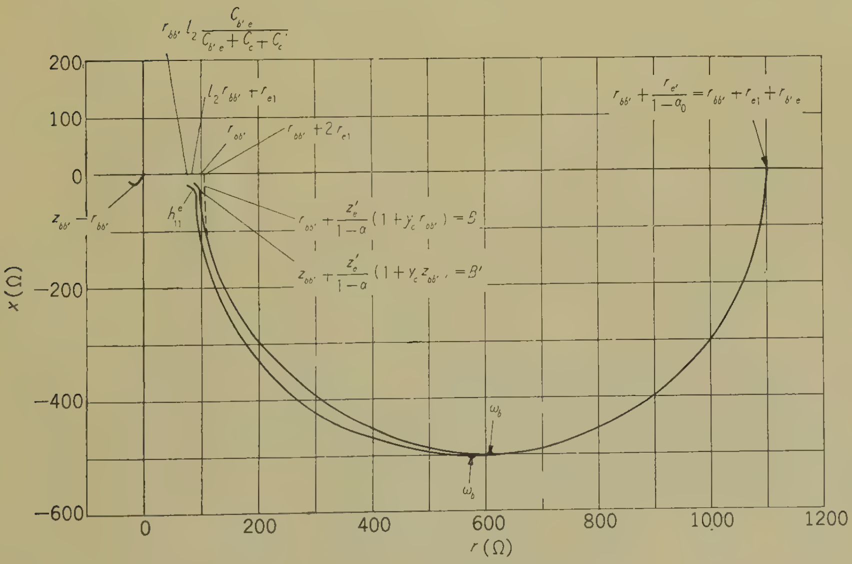

Fig. 14-5—h_{11}^e.

$$\alpha=\alpha_0\frac{\exp\left(-jm\dfrac{f}{f_\alpha}\right)}{1+j\dfrac{f}{f_\alpha}}=\alpha_0\frac{1-jm'n'\dfrac{f}{f_\alpha}}{1+jn'\dfrac{f}{f_\alpha}}. \tag{4}$$

Still we estimate m_1, n_1, appearing in following equation

$$Z_e=r_e\frac{1+jm_1n_1\dfrac{f}{f_\alpha}}{1+jn_1\dfrac{f}{f_\alpha}}, \tag{5}$$

which is derived from dependency of α by I_E.

(2) Next, for frequencies below $0.3f_\alpha$, $r_{b'e}$ is obtained from the frequency characteristic of $\{h_{11}{}^b/(1-\alpha)\}(\doteqdot h_{11}{}^e)$ which is a semicircle on the complex plane at low frequencies (2 to 10 Mc), and comfirmed whether it satisfies following equation; therefore r_e and $r_{ee'}$ are determined.

$$\frac{r_{b'e}}{1+b_0}=r_e+r_{ee'}-\frac{n''r_e+r_{ee'}}{(1+\alpha_0m')(1+b_0)}\quad\left(r_e\doteqdot\frac{kT}{qI_E}\right)$$

($r_{ee'}$ is difference between grounded emitter saturation resistance and grounded base saturation resistance)

Next, we obtain the low frequency value of $Z_{bb'}$

$$r_{bb'}=h_{110}{}^e-\left(r_{b'e}+\frac{r_{ee'}+n''r_e}{1+\alpha_0m'}\right)$$

$$=h_{110}{}^e-(1+b_0)(r_e+r_{ee'}).$$

And similarly in the low frequency range, $C_{b'e}$ is calculated from real part r of the $h_{11}{}^b/(1-\alpha)$ $(\doteqdot h_{11}{}^e)$ locus semicircle

$$C_{b'e}=\frac{1}{2\pi fr_{b'e}}\sqrt{\frac{r_{b'e}}{r}-1}.$$

It should coincise with the value obtained from the following equation.

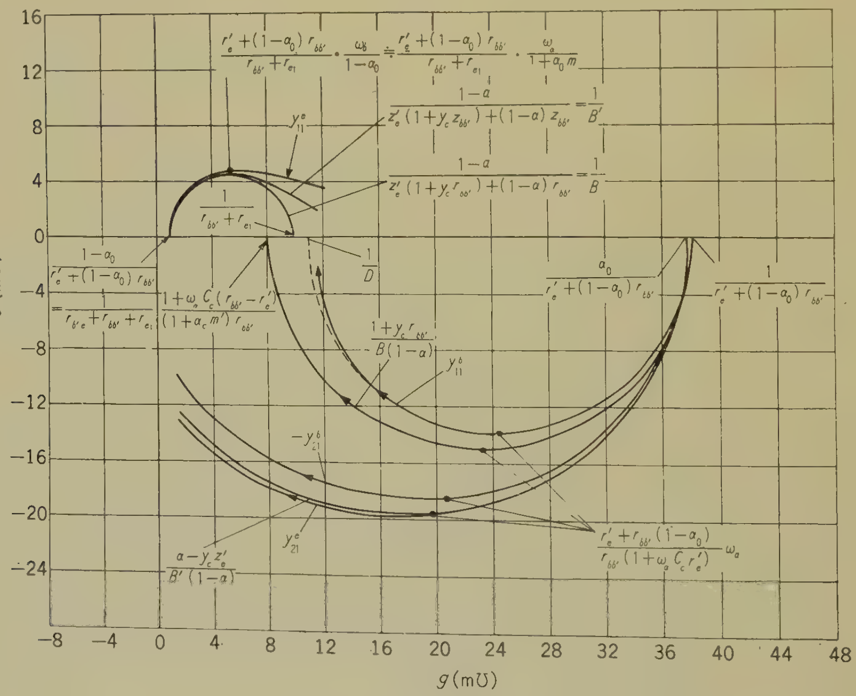

Fig. 14-6— $y_{11}{}^e$, $y_{11}{}^b$, $-y_{21}{}^b$, and $y_{21}{}^e$.

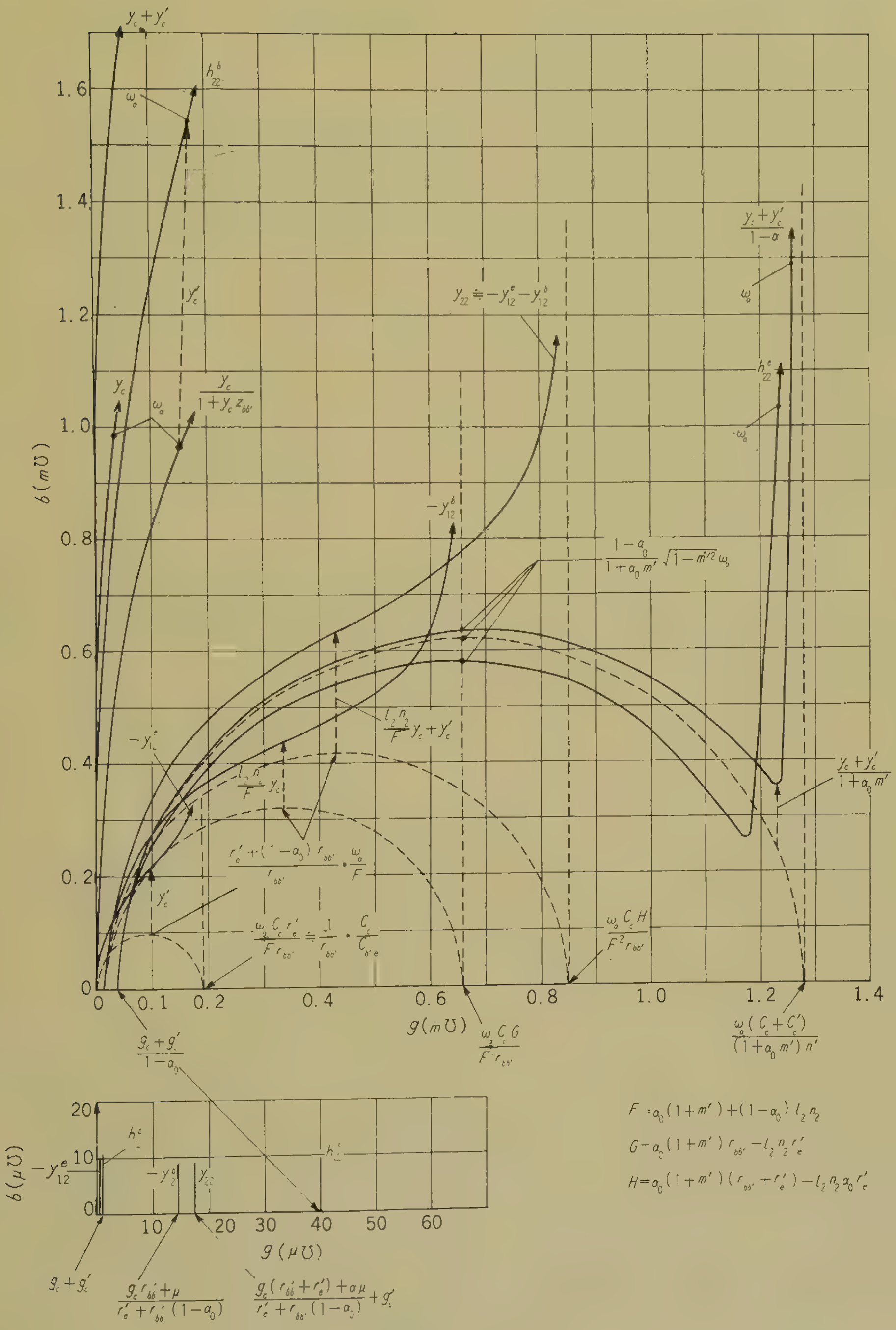

Fig. 14-7—h_{22}^b, $-y_{22}^e$, $-y_{12}^b$, y_{22}, and h_{22}^e.

$$C_{b'e} = \frac{1+\alpha_0 m'}{1-\alpha_0} \cdot \frac{n'}{2\pi f_\alpha r_{b'e}}.$$

$C_{b'e}$ is nearly constant at frequencies below $0.2f$ and

$$f_b = \frac{1}{2\pi C_{b'e} r_{b'e}}, \quad f_t = b_0 f_b.$$

(3) Next, at frequencies above $0.3f_\alpha$ we calculate Eq. (5), and obtain $(Z_e + r_{ee}')/(1-\alpha)$ and remainder B which is subtracted from $h_{11}^b/(1-\alpha)$, is

$$B = \frac{Z_{bb'}}{1+y_c Z_{bb'}}$$

and $Z_{bb'}$ is obtained from following

$$Z_{bb'} = \frac{B}{1-h_{11}^b}.$$

(4) Similarly, in the frequency range in which μ is neglected, we obtain

$$y_c = \frac{h_{12}^b}{B}, \quad y_c' = h_{22}^b - (1-h_{12}^b) y_c.$$

(5) At low frequencies

$$g_{c0} \fallingdotseq h_{220}^b, \quad \mu_0 \fallingdotseq h_{120}^b - g_{c0} r_{bb'}$$

are obtained.

7. Method of Measuring Four-Terminal Parameters

To measure these parameters, a transfer-function phase meter, high frequency bridge, or standing wave detector can be used. In the high frequency region, to realize the terminal condition (open or short) resonance of a low loss line can be used. When specific impedance is placed at the terminal, it may be rejected by the following equations.

$$h_{21} = \frac{H_{21}}{1-H_{22} z_2},$$

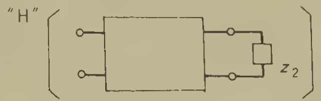

$$h_{12} = \frac{H_{12}}{1-H_{11} \cdot y_2}.$$

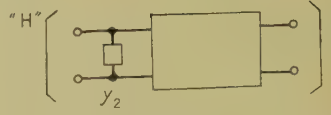

In order to obtain the transfer-function from the two terminal immittance parameters, only we measure these parameters changing the ground configuration, and compute using the following equations

$$H_{21}^e = \frac{1}{2}\left[A + \sqrt{A^2 + 4(H_{22}^e - Y_{22}^e) H_{11}^e}\right]$$

$$\left(A = \frac{H_{11}^e}{H_{11}^b} - 1 - Y_{22}^e \cdot H_{11}^e\right)$$

$$H_{12}^e = (H_{22}^e - Y_{22}^e) \cdot \frac{H_{11}^e}{H_{21}^e}.$$

Using Table 3, we can change on set of parameters to the others. In all cases, care must be taken to satisfy the small signal condition.

8. Four-Terminal Parameters and Measured Examples of Equivalent Circuit

Measured examples of H parameters and equivalent circuit of each transistor are shown in Figs. 15 to 37 and Table 8.(5)~(7)

9. Conclusion

This study was carried out for the purpose of analyzing the frequency characteristics of equivalent circuits and the four-terminal parameters of high frequency transistor. The following results were obtained:

(1) For both transistors of carrier diffusion type and carrier drift type, strict theoretical curves for frequency characteristics of equivalent circuit elements of the inner region are obtained, and they are represented approximately in the low to approximately cutoff frequency region.

(2) Equivalent circuit, (from the measuring point of view) commonly adaptable to various high frequency transistors obtained from grounded base H parameter is decided.

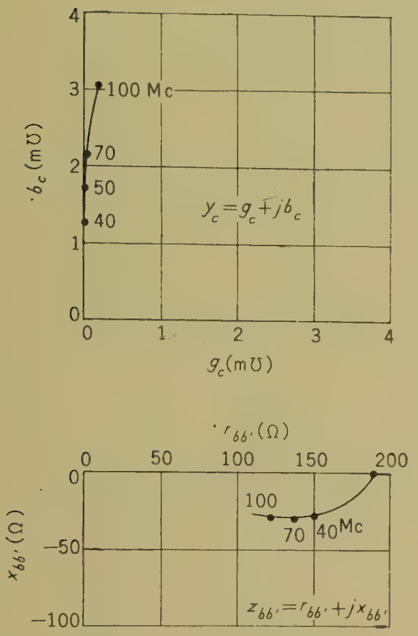

Fig. 15—Frequency characteristics of y_c and $z_{bb'}$ of ECL-1205.

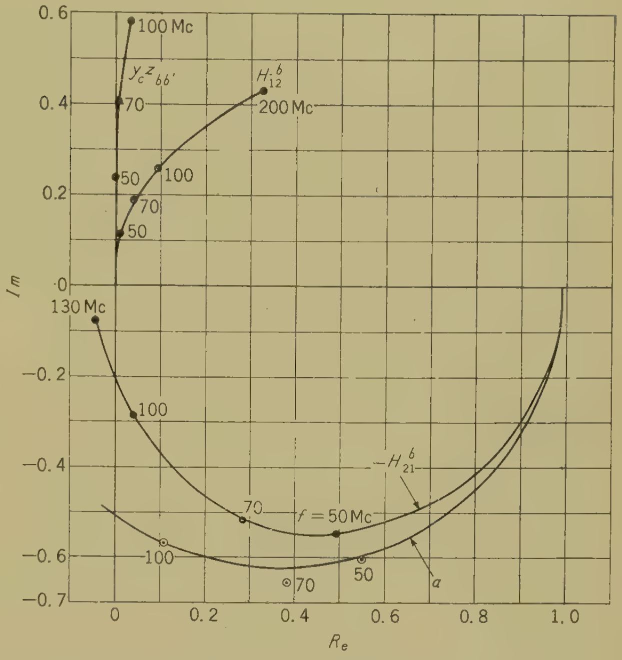

Fig. 16—Frequency characteristics of FT-100 (Micro Alloy).

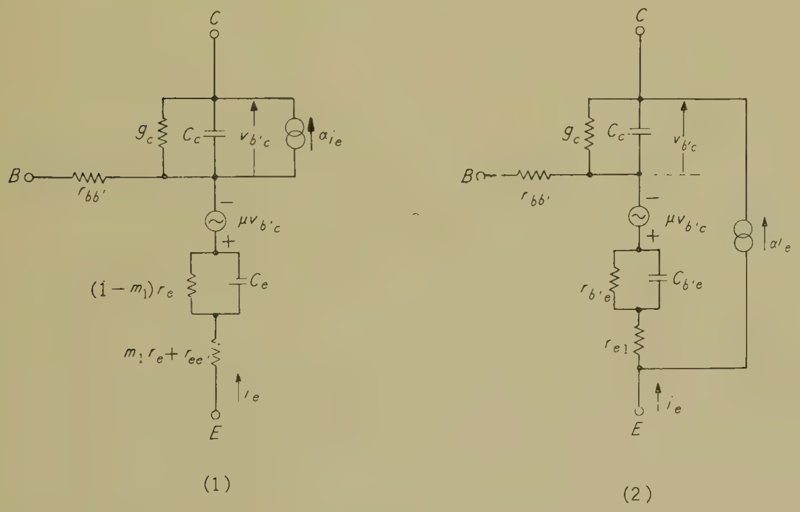

$$a=a_0\frac{e^{-jm\frac{f}{f_a}}}{1+j\frac{f}{f_a}}$$
$$(\mu)\ (\mu_0)$$

Fig. 17—Equivalent circuit of FT 100 (below middle frequency).

Table 8 MEASURED VALUES OF VARIOUS CONSTANTS (FT100)

Connection	No. 1 N	No. 1 I	No. 2 N	No. 2 I	No. 3 N	No. 3 I
$h_{11}^e(\Omega)$ at $f=270\sim$	3850	428	1012	520	5400	550
$h_{11}^b(\Omega)$ 〃	29.7	36	36.4	35	28.9	31.4
$h_{12}^b(\times 10^{-4})$ 〃	10.7	14	13.3	13.5	12.7	12.5
$g_c=h_{22}^b(\mu\Omega)$ 〃	1.16	4.46	1.02	3.03	0.77	3.1
$b_0=h_{21}^e$ 〃	128.5	10.87	26.8	13.84	185.5	16.5
$\alpha_0=b_0/(1+b_0)$ 〃	0.992	0.915	0.9652	0.9323	0.9945	0.943
$r_{b'e}$ (Ω)	3625	298	772	364	5200	441
$r_e+r_{ee'}$ (Ω)	28	25.1	27.8	24.53	27.85	25.2
m_1	0.1	0.1	0.1	0.1	0.1	0.1
$r_{bb'}$ (Ω)	217	127	237	153	197	105
r_{e1} (Ω)	3	3	3	3	3	3
$C_{b'e}$ (pF)	86.4	574	67.15	495.5	62	537
$f_b=1/(2\pi C_{b'e}r_{be})$ (Mc)	0.508	0.93	3.07	0.8825	0.494	0.672
$f_t=b_0f_b$ (Mc)	65.3	10.11	82.3	12.21	91.6	11.1
$f\alpha$ (Mc)	79	13.1	102	15.6	110.5	14
C_e (pF)	82.6	519	64	446	59.2	485
C_0 (pF)	3.5		3.6		3.9	
μ_0 $(\times 10^{-4})$	8.13	8.13	8.74	8.86	11.184	9.24

Connection N : Normal I : Emitter, Collector Inversed
$T_a=25°C$, DC Bias ($V_C=-6V$, $I_E=1$ mA)
Equivalent Circuits are Shown in Fig. 17.

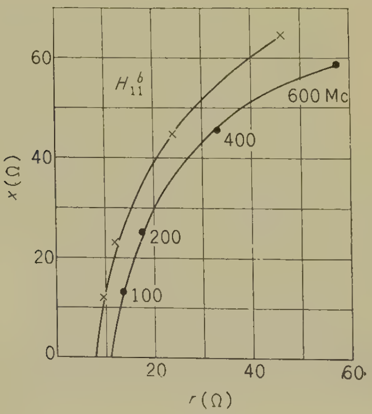

Fig. 18—Measured of ECL 1206 (Ge Mesa) characteristics.

●: $V_c=-6^V$, $I_E=3^{mA}$
×: $V_c=-6^V$, $I_E=5^{mA}$ (same as follow)

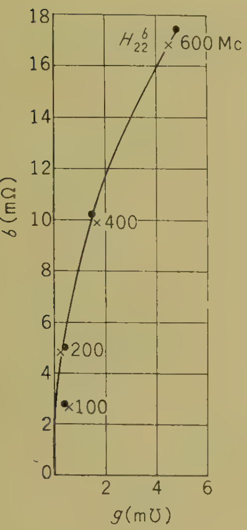

Fig. 19

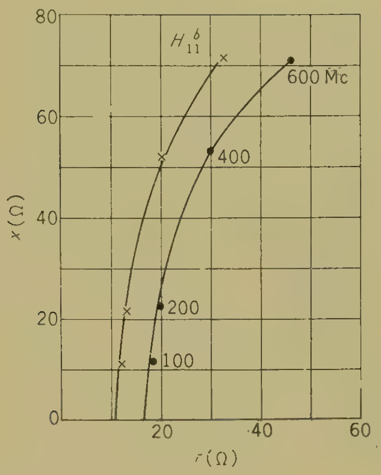

Fig. 22

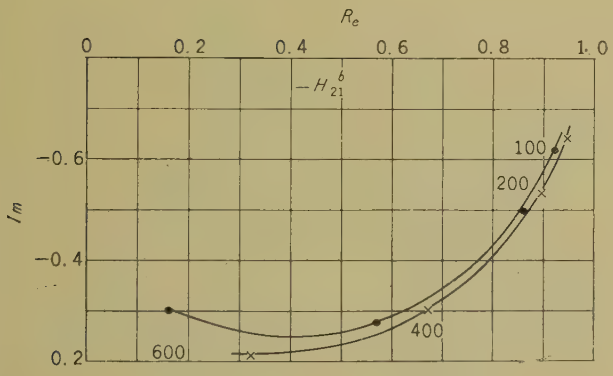

Fig. 20

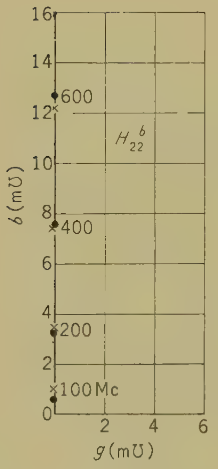

Fig. 23

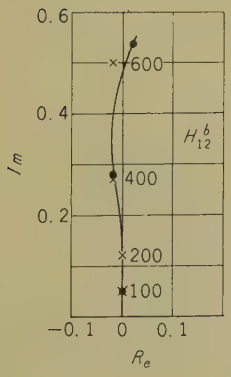

Fig. 21

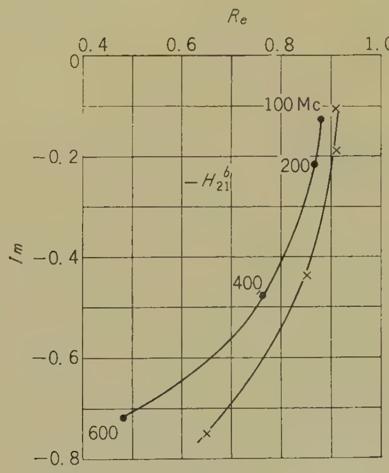

Fig. 24

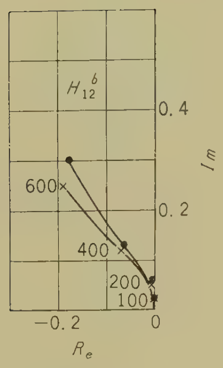

Fig. 25

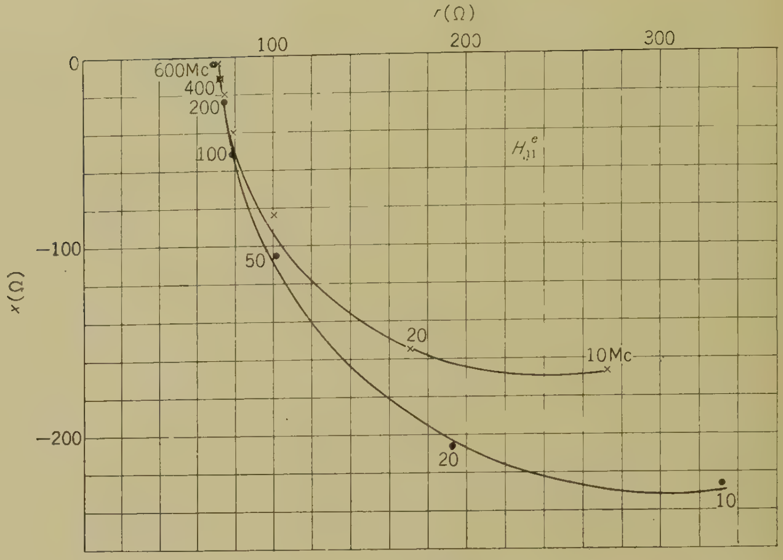

Fig. 26

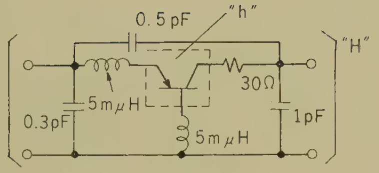

Figs. 27 to 30 are excluded curve of parasitic elements from Fig. 28 to 21.

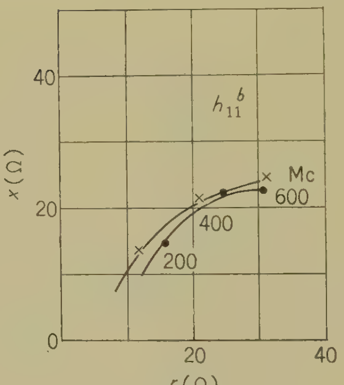

Fig. 27

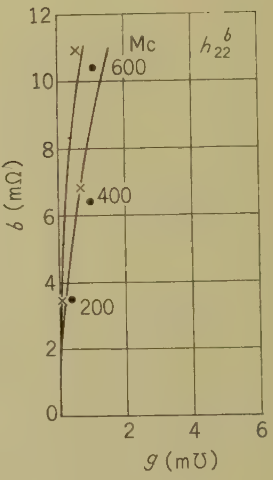

Fig. 28

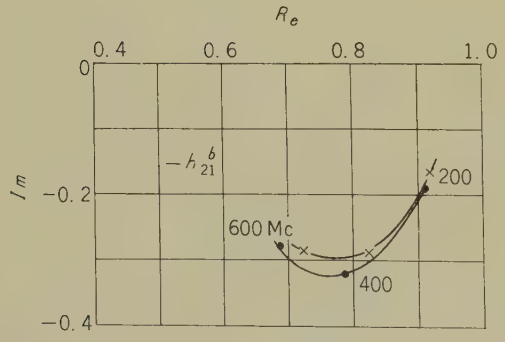

Fig. 29

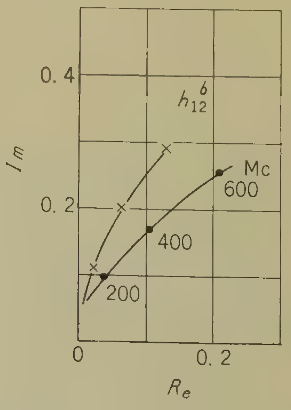

Fig. 30

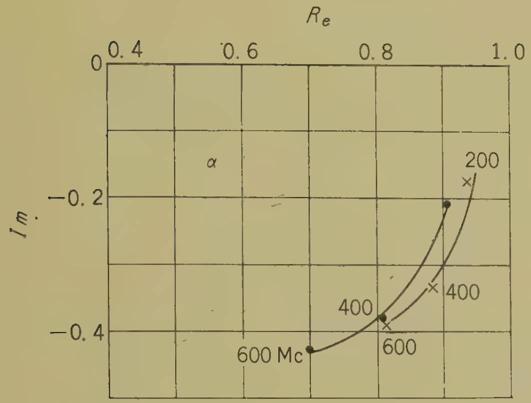

Fig. 31—Example of α (ECL 1206).

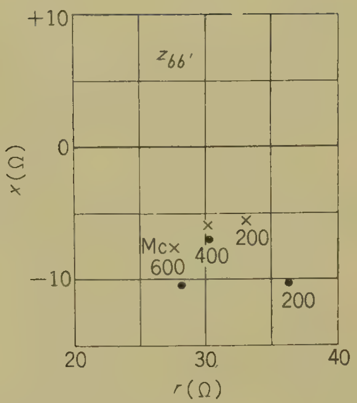

Fig. 32—Example of $z_{bb'}$ (ECL 1206).

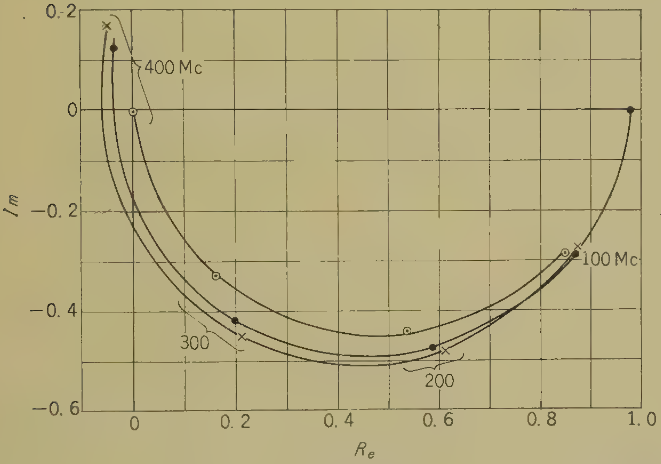

Fig. 33—$H21^b$.

Figs. 33 to 37 show measured curves of LST11 (Si diffused base).

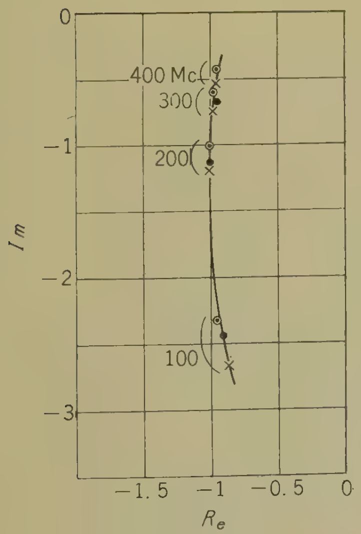

Fig. 34—H_{21}^e.

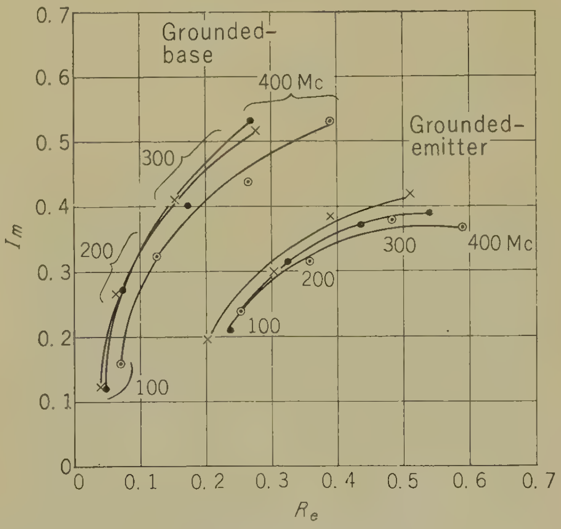

Fig. 35—H_{12}^b and H_{12}^e.

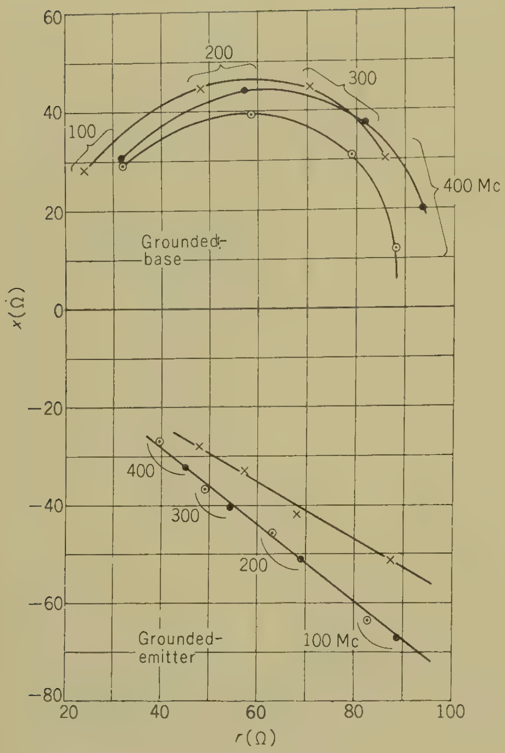

Fig. 36—H_{11}^b and H_{11}^e.

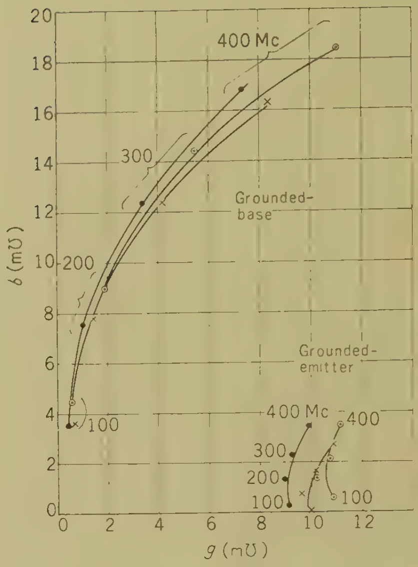

Fig. 37—H_{22}^b and H_{22}^e.

(3) Four-terminal parameters of transistors are expressed by equivalent circuits, and frequency characteristics are analyzed.

(4) Measured examples of H and h parameters for several high frequency transistors are given.

References

(1) H. Kröemer: Zur Theorie des Diffusions und des Drifttransistors", *AEÜ.*, 8, 1954, p. 223–228.

(2) J. Almond and R. J. McIntype: The Equivalent Circuit of the Drift Transistor", *RCA Rev.*, **18,** 3, Sep. 1957, p. 361–384.

(3) R. L. Pritchard: "Two-Dimensional Current Flow in in Junction Transistors at High Frequencies", *Proc. I.R.E.*, June, 1958, pp. 1152-1160.

(4) S. Kawaguchi and M. Hirai: "Equivalent Circuits and Four-Terminal Parameters of High Frequency Transistors," *Paper of Technical Group on Transistor*, Feb. 1960.

(5) M. Hirai and S. Kawaguchi: "Measurement of Complex Four-Terminal Parameters of High Frequency Transistor," *Paper of Technical Group on Transistor*, Nov. 1959.

(6) S. Yoshida, S. Kawaguchi, M. Hirai, and T. Koshio: "Characteristics of Alloyed High Frequency Transistor by way of Trial", *Transactions of the 1959 Joint Convention of the Four Electrical Institutes of Japan*, p. 945.

(7) S. Kawaguchi, and M. Hirai: "High Frequency Equivalent Circuit of Transistor", *The 1959 National Convention Record of the I.E.C.E. Jap.*, p. 329.

(8) S. Yoshida and T. Koshio: "High Frequency Alloyed Transistor", *Internal Report (Seika-Hokoku) of the Electr. Comm. Lab. N.T.T.*, No. 1354, 1960-2.

*　*　*　*

REVIEW OF THE ELECTRICAL COMMUNICATION LABORATORY
VOLUME 9, NUMBERS 11-12, NOVEMBER-DECEMBER 1961

U.D.C. 621. 391. 812 : 551. 593] : 621. 371. 029. 63

Microwave Propagation Test in Mirage District*

Shigetaka UGAI†, *Yoshiie KANEDA*‡, and *Tadashi AMEKURA*‡

This paper deals with countermeasures against fading phenomena and also with the results of field tests held to examine the causes of fading.

The tests were carried out in the circuit between Toyama and Asahi running along the seaside of Toyama Bay, where mirages frequently occur; and the characteristics of both frequency and space diversity against deep fadings have been clarified by comparison tests.

A space diversity system provides more effective relief, and particularly it was confirmed that deep fadings have been relieved more effectively under the system where the radio frequency outputs of two antennas are combined in the same phase.

As the fadings occurred more frequently than expected, the observation of mirages and radio ducts as well as the measurement of general factors of radio meteorology have been carried out midway on the radio wave route to examine the causes of these deep fadings, thus clarifying the general character of heavy fadings.

1. Introduction

In this propagation test, importance has been attached to the fact that the fadings, which occurred on the *Hokuriku* microwave circuit route in May 1958, proved to be much heavier than expected. Thus, major efforts have been made on the examination of the experimental relief measures against these intense fading phenomena; of whether the phenomena were characteristic of the mirage district; whether they were due to specific meteorological conditions connected with the mirage district; and the cause, if such characteristics existed. In other words, tests were made on the relief measures on the one hand, and fundamental experiments have been made, on the other, whereby clues might be obtained to the variation characteristics and generation structure of fadings. That is, not only the observation of radio ducts but also measurements of the temperature of sea-water, the atmospheric temperature, the direction and velocity of wind and general meteorological factors, have been conducted.

As the test results have been examined, their relation to mirage phenomena characteristic of the district have gradually been clarified. Furthermore, the fact has been brought to light that the causes of the heavy fadings in this circuit, contrary to expectation, have been deeply related to the larger scale of meteorological phenomena—the generation condition and characteristics of various air masses.

2. Test Plan and Process

The test circuit was taken from the span between Toyama and Asahi, where fadings frequently took place. The reason is that unexpectedly heavy fadings have been found in spring and they were presumed to be closely connected with meteorological conditions, (generation condition of mirage phenomena). Also, it is thought that the meteorological conditions are in general characteristic of the areas along the Japan Sea. Furthermore, the span selected for the test was considered most

---

* MS in Japanese received by the Electrical Communication Laboratory, on August 10, 1960. Originally published in the *Kenkyu Zituyôka Hôkoku* (*Electrical Communication Laboratory Technical Journal*), N.T.T., Vol. 10, No. 2, pp. 155–191, 1961.

† Assistant Chief, Radio-Wave Propagation Section.

‡ Radio-Wave Propagation Section.

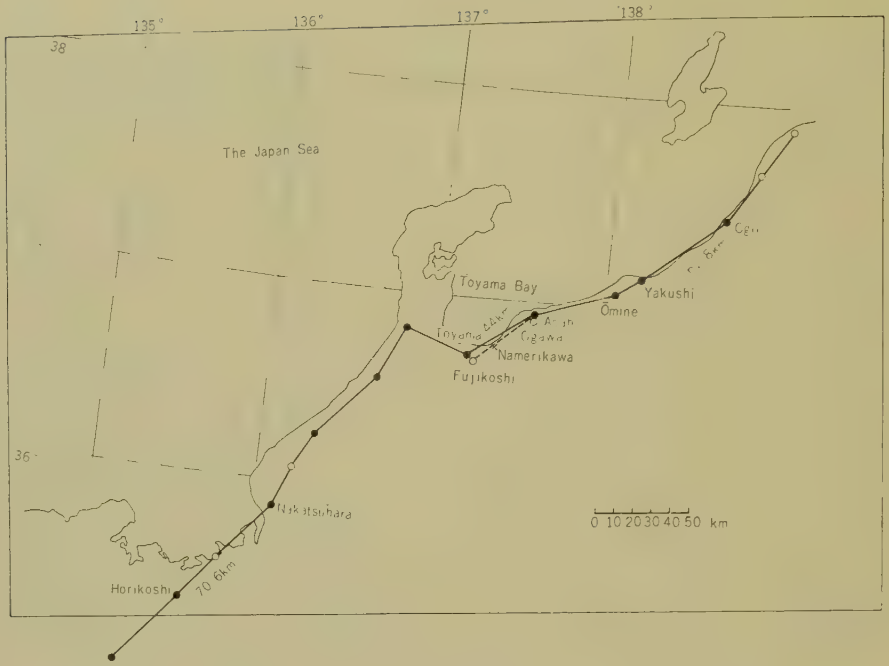

Fig. 1—Microwave relay route along the Japan Sea coast.

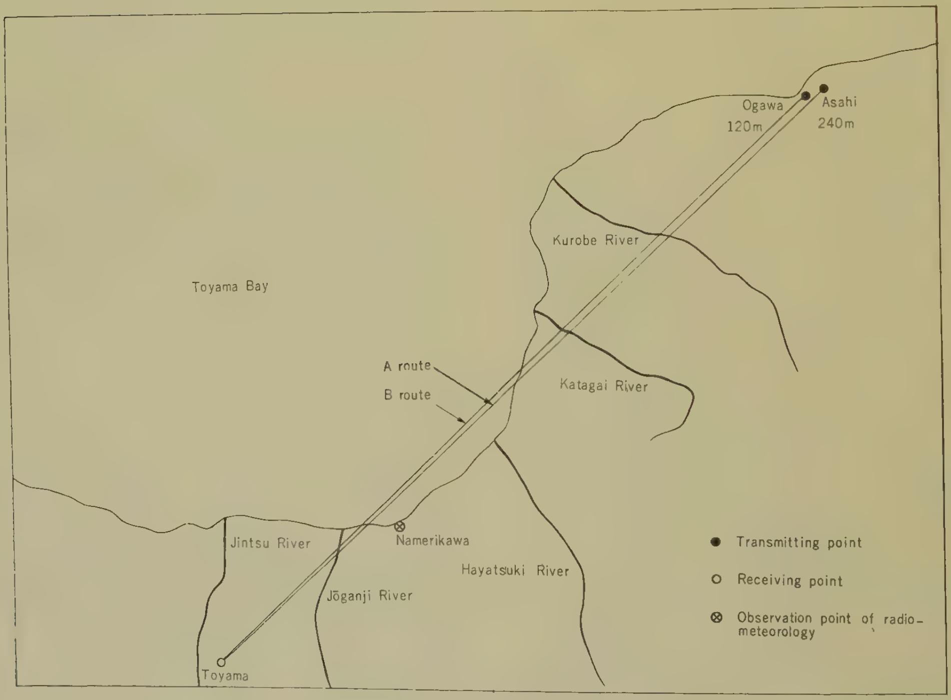

Fig. 2—Plan of test circuits between Toyama and Asahi.

liable to have mirages; to be most affected, and to suffer from heavy fadings.

2.1. Test Circuit

Fig. 1 is a plane topographical map showing the microwave relay route in the areas along the Japan Sea, including the Toyama–Asahi span. Fig. 2 shows the plan of the test circuits, and Fig. 3 the profiles of the propagation paths. Fig. 3 shows the relation of antenna locations at Asahi, Ogawa, and Toyama. Route A is the profile of the active microwave (4000 Mc) relay route on which various tests were carried out to actually relieve fading, and Route B is the profile of the experimental circuit. For the two routes fadings were compared concerning the effects of mirage, effects of inclination in the propagation route, and effects of topography upon fading.

2.2. Term of Tests

The tests were carried out for fading relief and also for investigation of fading characteristics of the district. The tests were carried out during the summer (Aug. 1958), when fadings took place most frequently, and during the mirage season (May 1959).

Radio meteorological observations were simultaneously carried out during the above period. Furthermore, propagation tests have been continued for long term investigation over the period of one year between the above two periods, to ascertain whether fadings in the district were different from these characteristics as observed in the Pacific side of Japan in the past.

2.3. Test Process

2.3.1. Test Process of Reduction of Fading

Fig. 4 shows the arrangement of frequency diversity effect measuring apparatus installed in August 1958 on the roof of the Toyama Toll Office Building for 4000 Mc and three other frequencies. (1500 Mc, 6720 Mc, and

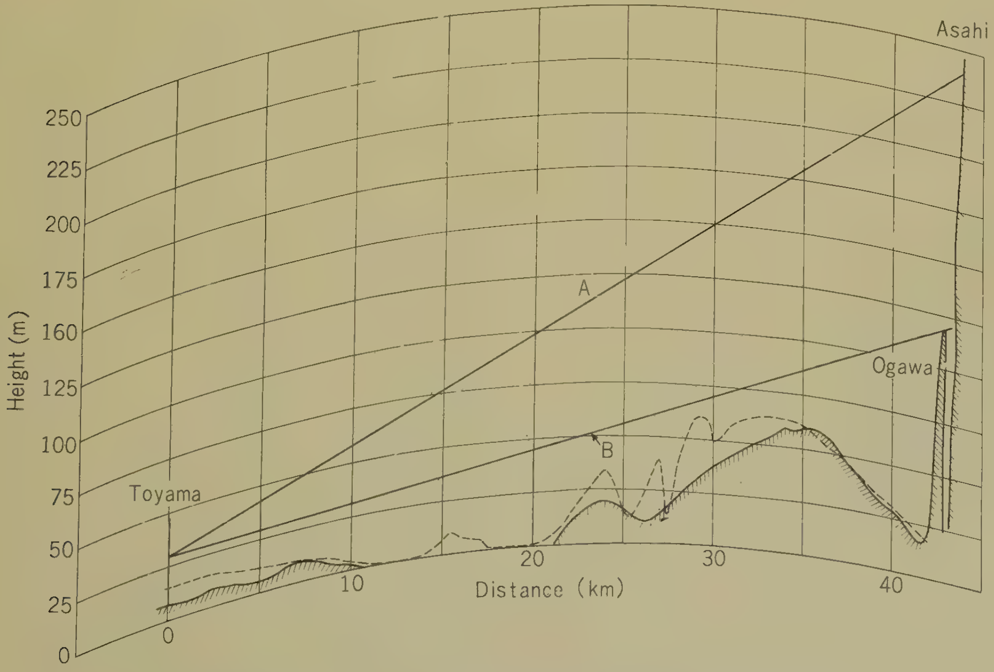

Fig. 3—Profile of test circuit between Toyama and Asahi.

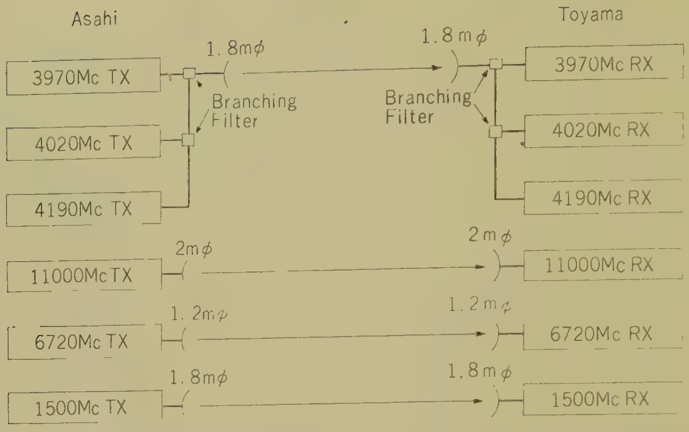

Fig. 4—Arrangement of frequency diversity effect measuring apparatus. (The letter, ϕ shows diameter of antenna)

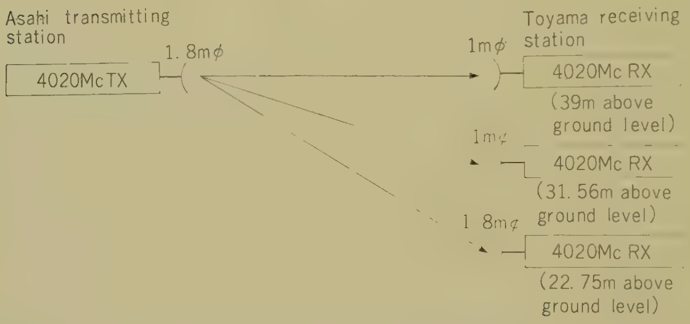

Fig. 5 (a)—Arrangement of space diversity effect measuring apparatus.

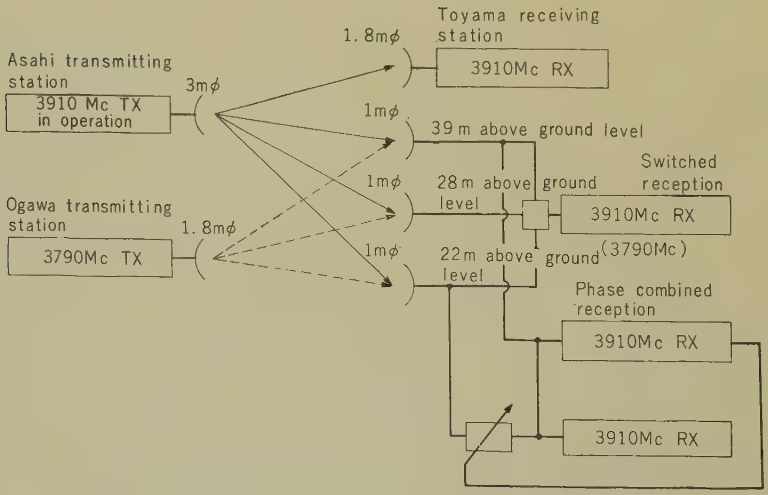

Fig. 5 (b)—Arrangement of space diversity effect measuring apparatus.

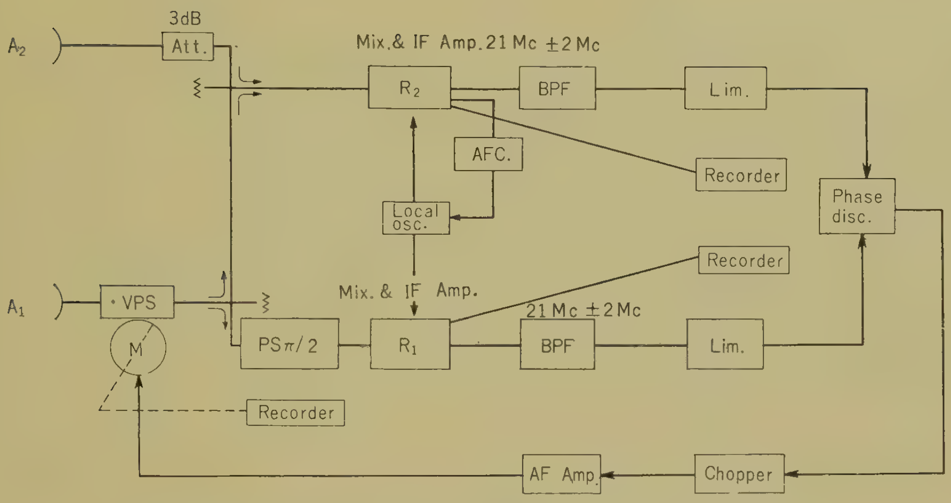

Fig. 6—Block diagram of combined-phase receiving system.

11000 Mc). Fig. 5 (a) shows the arrangement of antennas for measuring space diversity effec tduring Aug. 1958, and Fig. 5 (b) that during May 1959. Fig. 6 shows block diagram of the receiving system to combine the outputs of two antennas in the same phase by utilizing space diversity effects.

In this system was used an endless phase shifter, VPS which is fitted in a circular waveguide, with a half wavelength plate of dielectric material, so as to make it revolve around the axis of the waveguide. This rotating phase shifter can be controlled by a motor M, which is driven by the output voltage obtained by phase discrimination of the phase difference between outputs of receivers R_1 and R_2 in Fig. 6.

Fig. 7 shows the phase relationship of received signals from antennas A_1 and A_2 shown in Fig. 6. Vector $\overrightarrow{OA_1}$ corresponds to the output of antenna A_1, and $\overrightarrow{OA_2}$ to the combined output of A_1 and A_2. Vectors $\overrightarrow{OB}$ and $\overrightarrow{OC}$ correspond to the output of A_1 with phases shifted by $\pi/2$ relative to the vector $\overrightarrow{OA_1}$. It is arranged that the signals from A_1 and A_2 may be added in the same phase by revolving the variable phase shifter which is controlled by dicriminating the difference between the phase angles, $\angle A_2OB$ and $\angle A_2OC$.

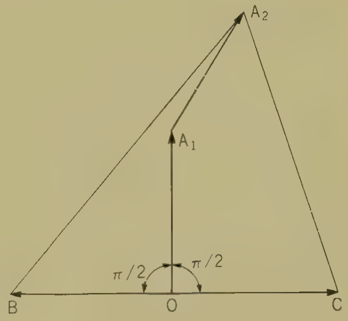

Fig. 7—Vector diagram showing the phase of combined receiving signal.

2.3.2. Measurement of Fading Characteristics and Radio Meteorology

In order to obtain fading characteristics of various wavelengths, fadings were measured for four frequencies (1500 Mc, 4000 Mc, 6700 Mc, and 11000 Mc) in August 1958 and May 1959; and for three frequencies (1500 Mc, 4000 Mc, and 6700 Mc) from September 1958 to May 1959, respectively.

Observation of radio duct was made at Namerikawa Seaside where mirages are likely to occur.

In measuring atmospheric duct, a pair of dry and wet thermistors were used and a pair of thermistors were placed in a shelter hung from a balloon. The M-protile was obtained by raising and lowering balloon from the surface up to about 300 m above the ground. To maintain standard ventilation in the shelter an electric fan driven by batteries was used.

Fig. 8 shows the actual arrangement for radio meteorological observation. Atmospheric temperature and humidity were recorded in the testing room on the ground by measuring electric resistance variation of the thermistors calibrated to read temperature in degrees centigrade.

Also to measure movements of temperature and humidity inversion layer near the ground surface, a tree about 20 m high on the coast was used, and Agari-type remote measuring thermometers were set on the tree at heights of 1.5 m, 5 m, 10 m, 15 m and 20 m above the ground. The sea water temperature at 1 m below surface was also measured. Furthermore, the direction and velocity of the wind at a point 7 m above the ground were recorded by a Skyvane.

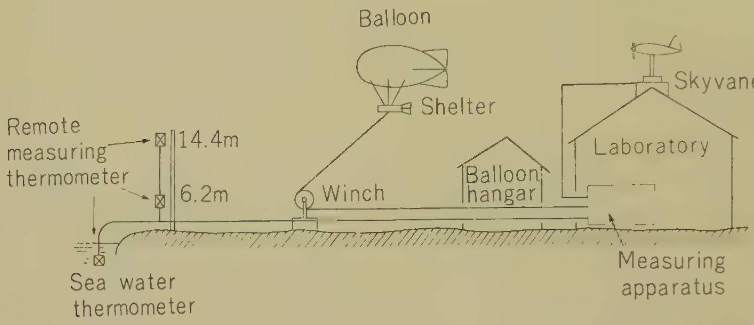

Fig. 8—Arrangement of radio meteorology observation apparatus.

3. Results of Fading Reduction Test

3.1. Deep Fading to be Relieved

During observations of this circuit in the summer lasting about one month, the fadings were moderate and not so heavy as to require relief.

During about one month in late spring, however, the fading took place to a considerable extent and were frequent; therefore it was thought countermeasures were necessary to relieve communication troubles.

Examples of these fadings are shown in Figs. 9 and 10, where the fading range is represented by maximum variation amplitude (dB value) of received power every hour. In Fig. 11 is shown an example of a variation mode of deep fadings which took place on May 27 and June 3.

The above are the outlines of deep fadings requiring relief during the test period. The causes of these fadings are considered in connection with meteorology in Section 4.

3.2. Diversity Characteristics

To relieve deep fadings liable to occur on the microwave circuit diversity receiving systems are commonly used at present.

Diversity effects are roughly classified into three types:

(1) Frequency diversity effect
(2) Space 〃 〃
(3) Arrival angular 〃 〃

A system which uses arrival angular diversity is not considered advantageous except at extremely high frequencies, because sharp directivity to separate arrival angles is required. In a 4000 Mc relay circuit, equipment utilizing effects (1) and (2) is more easily realized and more suitable.

Thus, in the diversity experiments, a test plan was undertaken on both frequency and

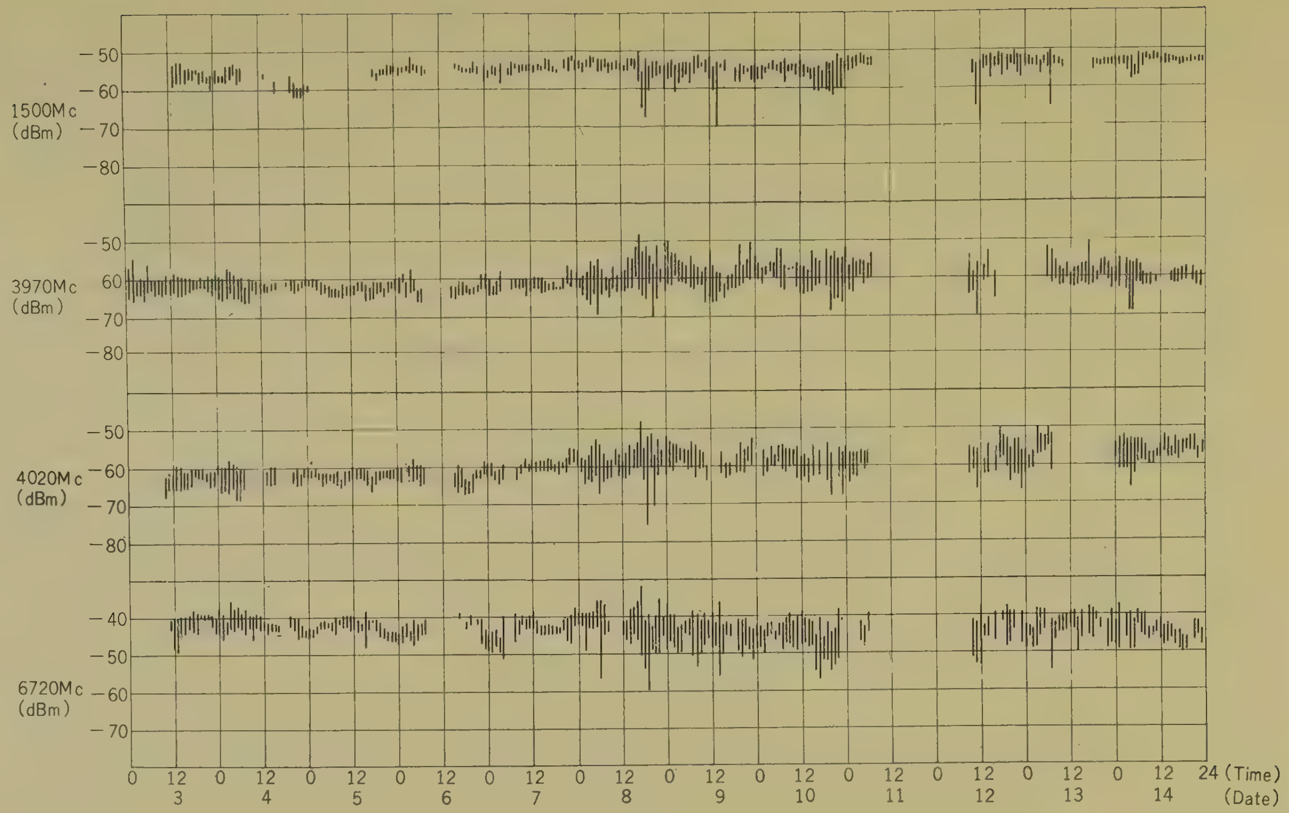

Fig. 9 (a)—Hourly fading variations (Asahi–Toyama; May 11–22, 1960).

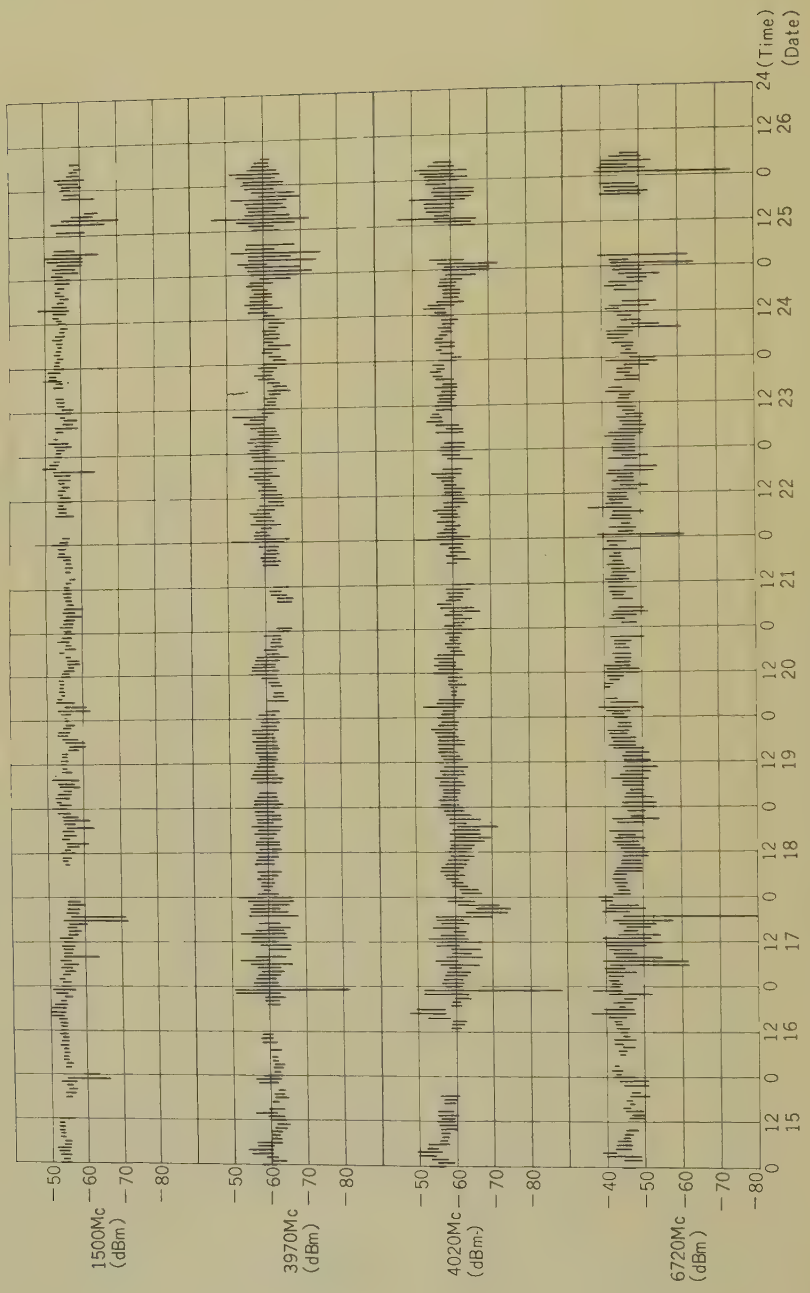

Fig. 9 (b)—Hourly fading variations (Asahi–Toyama; May 23–June 3, 1959).

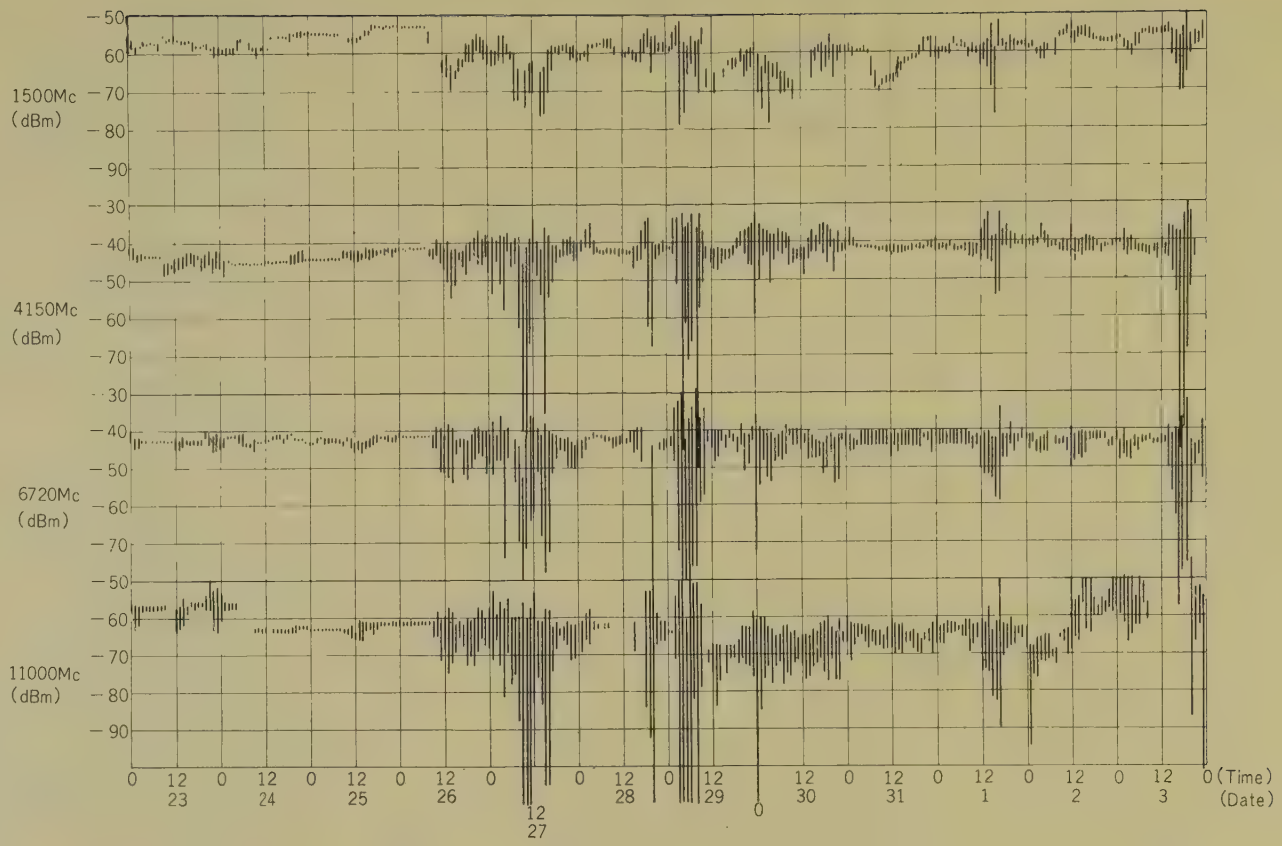

Fig. 10 (a)—Hourly fading variations (Asahi–Toyama; Aug. 3–14, 1958).

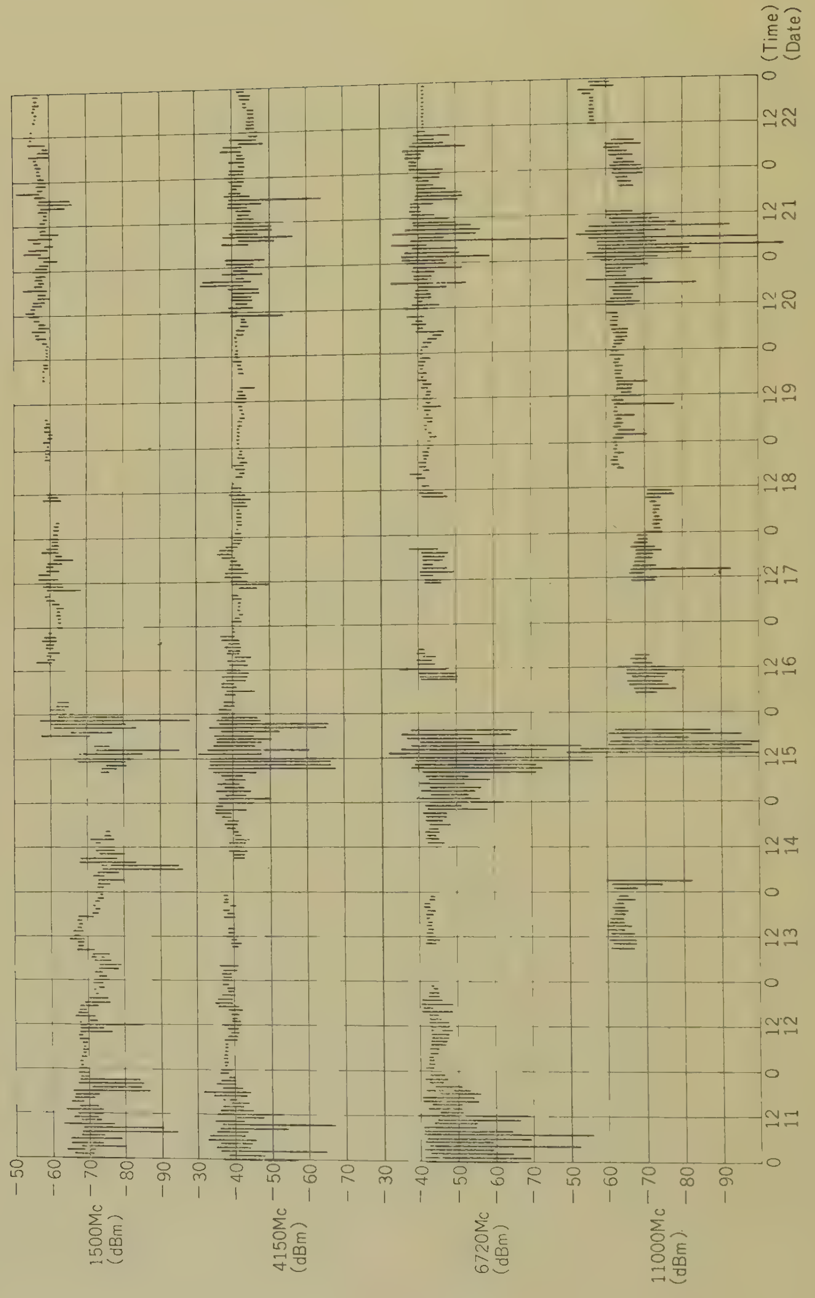

Fig. 10 (b)—Hourly fading variations (Asahi–Toyama; Aug. 15–26, 1958).

space diversity in order to obtain fundamental data on diversity effects in summer. From the consideration of the fundamental frequency diversity test results, a space diversity experiment was carried out the following spring.

3.2.1. Frequency Diversity Characteristics

Signal amplitude and simultaneity of fading depending on frequency are considered important in diversity characteristics. Therefore for three frequencies (3910 Mc, 4020 Mc, and 4190 Mc) the received outputs were recorded by a pen writing oscillograph so as to be able to compare the structures of fadings in detail by using three antennas connected to channel filters as shown in Fig. 4. Results of observations of frequency diversity characteristics in the 4000 Mc band will be

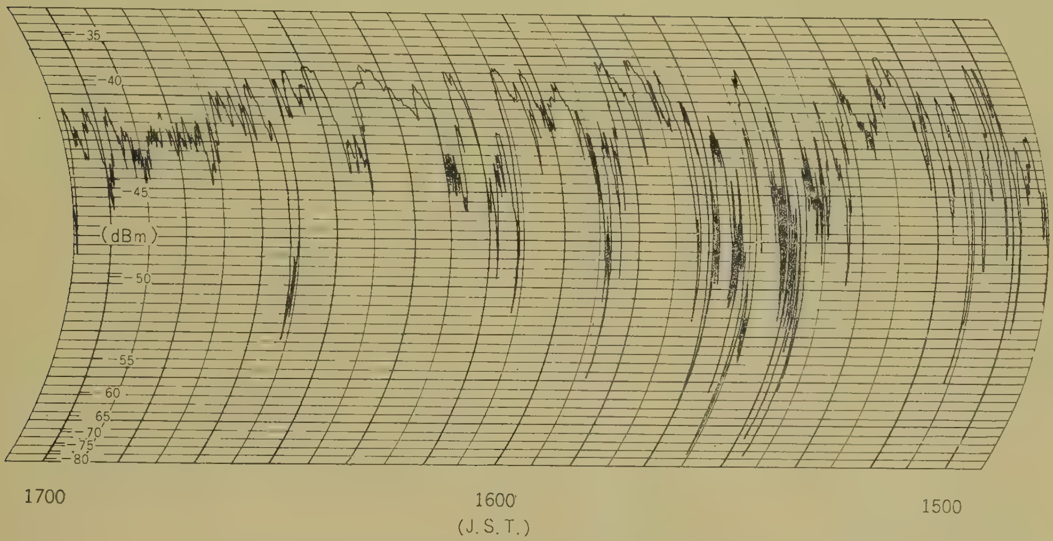

Fig. 11 (a)—Examples of deep fading at 4150 Mc on May 27, 1959.

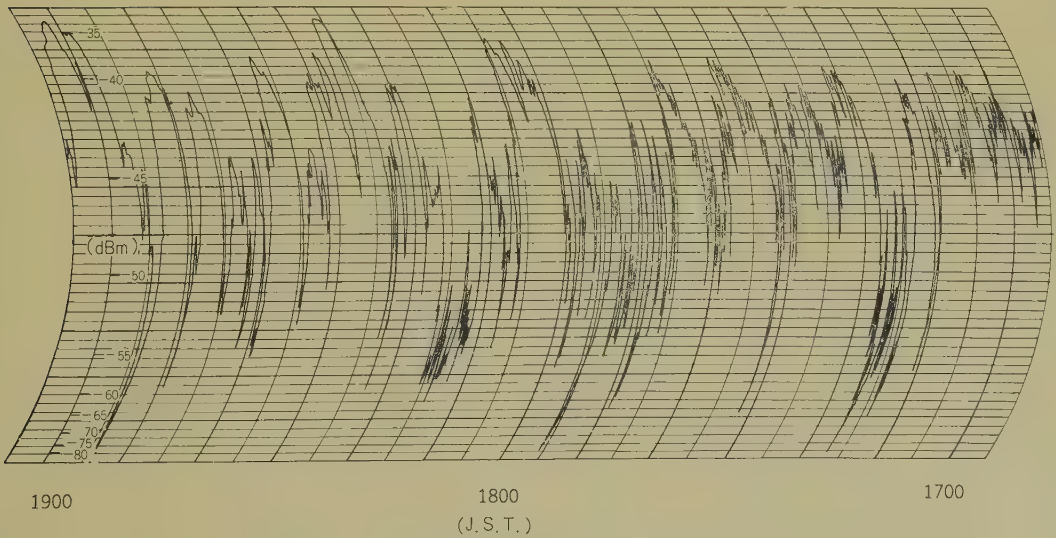

Fig. 11 (b)—Examples of deep fading at 4150 Mc on June 3, 1959.

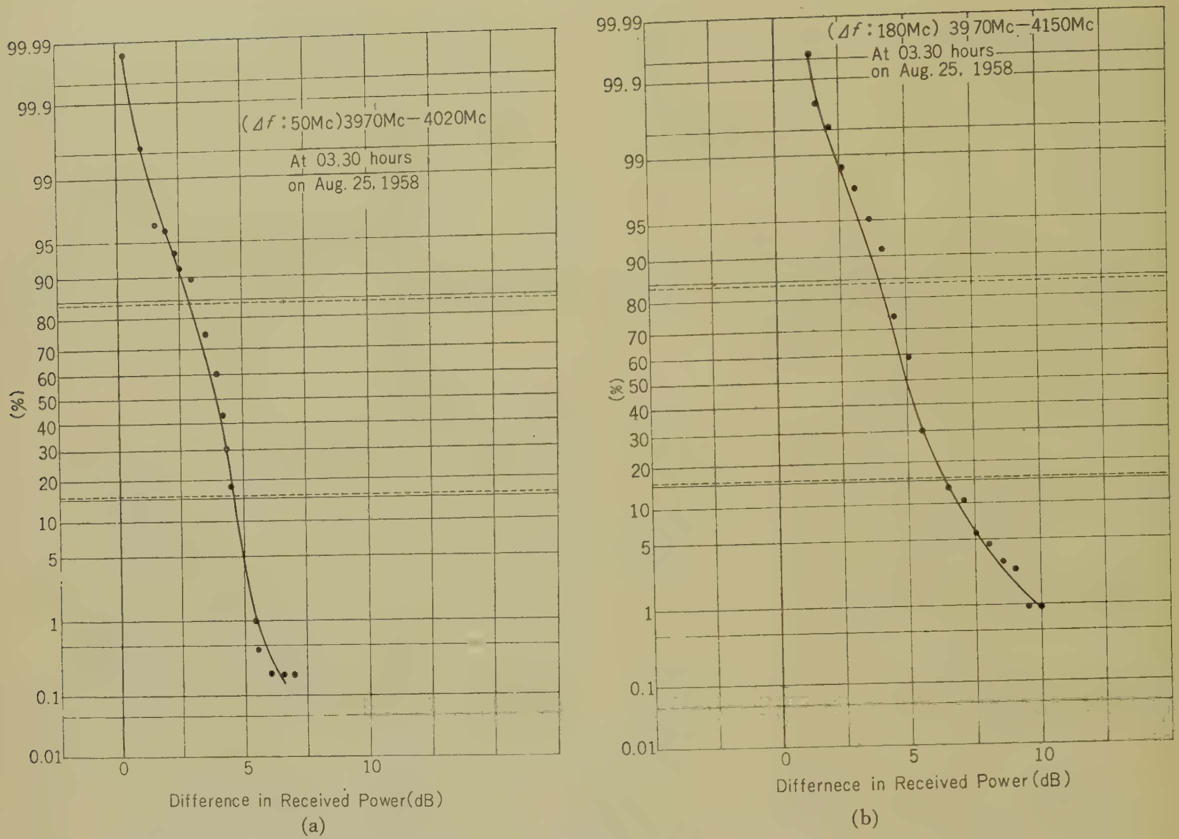

Fig. 12 (a) and **(b)**—Cumulative distribution curve of received power difference with frequency diversity.

given here. The time during which one wave faded out more than −10 dB from its free space value was determined from the fading record on the day when deep fadings took place. Fig. 12 shows an example of cumulative distribution of the difference of power between received powers at these frequencies. In Fig. 13 is given a cumulative distribution curve obtained from space diversity measurement on the same antenna condition. These examples correspond to cumulative distributions of received power for the case where ideal switching diversity reception is made when the switching level is set at −10 dB. It further shows that deep fade-out is statistically improved. DB values for the 1 %-99 % range of cumulative distributions are given in Table 1. It means that the greater these values are, the more improvement is obtained. The

Table 1

AN EXAMPLE OF FADING RANGE DURING SWITCHED RECEPTION

Item	1 %~99%
Difference in frequency (Δf)	
50 Mc	4 dB
180 Mc	7 dB
Difference in height of antennas (Δh)	
6.94 m	25 dB
9.31 m	26 dB
16.25 m	29 dB

improvement is a little greater for frequency separation $\Delta f=180$ Mc than for $\Delta f=50$ Mc. For this order of frequency separation simultaneous fadings still occurred and large improvement from frequency diversity is not expected. As will be seen from Table 1, space diversity is considered more effective than frequency diversity.

3.2.2. Space Diversity Characteristics

For the measurement of space diversity effect, was used a waveguide switch made of ferrite. As shown in Fig. 14, this switch was used in order to compare the outputs of three antennas, with particularly high accuracy. The outputs of these antennas were fed to a receiver through the waveguide switches and the output was recorded on each channel of a three-channel pen writing oscillograph by switching.

On the day when the heaviest fading occurred instantaneous values of received power for every ten seconds for the worst one hour were chosen and correlation diagrams of the received power were obtained for three pairs of two antennas, with heights of 3 m • 9 m, 3 m • 20 m, and 9 m • 20 m respectively as shown in Fig. 15. The spacing between antennas was 6 m, 17 m, and 11 m, respectively. From these figures, correlation coefficients obtained are given in Table 2 for each value of antenna spacings.

Fig. 16 shows examples which give movement of the points on the correlation diagram for a short period (several minutes). Arrow marks in the figure show direction of motion of the correlation.

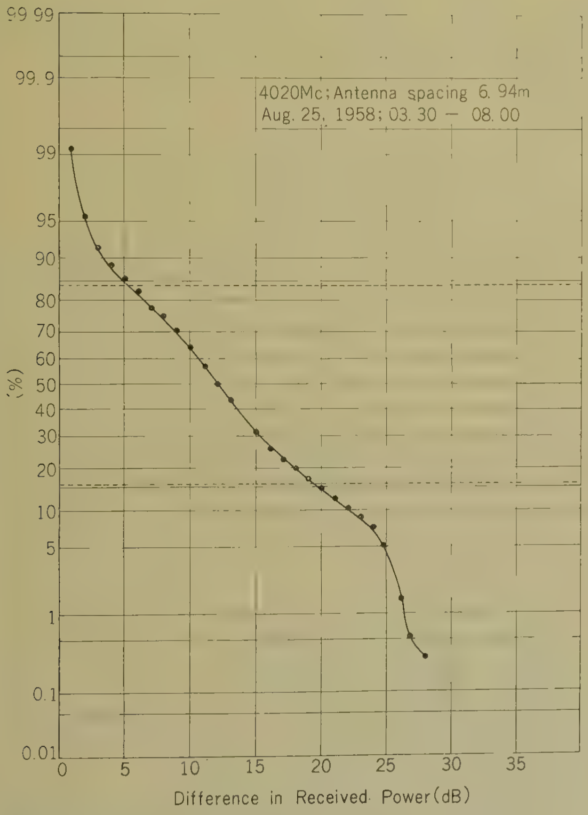

Fig. 13 (a)—Cumulative distribution of difference in received power (space diversity).

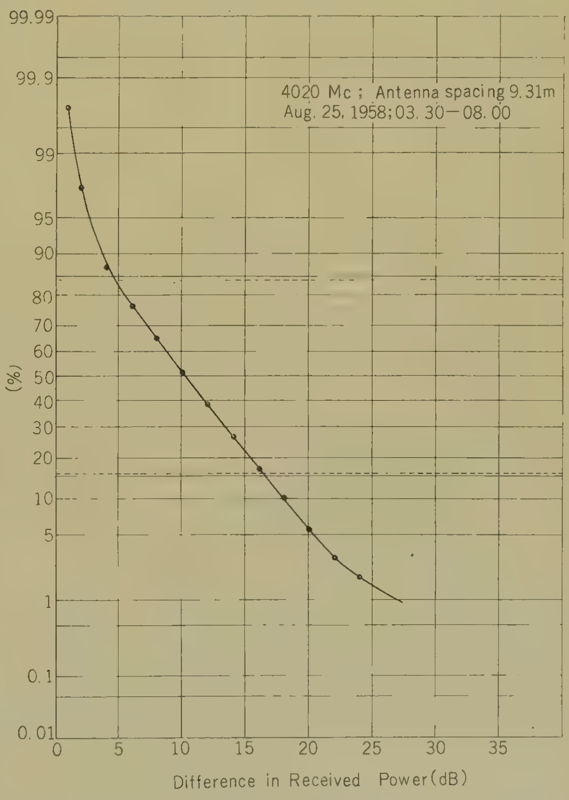

Fig. 13 (b)—Cumulative distribution of received power (space diversity).

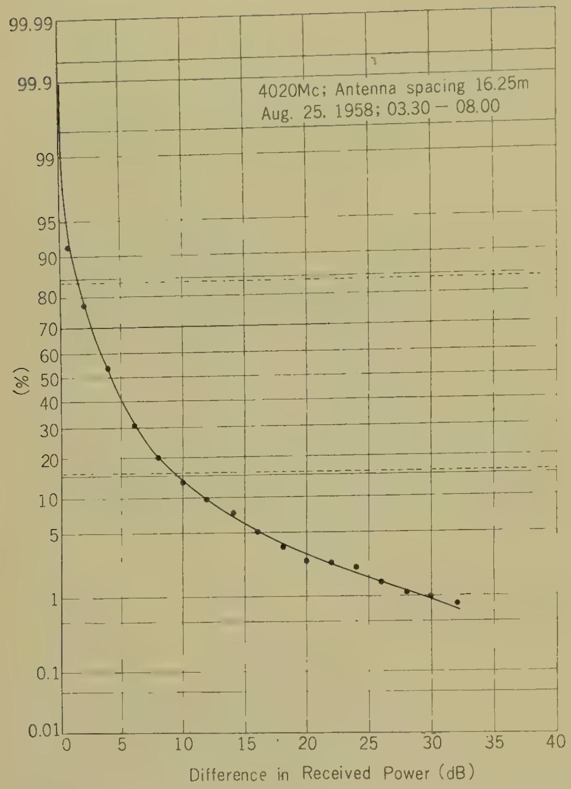

Fig. 13 (c)—Cumulative distribution of received power (space diversity).

Table 2

CORRELATION COEFFICIENT FOR EACH ANTENNA SPACING

Date	Spacing (in m)	Maximum & Minimum Value	Correlation Coefficient
Frequency : 3910 Mc			
May, 29, 1959	6	15～23 dB	−0. 39
〃	11	15～18 dB	0. 334
〃	17	15～23 dB	−0. 326
Frequency : 3790 Mc			
May, 27, 1959	6	21～19. 5 dB	−0. 306
〃	11	20～21 dB	0
〃	17	19～20 dB	0. 129

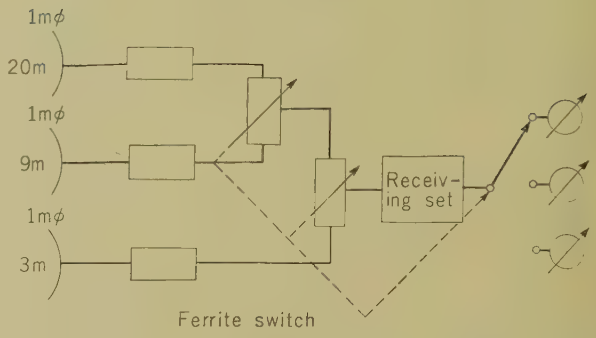

Fig. 14—Switched receiving system.

They show how correlation changes with time. During a short period, correlation exists, but for a long period (about one hour, for example) it disappears as will be understood from Fig. 15. From these data it is admitted that the diversity effect is greater for space diversity than for frequency diversity.

3.3. Results of Phase Controlled Diversity Reception

A phase controlled diversity system shown in Fig. 6 was used experimentally to relieve fading. Antennas were the same as those used for the space diversity measurement.

In Fig. 17 are shown the received signal variation during phase controlled diversity reception compared with the received signal variation during single antenna reception (non-diversity), and phase difference (in degrees). And also, in this figure are plotted the values of phase angle rotation necessary to be controlled in-phase (phase equalization).

This experiment was conducted for heavy fadings where the range between the maximum and the minimum signal during one hour was over 20 dB.

Fig. 18 shows an example of cumulative distribution curves of received power by single antenna reception (R_1) and by phase controlled diversity reception (R_2), for one hour during the day when strong fadings took place.

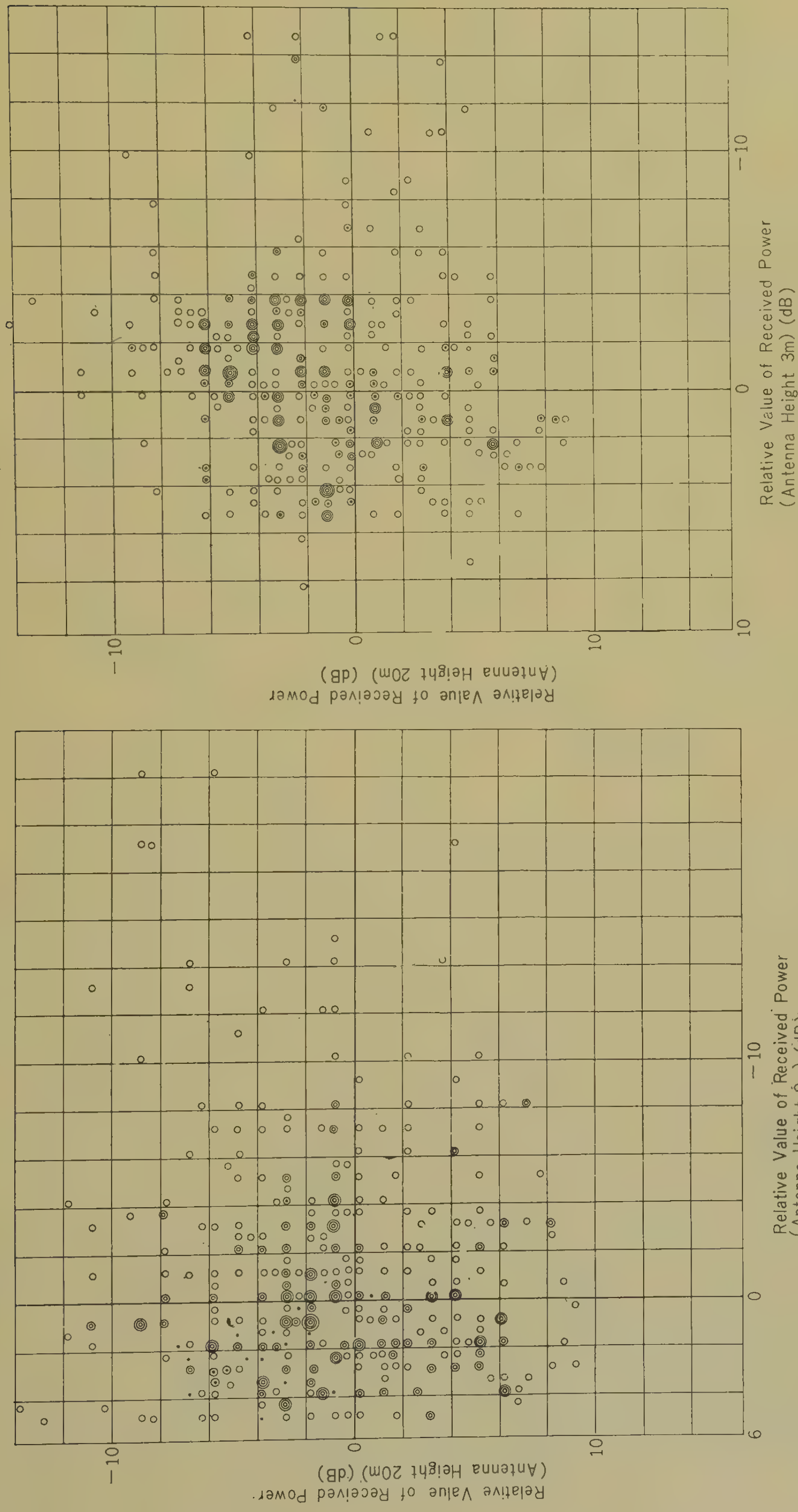

Circuit: Asahi-Ogawa 3790 Mc
May 27, 15–16 hrs.
Antenna heights; 9 m • 20 m

Circuit: Asahi-Ogawa 3790 Mc
May 27, 15–6 hrs.
Antenna heights; 3 m • 20 m

Fig. 15—Spacing correlation diagram (Unit: Correlation value dB).

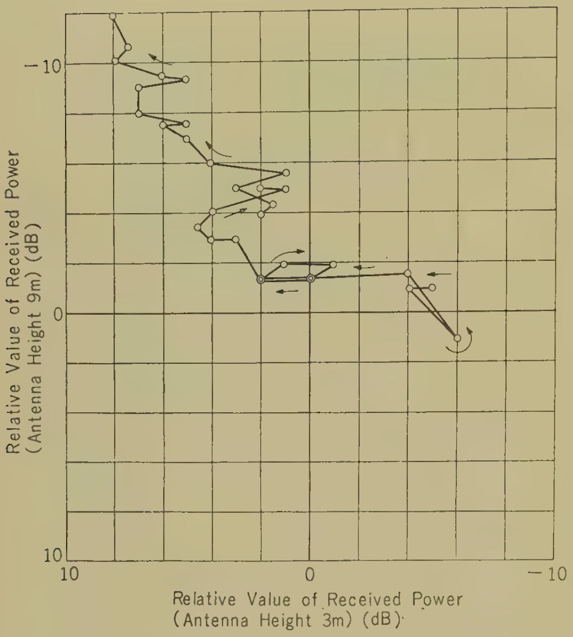

Fig. 16 (**a**)—Example of space correlation for short period.

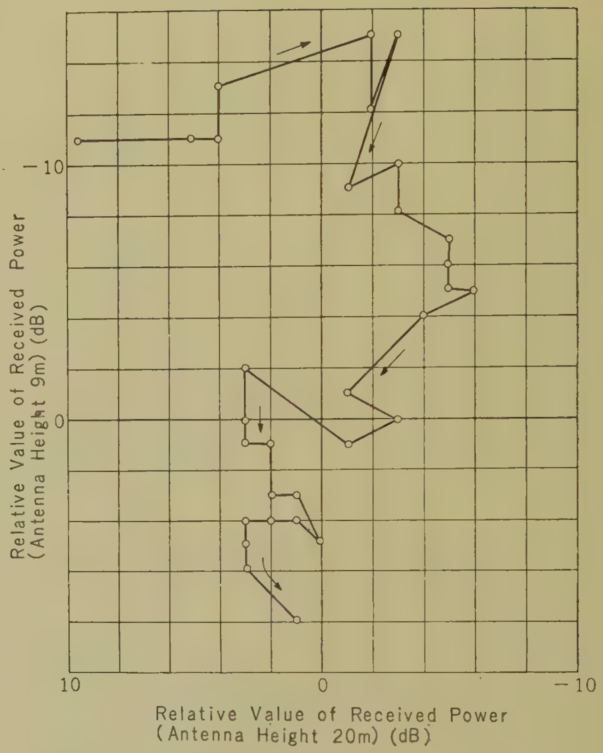

Fig. 16 (**c**)—Example of space correlation for short period.

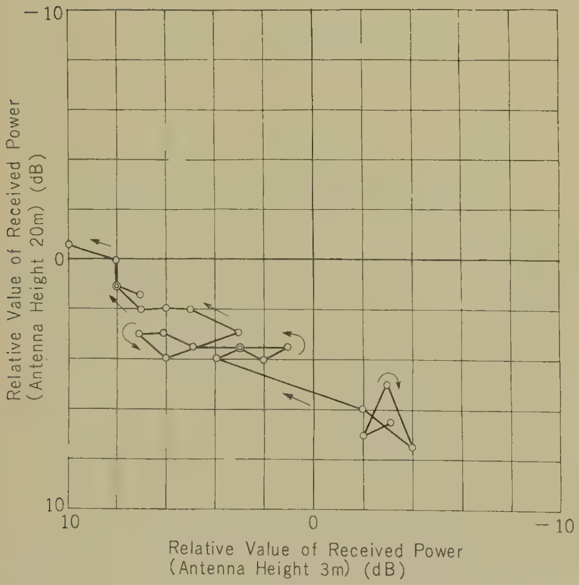

Fig. 16 (**b**)—Example of space correlation for short period.

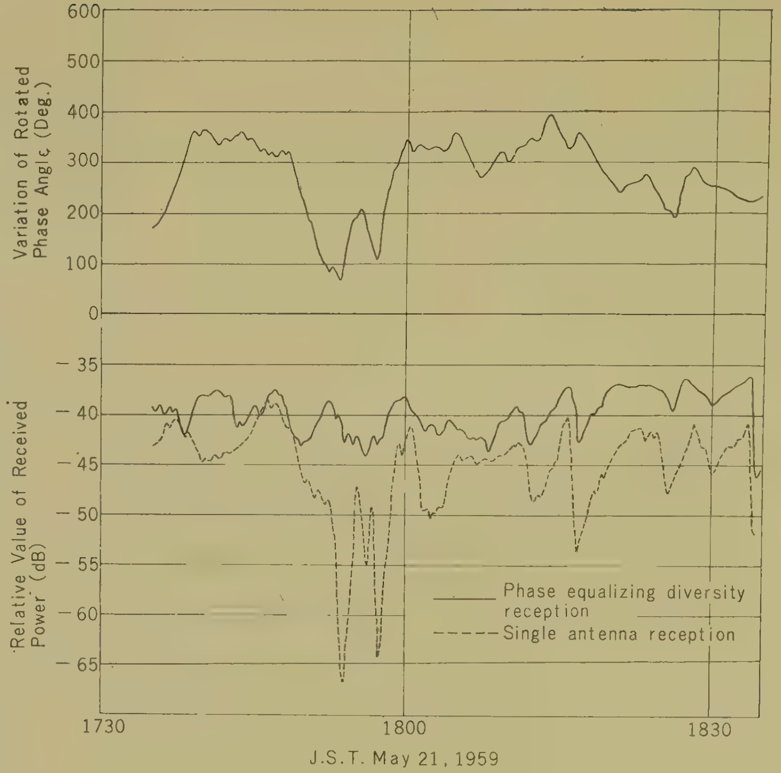

Fig. 17—Examples of received single variation in comparison between single antenna reception and phase equalizing diversity reception.

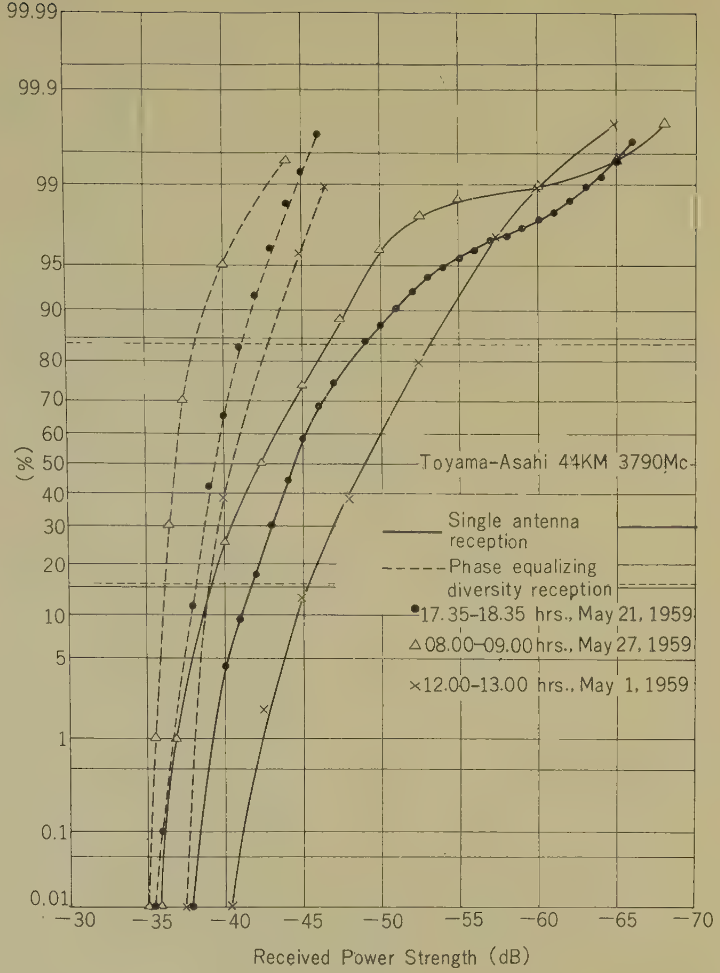

Fig. 18—Cumulative distribution curves of received power by phase diversity reception and single antenna reception.

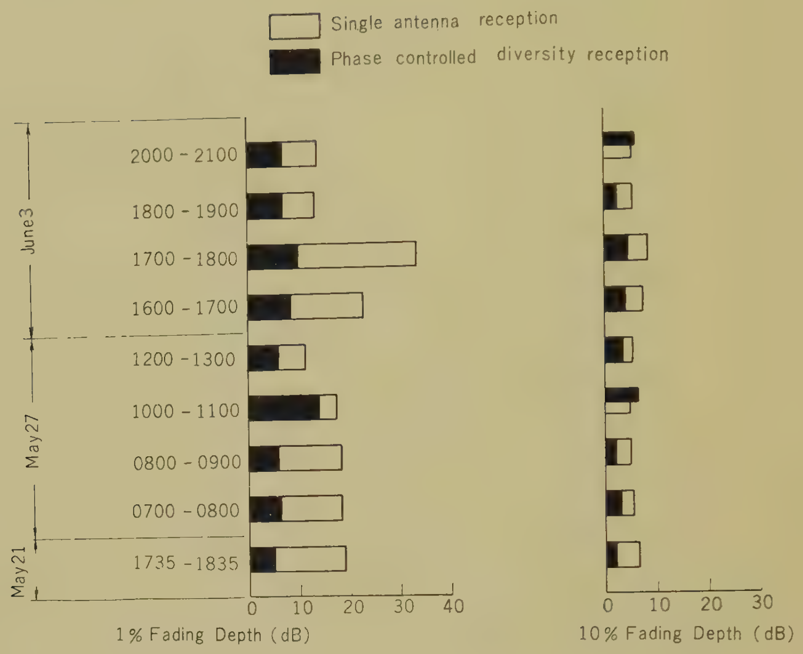

Fig.19—Improvement effect of fading relief.

In Fig. 19 is shown fading relief given by the diversity reception. As will be seen from these examples, large improvement is not always expected from diversity reception, but generally speaking, considerable improvement is recognized by this diversity reception for deep fading.

3.4. Variation of Rotated Phase for Equalization

It depends upon the rotation time constant of equalizing phase shifter following fading speeds whether phase aqualizing diversity reception acts effectively or not. Thus it is necessary for the designing of this system to know the magnitude of variation of phase angle and its velocity for rapid and deep fadings.

In Fig. 20 are shown examples of cumulative probability distribution curve of the magnitude of controlled phase angles produced by strong fading during one hour. It is readily seen from the figure how greatly it changes.

Fig. 21 shows cumulative distribution curve of phase angular shifting velocity for the worst hour in the day when the strongest fading took place. In this analysis, the phase angular shifting velocity was taken as the magnitude of phase angle shifted per second. It is shown that the distribution is almost log-normal distribution.

Phase angular velocity is about 0.6 degrees per second at 50 % of time (median value), about 3 degrees per second at 10 %, and nearly 10 degrees per second extrapolated at 1 % and it was found quite possible to design to make following the phase angular variation of general fadings.

From these results, phase equalizing diversi-

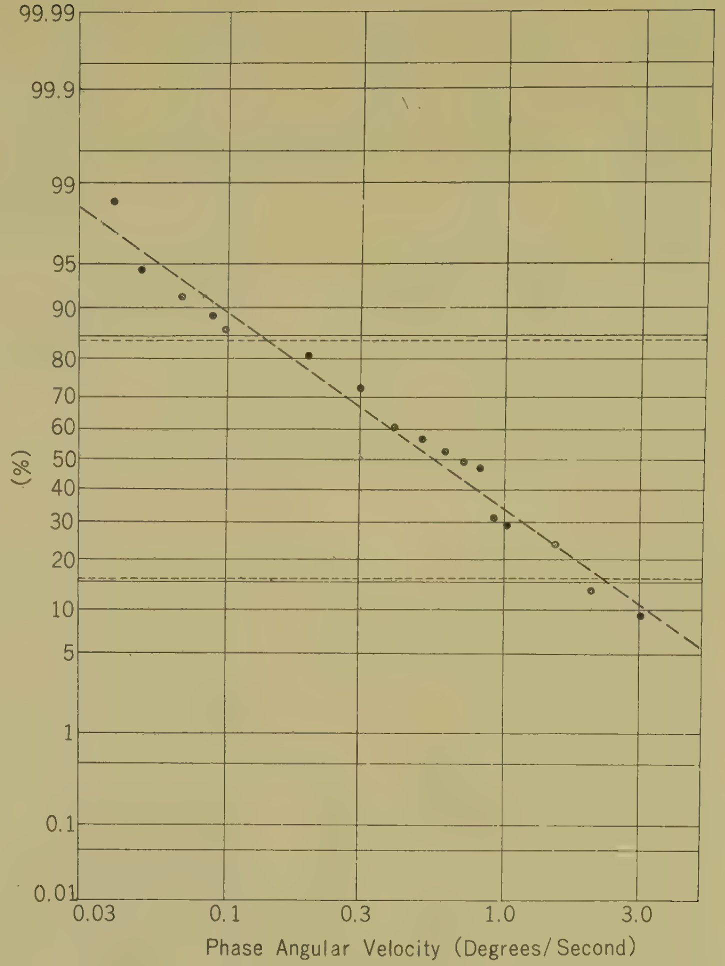

Fig. 20—Cumulative distribution curve of the magnitude of phase angles in the one worst hour.

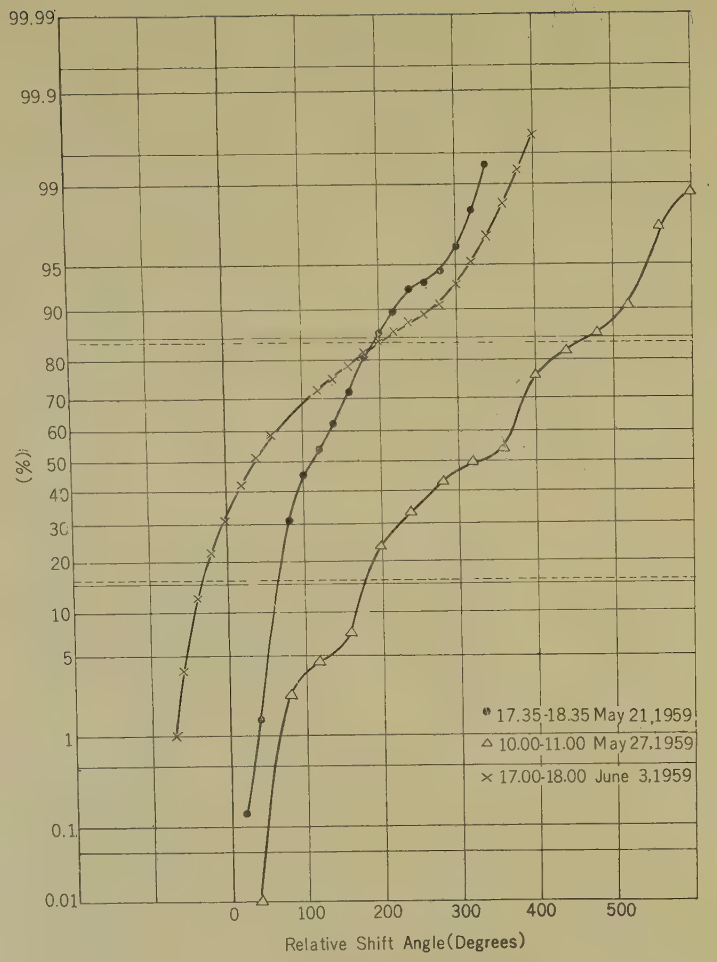

Fig. 21—Phase angular velocity distribution for one hour during the worst day (May 27, 1959).

ty reception is found considerably effective as a relief measure againt strong fading. As has already been stated, however, the deep fadings were not always relieved. As the so-called long term fanding usually has not space selectivity nor frequency selectivity, special relief measures should be considered for this type of fading.

4. Fading Characteristics in the District

4.1. Outline of Fading Characteristics

4.1.1. Features of Fading Characteristics

The calculated ground reflection point on the Asahi–Toyama circuit is located 7.7 km from the antenna at Toyama in standard atmosphere; the coast line is 10.5 km away from that at Toyama. Position of the reflection point with variation of *k* is limited to the range of 7 km to 9.5 km, if the value of *k* (equivalent earth radius factor) is varied from 2/3 to 2. Thus the reflection point is never liable to fall on the sea for actual changes of *k*.

Now a case will be considered where duct took place. Assuming that stratified ducts will form parallel to the earths surface, we classify them into surface and elevated ducts for convenience.

First, it is assumed that there is a surface duct and transmitting and receiving antennas are higher than the duct height. By the explanation in Fig. 22, the displacement of reflection point due to the surface duct newly produced in the uniform standard atmosphere $(dM/dh)_S$ can be calculated by considering that the surface is elevated by Δh in the $(dM/dh)_S$ atmosphere. And thereby the effect of surface duct formation on displacement of reflection point can be replaced, as shown in the figure. When transmitting and receiving antennas are at different heights, geometrical and optical calculation prove that the reflection point moves to the side of the lower antenna; in this case, to the side of Toyama.

Next a case may be considered where elevated duct is produced between the transmitting and receiving antenna heights as shown in Fig. 23. As seen from Fig. 23 the displacement of reflection point due to elevated duct may be considered as the location of the higher antenna being shifted by distance Δd. Thus, the reflection point moves closer to the lower antenna than when there was no duct.

Generally speaking, when duct takes place in part of such a uniform atmosphere, the average value of *k* is usually larger than that of *k* when there is no duct. Therefore the inclination in the change of *k* value generally corresponds to the above mentioned inclination in the displacement of reflection point.

As the measured values of the effective earth reflection coefficients on this circuit were 0.33 maximum, 0.14 minmum, and about

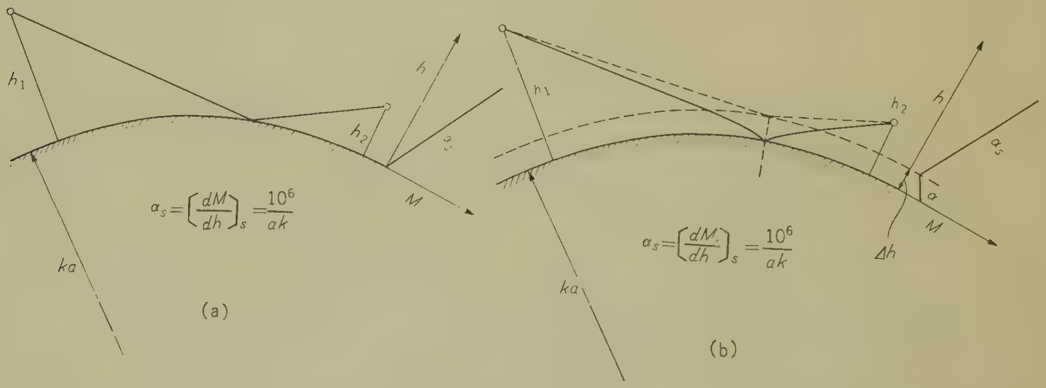
h_1
h_2
h
a_s
M
ka
$a_s = \left(\frac{dM}{dh}\right)_s = \frac{10^6}{ak}$
(a)
h_1
h_2
h
a_s
a
M
Δh
ka
$a_s = \left(\frac{dM}{dh}\right)_s = \frac{10^6}{ak}$
(b)

Fig.22—Explanation of displacement of reflection point due to surface duct.

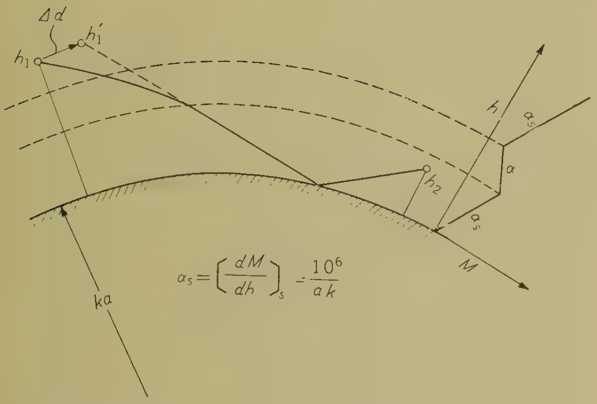

Fig. 23—Explanation of displacement of reflection point due to elevated duct.

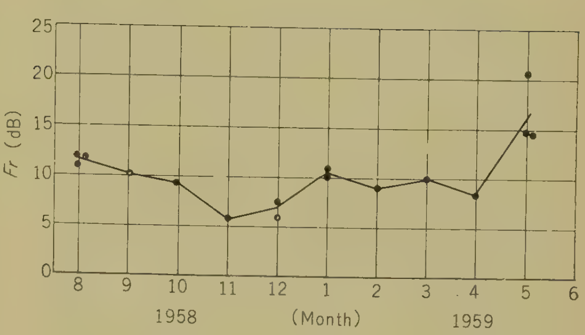

Fig. 24—Monthly variation of fading range.

0.25 average, the *k* type fading itself cannot become large enough. Therefore it is considered that deep fadings are due to radio ducts.

4.1.2. Feature of Seasonal Variation in Fading and its Relation to General Meteorology

Monthly variation characteristics of fading range during the test period are shown in Fig. 24. Measurements were carried out on three frequencies, 1500 Mc, 4000 Mc and 6700 Mc, for ten months during the period August 1958 to May 1959. As except in August and May measurements were carried out unattended, there were many hours of no measurement. In the figure fadings are shown for 4000 Mc for a month when the data had been collected for over 20 days of the month; frequencies were converted by the following formula:

$$F_{rf}=K\sqrt{1+0.28f} \qquad (1)$$

where $K=3.73\left\{\frac{\sigma_\alpha}{\langle\alpha\rangle}\right\}^{1/2} d^{0.53}\phi(h_t, h_r)$

and F_{rf} = Fading range (dB)

K = constant.

As there were few months when data on three frequencies were simultaneously obtained for more than twenty days of the month, it may not be said that monthly variation characteristics of fading have been sufficiently obtained. It may be considered, however, that the figure shows the actual tendency, as the calculated values of fading ranges approximately agree with each other.

The feature of seasonal changes during this term were that the maximum fading range occurring during this year took place in May and also that the fading range appearing in August was not so large, as it was expected to be the maximum for the year. This tendency in seasonal variation is considered to be quite different from that in other districts in Japan (where its variation range was usually maximum in summer, minimum in winter, and medium in spring and autumn). Whether this difference is a general charcteristic of this specific district, or weather it was due to abnormal meteorological conditions during the particular year will have to be examined by the observation of radio meteorology, surface weather charts, and aerological data.

At first the relation between daily variation of fading and that of synoptic weather will be compared with the weather charts for August. Early in August a line of discontinuity remained over Honshû, with inclement weather generally prevailing in the Hokuriku District, where no frequent fadings took place. At about the 7th of August a high atmospheric pressure over the Japan Sea developed, pushing southward, and further combined with that on the Sanriku Coast, thus making the weather fine. This weather pattern continued until about the 10th; during this period remarkable fadings took place. About the 11th of August the front moved to the Japan Sea from the west, and the high atmospheric pressure over the Sanriku Coast moved southward, and developed into a powerful Pacific Anticyclone but the front passed across Honshû, again on the 13th. On the 14th and 15th of August, the front remained over Honshû, with bad weather, and during this period no remarkable fadings appeared. From the 16th it moved northward and considerably strong fadings took place. During the 16th to 18th this area was covered by the Pacific high atmospheric pressure after the passing of the front. Passing Honshû on the 20th and 21st, the front remained near Honshû until the 23rd and advanced southward on the 24th, causing heavy rain on the north side of central area of Honshû. At night of the 21st, immediately after the passing of the front, strong fadings occurred. Approaching Honshû from the

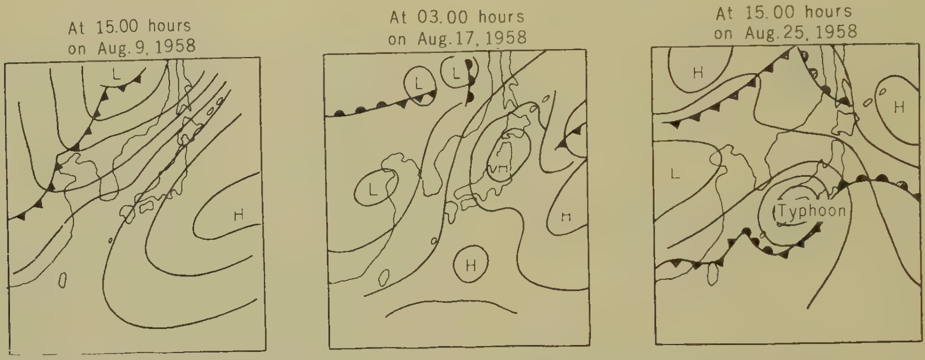
At 15.00 hours on Aug. 9, 1958

At 03.00 hours on Aug. 17, 1958

At 15.00 hours on Aug. 25, 1958

Fig. 25—Examples of weather charts on the days when strong fading occurred.

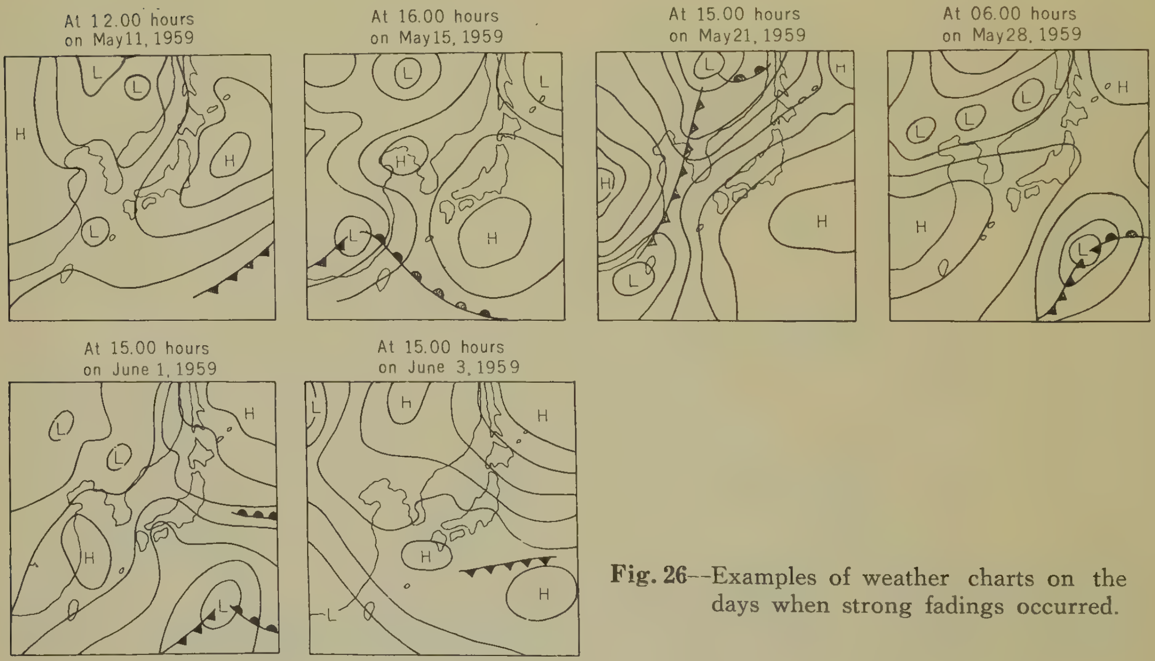
At 12.00 hours on May 11, 1959

At 16.00 hours on May 15, 1959

At 15.00 hours on May 21, 1959

At 06.00 hours on May 28, 1959

At 15.00 hours on June 1, 1959

At 15.00 hours on June 3, 1959

Fig. 26—Examples of weather charts on the days when strong fadings occurred.

south of Cape Ashizurimisaki on the 25th, Typhoon No. 17 passed the western part of Toyama Prefecture during the early morning of the 26th, degenerated into a tropical cyclone, and passed to the Tohoku District. Immediately before the passage of the cyclone through the eastern part of Toyama Prefecture, the north-eastern part of Honshû experienced temporary weather improvement, being located on the edge of the high atmospheric pressure region over the Sea of Okhotsk. At this time strong fadings occurred.

Fig. 25 shows examples of the pressure pattern on the days when strong fadings occurred. In August the weather was not good, generally speaking, with many rainy days. Thus less summery days than in an usual year were experienced. There were few such strong fadings as consequently fell down to the noise level, and thus the fading range seems to have been small.

Even during the test term of May strong fadings happened on May 11th, 15th, 20th–21st, 27th, 29th, and June 1st and 3rd, as shown in Fig. 10.

Fig. 26 consists of weather charts showing the pressure pattern on the days when strong fadings appeared in early summer.

Between the occurrence of three strong fadings and the general meteorological condition obtained from the weather charts is recognized the same relations as have been made clear in other districts.

From the barometric distribution on the days with such meteorological condition, it is found that the center of the high atmospheric pressure region generally exists over Pacific off the Sanriku Coast, with the propagation route on the back of the slow gradient of pressure on its western side.

4.2. Relation between Radio Meteorology and Fading

4.2.1. Results of Observation of Lower Duct

The general atmospheric condition during the summer month of August was already stated in the preceding paragraph; in general strong duct did not occur. From the 4th to 6th duct hardly occurred. From the early morning of the 7th, lower duct occurred, though with more or less development, until the early morning of the 11th. During this period remarkable fading appeared as has already been shown. On the 12th and later no steady strong ducts were observed, though some duct sometimes appeared. During the same period there were times when the atmospheric temperature deficit rate for height in daytime was small and less than standard. A condition for appearance of duct is remarkable temperature inversion at night. Decrease in humidity frequently appeared in the lower layer, usually of altitude lower than 100 m, and thus most of the ducts were surface ducts.

The surface duct usually observed on land has remarkable diurnal variation characteristics. In the present observation, on the contrary, no diurnal variation trend was observed

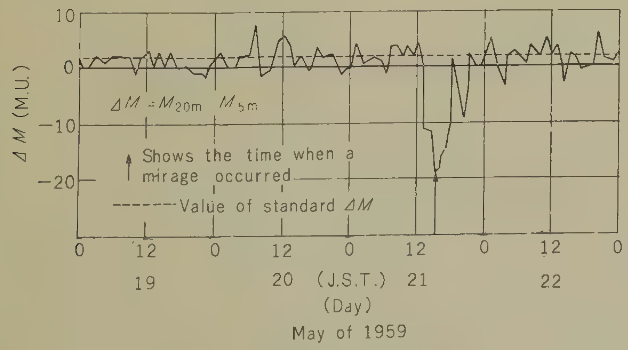

Fig. 27—Daily variation of modified index M gradient near the surface.

and distinctive surface duct has frequently occurred in the day time.

In the observation of lower duct in May, as in August, extremely good correspondence was observed between general atmospheric condition and the occurrence of duct. During this period surface ducts frequently occurred and those 50 m or less in altitude were mostly observed, with no fixed tendency of the time of occurrence. Lower surface ducts 20 m in altitude were almost continuously observed. Fig. 27 gives an example showing hourly change of ΔM, difference between the modified refractive index at 20 m altitude and that at 5 m on the coast of Namerikawa. It shows a perfect duct where the value of ΔM is negative. From 11.00 to 21.00 J.S.T. on the 21st extremely deep surface ducts were observed, particularly having developed into the deepest one at about 15.00 J.S.T., just when a mirage was observed.

Fig. 28 gives an example of lower duct observed from a balloon on May 21st. The figure shows profiles of spacial distribution of atmospheric temperature, humidity, and modified refractive index M on this day, compared with the occurrence of fadings in the 4000 Mc band (received at Toyama) at the same time. The two upper sections show spacial isopleth of atmospheric temperature and humidity observed nearly every hour; the third section is the profile of M. Symbol ● shows observed value when the balloon ascended and symbol ○ that when it descended. Inconsistency in values when it ascended and descended seems to be due to the change of atmospheric

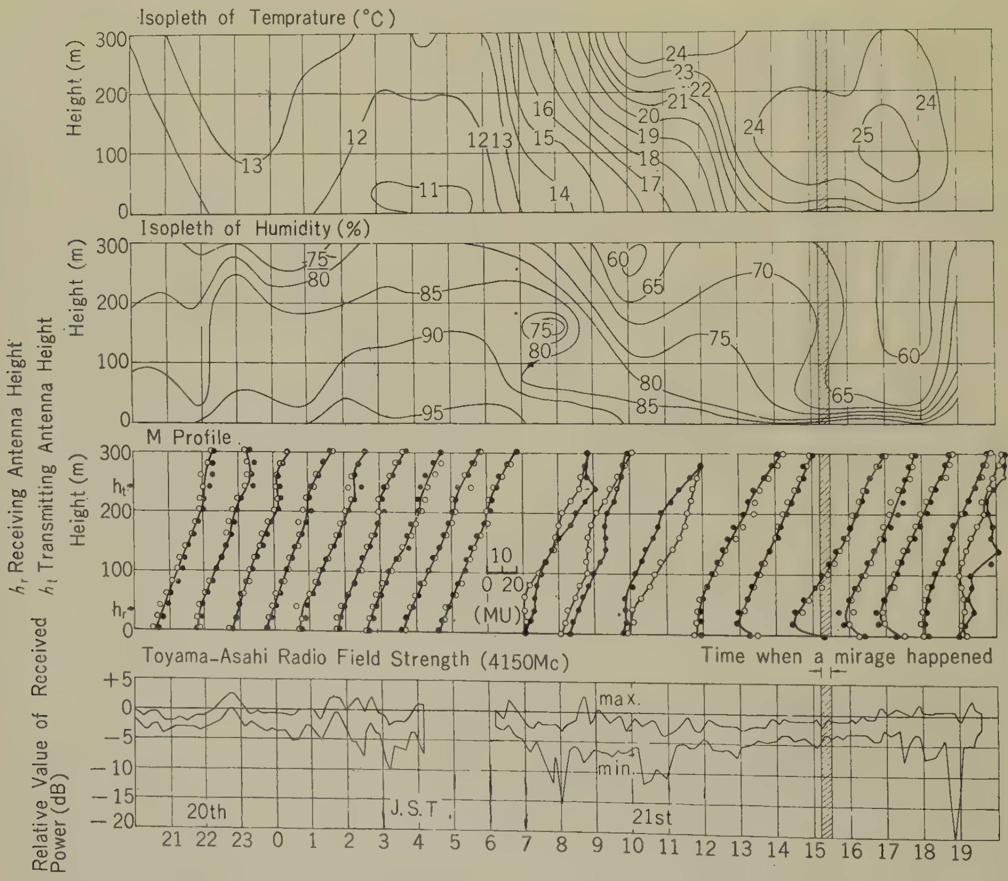

Fig. 28—Atmospheric vertical structure and received signal variation.

conditions with time. Considerable change was observed particularly between 07.00 hours and 13.00 hours.

With the aid of the weather chart for this day, for example, the mechanism of occurrence of duct will be considered.

The migratory anticyclone overlaying the Japan Sea at 15.00 hours on the 20th, passed Honshû at 03.00 hours on the 21st; and passing the southern part of Honshû, reached off the Sanriku Coast from 21st 15.00 to 22nd 03.00. It was a little windy and clear on the 21st in the Toyama district, which was located behind this atmospheric high pressure. Fig. 28 shows the transition of vertical structure of atmosphere on this day. Firstly, the temperature of the lower layer began to rise as a whole from about 07.00 hours, and the inversion of atmospheric temperature gradually happened and then slowly but intensely developed in the upper layer, up to 300 m from the ground. About 12.00 hours this inversion layer moved down to the surface again, becoming an extremely strong inversion layer near the surface. For the vertical distribution of humidity as well, the upper layer corresponded well to the distribution of atmospheric temperature, which, however, temporarily disappeared from 11.00 to 14.00. At about 15.00 hours the zone layer 100 m in height and more above the surface suddenly became low in humidity again, and, further moving down to the lower layer; formed the steep diminishing layer of humidity at 50 m and less above the surface. This continued for about three hours, then gradually disappeared. This transition is distinctly represented in the *M* curve. The weak elevated duct at about 200–250 m gradually moved downward, developed into a duct nearly on the surface at about 10.00 hours. This surface duct further developed, increasing in strength more and more and finally developed into the strongest duct at about 15.00 hours. It, however, disappeared at about 18.00 hours and changed into an elevated duct with complicated shape at 19.00 hours.

How the fading occurred at this time is shown in the lower part of the figure. The time of occurrence of deep fading corresponds well to the time of growth and disappearance of the duct. This shows that the propagation was disturbed only when there was duct in radio path.

Particularly interesting is the fact that mirage phenomena were observed when strong surface duct occurred, as has already been stated. It may be considered that there are some causes common to mirage phenomena and duct.

Futhermore, nearly the same fadings were observed at the same time even in the adjoining span between Ogijyo and Yakushi.

4.2.2. Relation between Mirage and Surface Duct

Mirage is an optical phenomenon due to super refraction of light passing through the medium in which vertical distribution of atmospheric density—in other words, vertical distribution of atmospheric temperature—is abnormal. From the viewpoint of the study on radio meteorology, distribution of air temperature and humidity with height in the lower atmosphere (up to about 300 m from the surface) has been observed in detail in several districts. According to the observation it has been found that surface and elevated inversion of the atmospheric temperature have occurred with considerable frequency. In cases where the refractive index of atmosphere has suddenly decreased with height, sudden increase of the atmospheric temperature and sudden decrease of atmospheric humidity have occured. The strength of duct is liable to be affected by the magnitude of humidity in summer and by that of temperature in winter. Thus optical mirage phenomena cannot entirely be independent on super-refraction phenomena due to radio duct, but be almost the same phenomena, though different in degree. Furthermore, mirages may be considered a kind of extreme surface duct with intense inversion of temperature.

From the above point of view, the causes and conditions, generally speaking, to generate duct can naturally be same as those to generate surface duct and mirages. They are not sole ones, but causes and surrounding conditions to make the temperature of lower atmosphere lower than that of upper layer are necessary for generating surface duct. The district facing Toyama Bay is a typical location fulfilling the above conditions. That is to say, the snow covering the Japan Alps during winter begins to thaw in spring and the cold fresh water rapidly carried by the rivers into Toyama Bay covers the sea surface. This, of course, is one of the conditions, but not a sufficient condition. For, even with these conditions mirage phenomena do not occur every day. And then the direction and velocity of wind, together with atmospheric pressure distribution will be considered as being closely related to the conditions growing mirages and duct.

In this district duct fading has already been shown to occur corresponding to type of atmospheric pressure distribution and statistical study shows the interesting fact that mirage phenomena are also well related to atmospheric pressure distribution type where duct fading occurs. Figs. 29 (a), (b), and (c) show types of atmospheric pressure distribution(2) corresponding to occurrence frequencies with which mirages have occurred in the past seventeen years. The corresponding frequencies are 57% (a), 26% (b), and 7% (c), respectively.

4.2.3. Duct Forming Mechanism foreseen from Surface Weather Chart

The air mass takes peculiar characteristics, being affected locally when it remains for a long time or moves slowly over a vast land mass or ocean. The principal air masses generated around Japan are the Siberian air mass, Yongtze Valley air mass, Equatorial air mass, Ogasawara air mass, and Okhotsk Sea air mass. Spring is the transition period during which the winter pressure pattern changes into the summer pressure pattern. The atmospheric high pressure, generated in Siberia or Manchuria, becomes migratory and is carried by upper westerlies, passing Northern Japan periodically. Characteristically low atmospheric pressure and pressure trough follow. And this is the reason why the weather is so changeable. It is in spring and autumn that migratory anticyclones appear periodically and frequently, only with different tracks and scales seasonally and yearly. In summer a pressure pattern is stabilized near Honshû, placed under the influence of the stable North Pacific anticyclone. Near the center a descending current to make up outflowing air occurs, which is called subsidence. The upper air with the least moisture, when it descends, adiabatically contracts causing temperature to rise and humidity to decrease.

When the center of migratory anticyclone moves away to the Pacific off the Sanriku Coast, the Hokuriku District on its western side has a south wind, together with which the comparatively dry warm air (Yangste air mass) originating on the Chinese Continent flows to Honshû (sometimes it comes to have higher temperature and further drying up under the effect of foehn when crossing over the Central Mountain Range) and stably

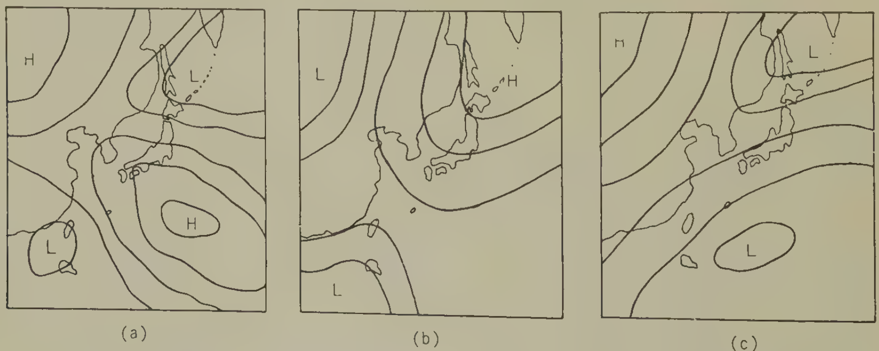

Fig. 29—Weather charts where mirages are liable to happen.

covers the cold surface of the Japan Sea. This is followed by the air mass with inversion of temperature and sudden decreace of humidity and in such conditions ducts and mirages are liable to appear.

4.3. Relation of Aerology to Fading

Further important meteorological phenomena regarding fadings are atmospheric subsidence and advection of different air mass. These phenomena will be outlined and their relation to fading characteristics clarified.

When upper and lower air masses make stable stratification due to subsidence, atmospheric temperature inversion and sudden lapse rate of humidity occur.

To simplify the considerations, it is assumed that air masses of uniform structure exist and that when they are perfectly mixed, atmospheric temperature and humidity decrease at a fixed decreasing rate for altitude. When an air mass descends from a higher altitude in the high pressure region, there should be difference between the meteorological nature of the air mass in the lower atmosphere and that in upper one. When strong elevated duct occurs; for example, difference in temperature, humidity, pressure, etc. in upper and lower atmospheres, it is considered, the differences between upper and lower atmospheres should considerably deviate from standard decreasing rate. The quantity directly corresponding to fadings is radio refractive index N of atmosphere of propagation route. The index should have an abnormal difference ($-\Delta N$) when vast difference exists in temperature, humidity, and pressure between lower and upper atmospheres. (In standard atmosphere the standard difference of refractive index per 1000 m in altitude is $-\Delta N = 39 M.U.$). The larger is $-\Delta N$ than $39 M.U.$, it is considered, the more abnormal refractive index distribution exists in the atmosphere. Namely, some ducts may be considered to exist.

Fig. 30 deals with aerological data furnished by the Wajima Aerological Observatory near the test circuit, for the period from Aug. 6 to 26, 1958. It compares the following data with each other; at two standard isobaric surfaces with 900 mb as higher atmosphere and 1000 mb as lower atmosphere, atmos-

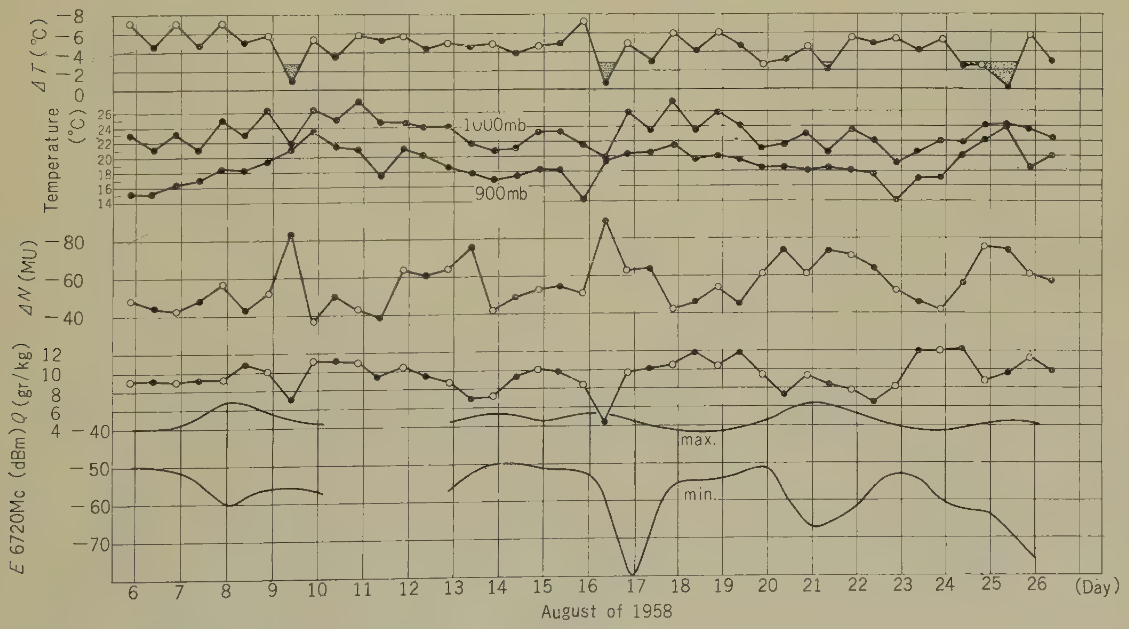

Fig. 30—Aerological data (by Wajima Aerological Observatory) and its relation to fading amplitude.

pheric temperature on each surface, temperature difierence ΔT(0°C) between these two surfaces, difference in refrative index ΔN (*M.U.*), atmospheric mixing rate of 900 mb, Q(gr/kg), and fading amplitude (dB) (maximum amplitude for one day) of 6700 Mc signal received at Toyama during the same period.

This seems to mean the existence of temperature inversion since ΔT becomes small on days when the absolute value of $-\Delta N$ increases in the relation of ΔN and ΔT in the figure. When ΔT became small, mixing ratio Q decreased exceedingly as well, as shown in the figure. The fading amplitude also corresponds well with the value of $-\Delta N$. The larger the value of $-\Delta N$, the larger is fading amplitude. If the respective correspondence of $\Delta N \leftrightarrow \Delta T$ and $\Delta N \leftrightarrow \Delta Q$ is taken into consideration, these fadings may be considered to be duct fadings causes by advection or subsidence phenomena.

The black parts on the $-\Delta T$ curve in the figure show the value of $-\Delta T$ with probability 10% or less during the period. From the above it follows that there exists excellent correspondence between fading amplitude and ΔT.

Correspondence between $-\Delta T$ and fading amplitude in May 1959 is shown in Fig. 31, which distinctly shows that the daily variation of $-\Delta T$ corresponds extremely well to that of the fading amplitudes of 4150 Mc and 6720 Mc.

4.4. Fading Characteristics in This District foreseen from Aerological Data

As already stated from the qualitative correspondence between ΔN (difierence of refractive indexes between two pressure levels of 900 mb and 1000 mb) and fading occurrence, ΔN may be considered as a measure of activity of air mass. Thus, the variation of ΔN furnished by the Wajima Aerological

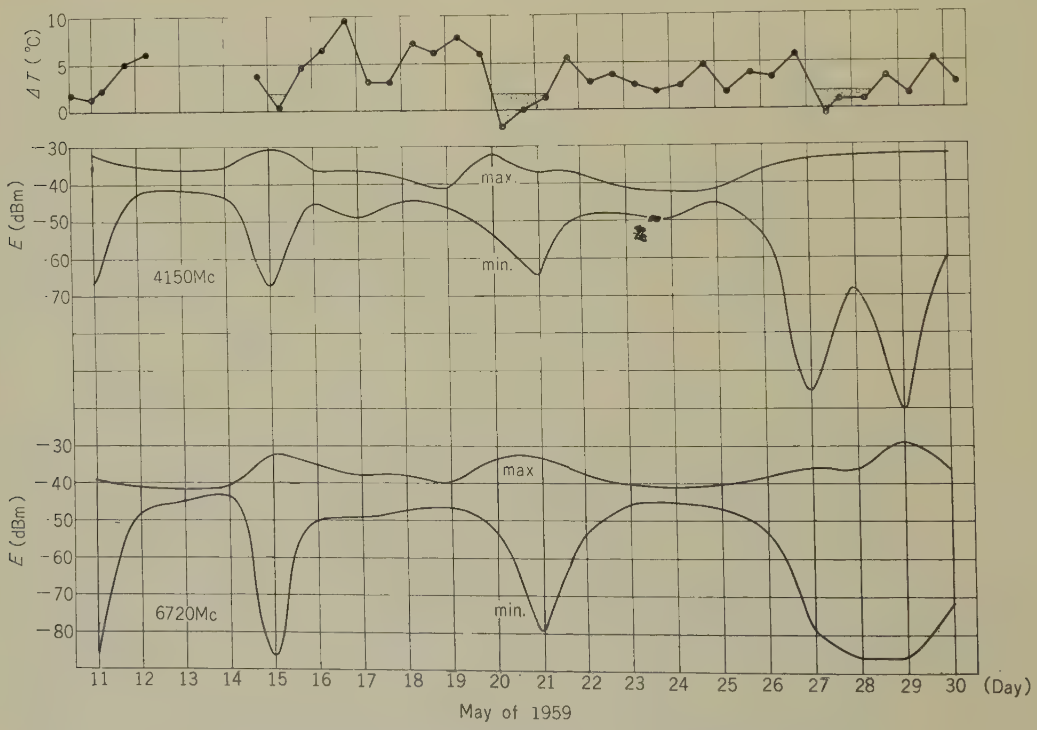

Fig. 31—Correspondence between ΔT and fading amplitude.

Observatory during a given period is used as values representing this district. If N is replaced by M, mean gradient $\alpha(=\Delta M/\Delta h)$ will be

$$\alpha = 0.157 - \Delta\dot{N}$$

where $\Delta\dot{N}$ is a gradient per unit height (m). Fig. 32 shows monthly average value $\langle\alpha\rangle$ and the standard deviation σ_α, which were worked out from 1954 to 1956 for Wajima.

Though the variation of the seasonal value of $\langle\alpha\rangle$ is not very marked, the seasonal variation of σ_α is large and much difference in values is observed for some years. This difference must be clarified by meteorological study in the future, and particularly one of the causes conceivable may be the movement of air mass. Will this not be the major cause of yearly changes! The values of $\langle\alpha\rangle$ and σ_α in 1958 and 1959 were computed for specific months as shown in Fig. 33 and were regarded to have occurred by chance. If special attention is paid to the fact that the generating condition of fading as already stated corresponds very closely to barometric distribution types and if the abnormal value of σ_α in spring may be attributed to the migration

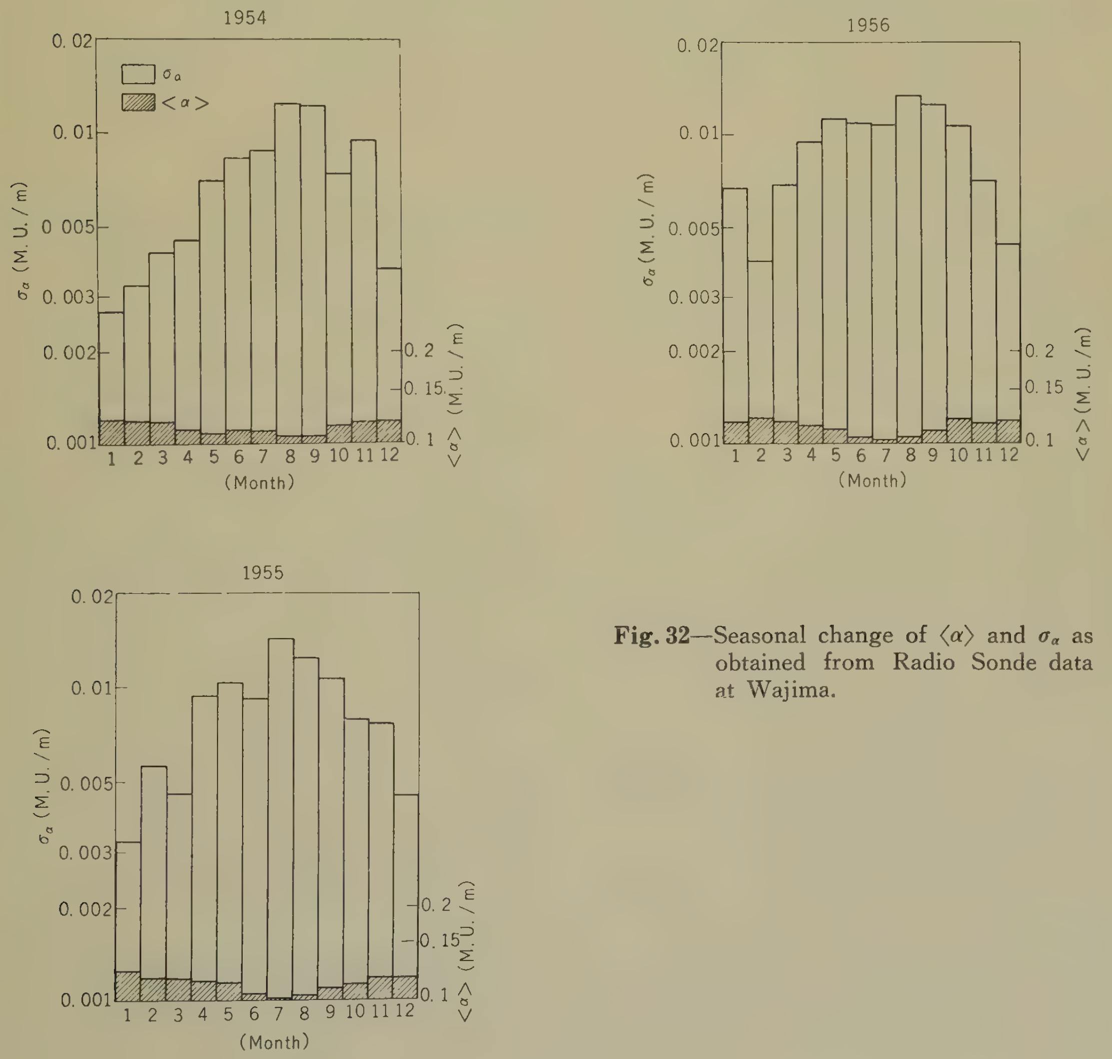

Fig. 32—Seasonal change of $\langle\alpha\rangle$ and σ_α as obtained from Radio Sonde data at Wajima.

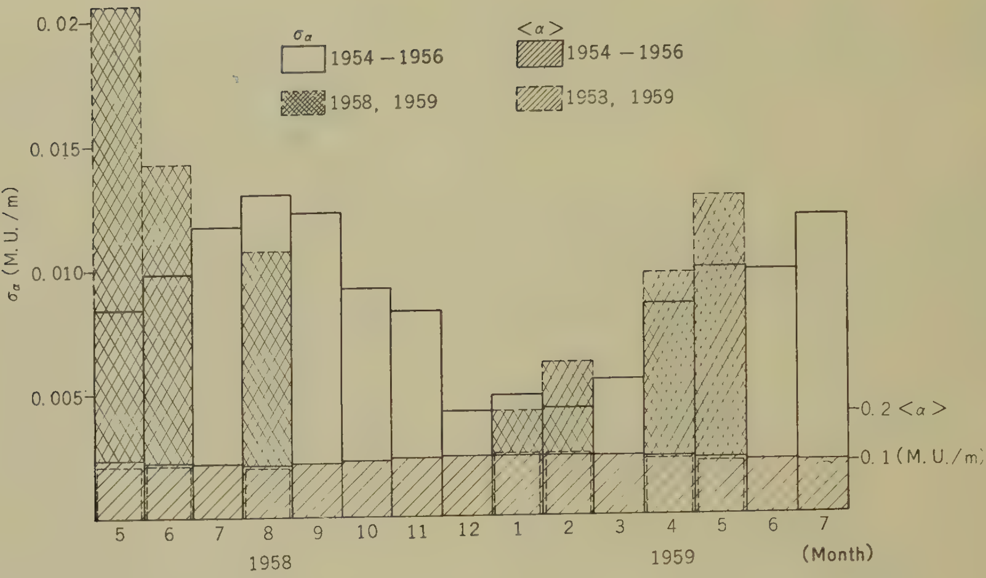

Fig. 33—$\langle\alpha\rangle$ and σ_α obtained from radio sonde data at Wajima.

of Siberian anticyclone or that of warm air mass liable to happen in the Chinese Continent in that year, it may be characteristic that the said district is placed in the geographical condition liable to cause the abnormality, or the geographical location.

5. Conclusion

Summarizing the results obtained in the test of fading relief, phase controlled space diversity reception is effective in the relief of deep interference fading. Thus it is also expected to be effective in decreasing wide band phase distortion due to multiple ray interference and it is considered to be an effective method to improve the quality of an actual circuit, though not effective against every type of deep fading. As this effectiveness depends on the system itself and also relates to the fading mechanism, it will be further studied in the future.

Further, the results obtained regarding the relation between fading occurrence and meteorology are as summarized below.

Whether the fading characteristics unexpectedly observed in this area in spring are peculiar to the area should be decided after observation over a long period and also over a wider area in the future. However, as far as they have been studied so far:

(1) It is unconceivable that there should be any local peculiarity in the fading phenomena themselves, as the estimation formula of fading quantity obtained from the actual measurement data for the Pacific side of Japan corresponds fairly well to the fading of the circuit.

(2) From this it follows that fadings unexpectedly experienced in spring were distinctly due to the unexpected values of radio meteorological constants (value at Wajima) for spring of that year. If compared with the values for three years, 1954 through 1956, it is clearly seen that the values for that year were abnormal.

(3) In spring the temperature on the sea surface in this region decreases remarkably, and constitutes a cause of generation of mirage phenomena, as well as more surface ducts than in other areas. For the formation of elevated ducts which are the cause of fadings in this circuit, it should not be over-looked that there are also Central Mountain Ranges topographically affecting the formations. The warm air advection, has been an important cause, together with subsidence phenomenon

in the atmospheric high pressure area.

Furthermore, between surface meteorological data and fading characteristics were the same relations as experienced in other areas.

If relation between the nature and activity of air mass and the characteristics of ducts formed is grasped in detail, it will be possible in the future to forecast locally the occurence of fadings abnormally deep—which are a hindrance to communication—by means of synoptic weather charts.

Acknowledgement

In the accomplishment of this study, the authors highly appreciate the valuable suggestions accorded by the technical staff of the Laboratory and also by cooperators in the within line-of-sight propagation study group. Their thanks are also due to the staff of Hokuriku Electrical Communication Bureau, and Telegraph and Telephone Offices in the district as well as to the staff of the Namekawa Fisheries High School, for their assistance granted in conducting actual tests.

References

(1) Shigetaka Ugai, Characteristics of Fading due to ducts and Quantitative Estimation of Fading, *Rev. Electr. Commun. Labor.*, **9**, (5–6), 1961.
(2) S. Fujiwara, T. Oomori, and K. Taguti, Shinkiro or the Japanese Fata Morgana, *Geophys.*, May 4, 1931.
(3) Shigetaka Ugai, Statistical Consideration of the structure of Atmospheric Refractive Index, *Reports of the Electr. Commun. Labor.*, NTT, Japan, **7**, 8, 1959.

* * * *

Review of the Electrical Communication Laboratory
Volume 9, Numbers 11-12, November-December 1961

U.D.C. 621.382.333:621.318.57]:621.395.345

Characteristics and Application of Three-Terminal pnpn Transistors for Speech-Path Switches*

Kingo YAMAGISHI† and *Ichiro ENDO*‡

The three-terminal pnpn switches, ECL-1202A and ECL-1202B, have both been made for trial to improve the early double-base diode with hook mechanism for the speech-path switches of space-division fully electronic exchanges. In this paper, the characteristics of the 1202A and 1202B are investigated from the viewpoint of the speech-path switch, and some practical circuits of applications are described. It is clarified that these devices have usable characteristics for speech-path switches.

1. Introduction

It is very important to choose suitable speech-path elements for realization of a space-division fully electronic exchange. Speech-path elements are classified into two types according to the presence or absence of a memory-function. Since speech-path elements without a memory function require additional holding circuits, it is desirable to use speech-path elements with negative resistance characteristics for simplification of control circuits. Among the speech-path elements with a memory function, the pnpn diode and the multi-terminal pnpn element are both promising considering all requirements⁽¹⁾ for the speech-path element. But it is very difficult to decide which is the better of these two devices. The multi-terminal pnpn element has a more complex structure in comparison with the pnpn diode, and the wiring for mounting speech-path circuits with the former device also becomes more complicated. But in the multi-terminal pnpn element, its breakdown voltage can be fixed by an external circuit, and uniform characteristics and good functional stability can be obtained comparatively easily. Furthermore, the control of speech-path circuits also becomes simple.

We have already complete an experimental fully electronic exchange⁽²⁾ using compound pnpn transistors⁽³⁾ as speech-path switches. But with this compound transistor, it is necessary to use each one pnp and one npn transistor for each one cross-point, and its wiring also becomes complex. Therefore, we have planned to develop a single-element switch which can be substituted for the compound transistor. And it was found that a double-base diode with hook mechanism, the ECL-1202⁽⁴⁾, made experimentally for trial at the Semiconductor Research Section of the Laboratory has satisfactory characteristics for our requirements.

The ECL-1202A and ECL-1202B described in this paper were experimentally made with the aim of obtaining simplification of the production process and an improvement of characteristics of the preceding ECL-1202. The characteristics of both devices experimentally made are described in the following sections.

---

* MS in Japanese received by the Electrical Communication Laboratory, on July 15, 1961. Originally published in the *Kenkyû Zituyôka Hôkoku* (*Electrical Communication Laboratory Technical Journal*), N.T.T., Vol. 10, No. 10, pp. 2173–2183, 1961.

† Switching Research Section.

‡ Chief, Electronics Research Section.

2. Structures and Fundamental Characteristics of 1202A and 1202B

Both the 1202A and 1202B have the same structure, shown in Fig. 1. In the 1202A, a p-type emitter terminal is made by bonding a gold wire on an n-type layer of a germanium npn grown junction bar. But in the 1202B, a p-type emitter terminal is made by bonding an aluminium wire on an n-type layer of a silicon npn junction bar. The fundamental circuit configuration of the three-terminal pnpn transistor as a speech-path switch and its typical emitter voltage vs. emitter current characteristics are shown in Fig. 2.

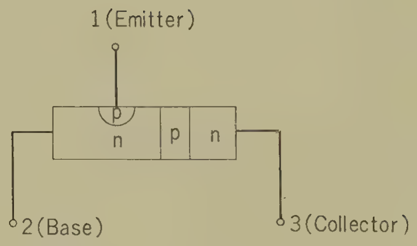

Fig. 1—Structure of 1202 A and 1202 B.

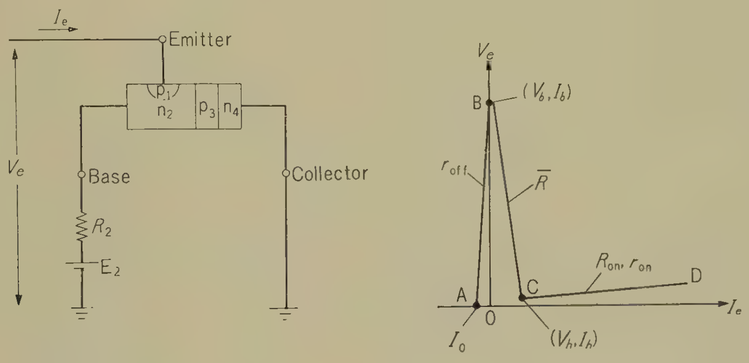

(a) (b)

Fig. 2—Fundamental circuit configuration of the three-terminal pnpn transistor as a speech-path switch and typical V_e—I_e characteristics.

2.1. The 1202A, a Germanium Three-Terminal pnpn Transistor

An example of the voltage-current characteristics between any two terminals of this device are shown in Fig. 3. The important characteristic curves in Fig. 3 for the speech-path switch are the following three curves.

(a) curve $\overset{+}{B}—\overset{-}{C}$

(b) curve $\overset{+}{B}—\overset{-}{E}$

(c) curve $\overset{+}{E}—\overset{-}{C}$

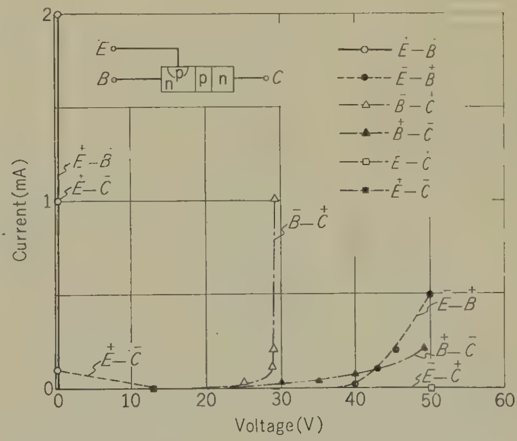

Fig. 3—Voltage-current characteristics between any two terminals of the 1202A.

Curve (a) affects the power consumption in the OFF state and the breakdown voltage of the speech-path switch. Therefore, this curve must present high resistance characteristics. Curve (b) must also present high resistance characteristics, because the characteristics of this curve determine the cutoff resistance r_{off} of the speech-path switch. For curve (c), a low resistance characteristics is desired because the characteristics of this curve determine the ac resistance r_{on} and dc resistance R_{on} of the speech-path switch in the ON state.

An example of the emitter voltage vs. emitter current characteristics of this device and their temperature dependence are shown together in Fig. 4. The breakdown voltage V_b of the speech-path switch using this device is most affected by the variation of temperature because its collector dark current I_{co} in the cutoff region varies with temperature. The breakdown voltage is approximately given by equation (1), and the collector dark current increases with the rise of temperature.

$$V_b \doteqdot E_2 - R_2 I_{co} \qquad (1)$$

Thus, it is expected that the breakdown voltage will decrease with the rise of temperature. The temperature characteristics of breakdown voltage of switches using this device is shown in Fig. 5. Furthermore, the values of other static characteristic parameters also more or less decrease with the rise of temperature.

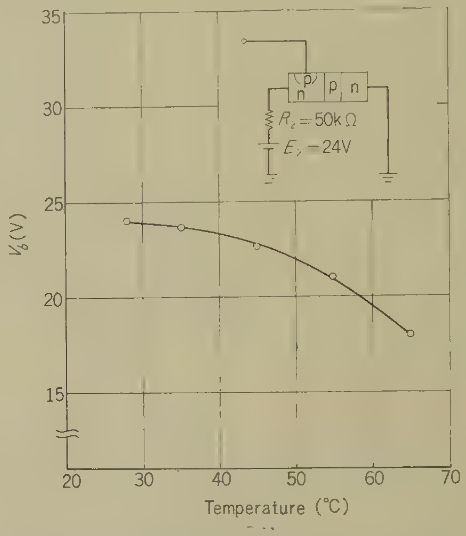

Fig. 5—Temperature dependence of the breakdown voltage of the 1202A.

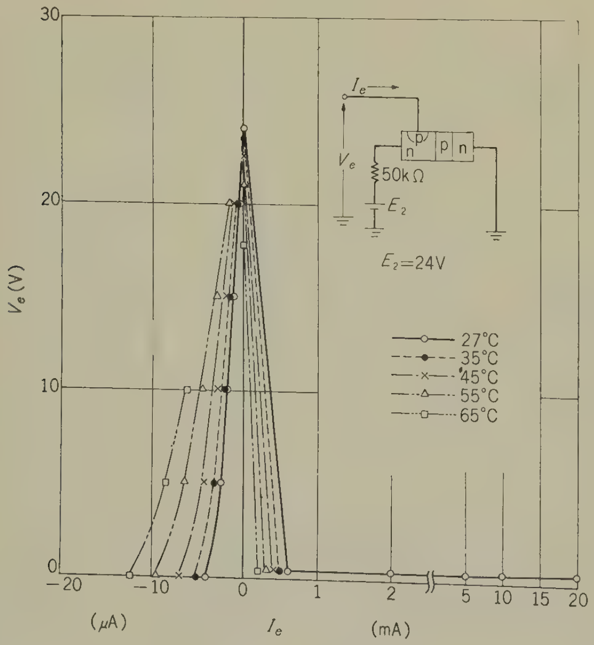

Fig. 4—V_e—I_e characteristics of the 1202A.

Table 1

C_{e-b} AND C_{b-c} OF THE 1202*A* AND 1202*B*

Sample Number	1202A				1202B			
Bias Voltage (V)	No. 2		No. 4		No. 1		No. 2	
Capacitance	6	24	6	24	6	24	6	24
C_{e-b} (pF)	1.2	1.15	1.25	1.2	1.3	1.2	1.4	1.25
C_{b-c} (pF)	6.7	6.4	9.0	8.8	2.6	2.9	2.45	1.9

If the values of static capacitances between any two terminals, namely emitter-base capacitance C_{e-b}, base-collector capacitance C_{b-c}, and emitter-collector capacitance C_{e-c}, of this device are too large, crosstalk will result. But in a three-terminal pnpn element of this type, there is the advantage that the quantity of crosstalk is substantially reduced by the dividing or screening effect of resistor R_2 connected to the base. An example of measured values of C_{e-b} and C_{b-c} in the 1202A and 1202B are shown in Table 1. In Table 2, an example of measured values of the static characteristic parameters of the 1202A are indicated.

Table 2 STATIC CHARACTERISTIC PARAMETERS OF THE 1202 A

	I_0 (μA)	V_b (V)	I_b (mA)	V_h (V)	I_h (mA)	r_{off} (MΩ)	R_{on} (Ω)	r_{on} (Ω)	C_{e-c} (pF)
E_1(V)						15~20			18
I(mA)							20	15~20	
measured values	6	25	0.1	0.44	1.1	12.5	30	10	0.9

where, $E_2=24.1$ V, $R_2=50$ kΩ, $T=23$°C

The turn-on characteristics of this device are shown in Fig. 6. And to turn-off this device when it is conducting a current I_{on} of 20 mA, a control pulse width of more than 30 μs is required. The pulse width required varies with the value of conduction current I_{on}.

The transmission characteristics of this device used in a speech-path network with a line impedance of 600 ohms are as follows, where a conduction current I_{nn} is 22 mA and signal frequency is 1 kc.

(i) Insertion loss in ON state	below 0.1 dB
(ii) Insertion loss at OFF state	above 60 dB
(iii) Frequency characteristics	flat response in the voice frequency range
(iv) Distortion	below 0.25% with an input level of +20 dBm

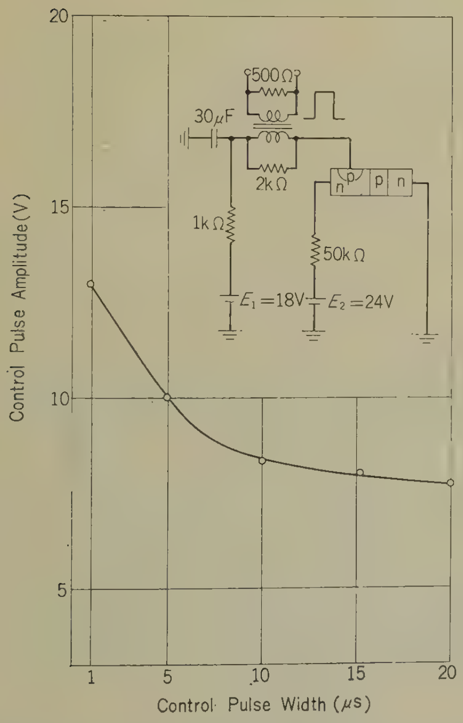

Fig. 6—Turn-on characteristics of the 1202A.

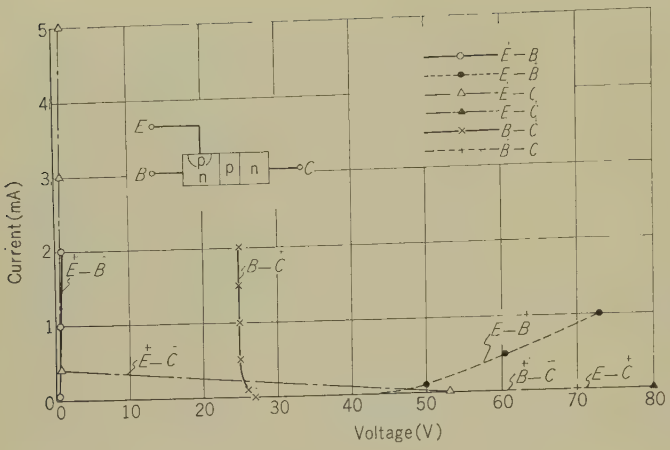

Fig. 7—Voltage-current characteristics between any two terminals of the 1202B.

2.2. The 1202B, a Silicon Three-Terminal pnpn Transistor

The problems of improving the collector dark current I_{cn} and the temperature characteristics are remained for 1202A because this device is made of germanium. These problems may be solved by using silicon materials. The 1202B was made to meet the above requirements.

An example of voltage-current characteristics between any two terminals of this device are shown in Fig. 7. Fig. 8 shows the emitter voltage vs. emitter current characteristics of this device. From measured results, it was found that the breakdown voltage of this element is about 2 to 4 volts higher than its base bias voltage E_2. This result is based on the fact that a total current amplification factor α of this device cannot become larger than unity unless its emitter current I_e becomes larger than 0.08 to 0.25 mA, because this device is made from a silicon npn junction bar with a small current amplification factor. In this connection, the α of a 1202A becomes larger than unity when its emitter current is 0.01 mA. An example of the measured values of the static characteristic parameters of 1202B are indicated in Table 3. In the temperature range of 20°C to 60°C, no appreciable variation in the characteristics of this device were found. Fig. 9 shows the turn-on characteristics of this device, and it shows that this device can be easily turned on by a control pulse of less than 1 μs. And this device can be turned off by a control pulse of 5 μs.

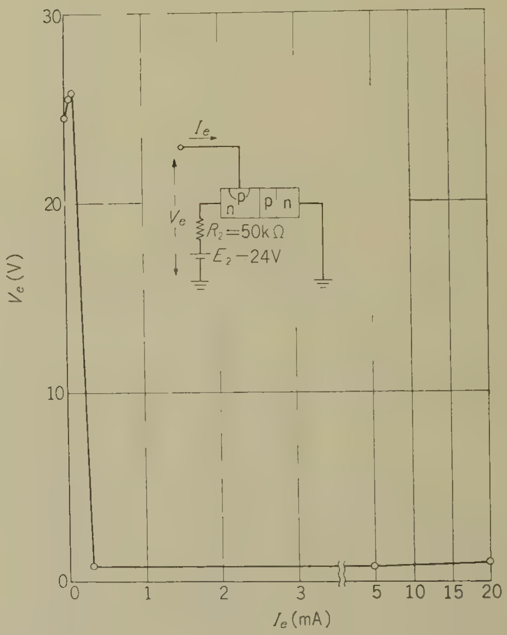

Fig. 8—V_e—I_e characteristics of 1202B.

The transmission characteristics of this device are almost similar to those of the 1202A. Fig. 10 shows a photograph of the 1202B.

3. Practical Speech-Path Circuits

The general circuit constructions using three-terminal negative resistance devices as

Table 3 STATIC CHARACTERISTIC PARAMETERS OF THE 1202 B

	I_0 (μA)	V_b (V)	I_b (mA)	V_h (V)	I_h (mA)	r_{off} (MΩ)	R_{on} (Ω)	r_{on} (Ω)	C_{e-c} (pF)
E_1(V)						15～20			18
I(mA)							20	10～20	
measured values	<0.1	25.8	0.09	0.79	0.3	>200	49	8	1.8

where, $E_2=23.9$ V, $R_2=50$ kΩ, $T=24°$C

speech-path switches for the space-division fully electronic exchange have already been presented.⁽¹⁾ But according to the adoption of a link-control method or an end-marking method for the control of speech-path circuits, the circuit details naturally differ. In this section, a fundamental circuit using 1202A's or 1202B's as speech-path switches and a method of control are described.

Fig. 11 shows a switch-matrix of $m \times n$ using these devices. In this switch-matrix, all bases of switching devices connected to a common output are gathered through each base resistor R_2, and are connected to a pulse source for base control. And a positive bias

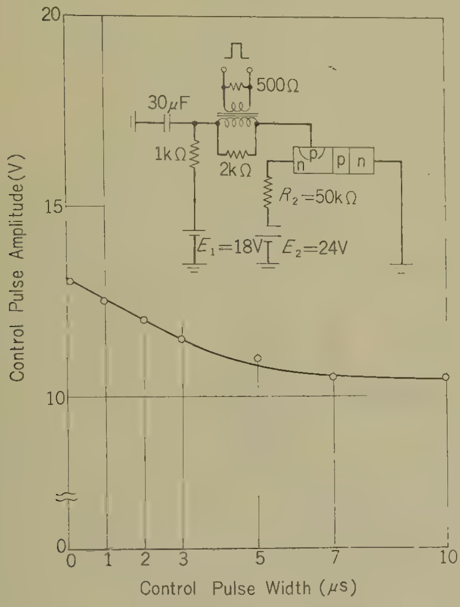

Fig. 9—Turn-on characteristics of the 1202B.

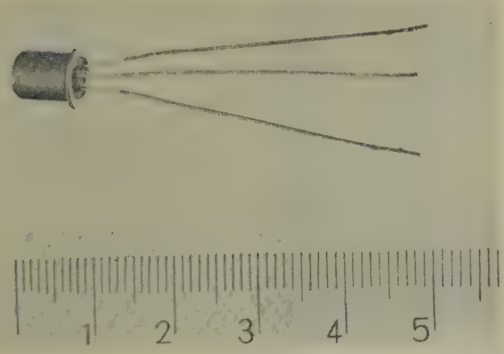

Fig. 10—Photograph of the 1202B.

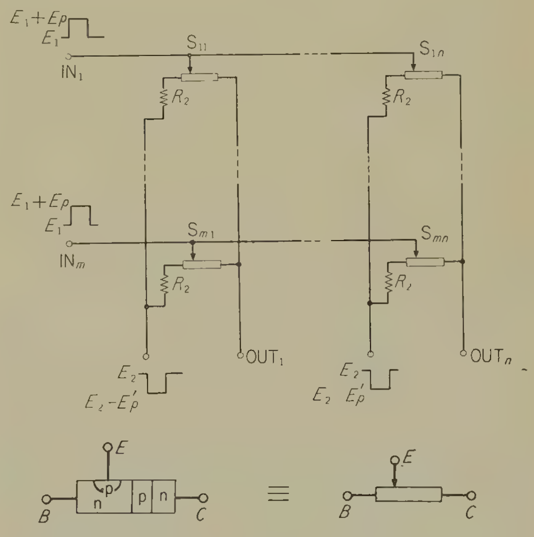

Fig. 11—Switch-matrix with three-terminal pnpn transistors.

voltage E_2 is normally applied to these bases.

On the other hand, all emitters of switching elements connected to a aommon input are gathered, and are connected to a pulse source for emitter control. And a positive bias voltage E_1 is normally applied to these emitters.

Now as an example, in order to turn on a switching element S_{11}, a positive control pulse having an amplitude of E_p must be delivered to the terminal of IN_1 from a pulse source for emitter control. Synchronized with this positive control pulse, a negative control pulse having an amplitude of E_p' must be delivered to bases of switching elements connected to the common output OUT_1 from a pulse source for base control. In this case, voltage relations presented in the following equation must be previously satisfied.

$$E_2 > (E_1 + E_p \pm E_s) > (E_2 - E_p') > (E_1 + E_s). \quad (2)$$

Where E_s signifies a maximum amplitude of transmitted signal.

And in the multi-stage connection of these switch matrices, a direct-coupled tandem connection is possible.

4. Conclusion

As described above, it was found that the 1202A and 1202B possess usable properties for speech-path switches. But these devices are still in the experimental stage, and some characteristics must be improved. Especially, some problems on uniformity of characteristics and long-term stability still remain to be solved.

Furthermore, these devices can be also used in the various circuits which can be realized with silicon controlled rectifiers, double-base diodes, and grid-controlled gas discharge tubes.

5. Acknowledgement

The authors wish to express their thanks to Dr. Y. Takeda and A. Sato of the Nippon Electric Company Ltd. for their efforts in making these devices, and to T. Tominaga, Semiconductor Research Section, for his good advice on design of these devices.

References

(1) I. Endo, S. Yoshida: Semiconductor Speech-Path Switches Suitable for Direct Coupled Connection, *Rev. Electr. Commun. Labor. NTT*, Jap., **8**, 3-4, p. 105, 1960.
(2) Kiyasu Zen'iti, I. Endo, K. Hanawa, S. Yoshida, K. Tomaru, K. Goto: An Experimental All Electronic Exchange Using Negative Resistance Elements as Speech-Path Switches, *J. Inst. Electr. Commun. Eng. Jap.*, **44**, 2, p. 197, 1961.
(3) I. Endo, K. Yamagishi, S. Yoshida, K. Goto: Properties of Compound Transistors for Speech-Path Swicthes, *Rev. Electr. Commun. Labor. NTT*, Jap., **8**, 5-6, p. 211, 1960.
(4) T. Tominaga, S. Kanai, A. Sato: A Double Base Diode with Hook Mechanism, *Rep. Electr. Commun. Labor. NTT*, Jap., **7**, 5, p. 133, 1959.

* * * *

U.D.C. 621.372.852.5

Mode Conversion in the Excitation of TE_{01} Waves in a TE_{01} Taper Type Mode Transducer*

Shin-ichi IIGUCHI†

The concise formulas for determining magnitudes of unused modes generated in a TE_{01} *taper type mode transducer are obtained by the use of the stationary phase principle from the equations of integral forms which are derived from the Reiter's telegraphist's equations for a nonuniform waveguide with a straight axis.*

The calculated values of the magnitudes of the unused TE_{11}, TE_{21}, *and* TM_{11} *modes generated in the mode transducer of 22.2 mm inside diameter and 220 mm length are −15.4 dB, −18.4 dB, and −17.6 dB, respectively at a frequency of 24 kMc/s.*

These values agree with the results of the author's previous calculation, which have been derived on the basis of Maxwell's Equations in oblique coordinates, within 1 dB.

Introduction

Mode conversion in a taper type TE_{01} mode transducer was calculated by use of Maxwell's Equation in oblique coordinates of a helix system⁽¹⁾ a few years ago.

But the calculation was complicated and the results were obtained in integral forms. Therefore, numerical integration was inevitable to determine the magnitudes of the generated unused modes.

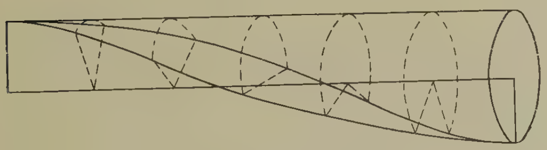

Fig. 1—TE_{01} wave transducer.

The paper concerning the telegraphist's equations for nonuniform waveguide with a straight axis was published by G. Reiter in 1959.⁽²⁾,⁽³⁾ By Reiter's method, integral forms of the magnitudes of the unused modes generated in this TE_{01} mode transducer can be derived fairly easily.

Sector TE_{11}, TE_{21} and TM_{11} modes, which are spurious modes in the mode transducer, build up mainly in the neighbourhoods where these modes degenerate with sector TE_{01} mode respectively. Approximate calculation based on the principle of stationary phase can be applied to these phenomena.⁽⁴⁾

In the present paper, by use of the principle of stationary phase, the concise formulas for determining the magnitudes of the unused modes generated in the TE_{01} mode transducer were obtained from the integral forms, which were derived by Reiter's method.

From the concise formulas, the magnitudes of the unused modes can be determined directly. The calculated values of the magnitudes of the unused TE_{11}, TE_{21} and TM_{11} modes generated in the transducer of 22.2 mm inside diameter and 220 mm length agree with the results mentioned in the author's preceding paper⁽¹⁾ within 1 dB at a frequency of

---

* MS in Japanese received by the Electrical Communication Laboratory, November 13, 1961. It will be published in the *Kenkyû Zituyôka Hôkoku* (*Electrical Communication Laboratory Technical Journal*), N.T.T.

† Assistant Section Chief, Hyper-Frequency Research Section.

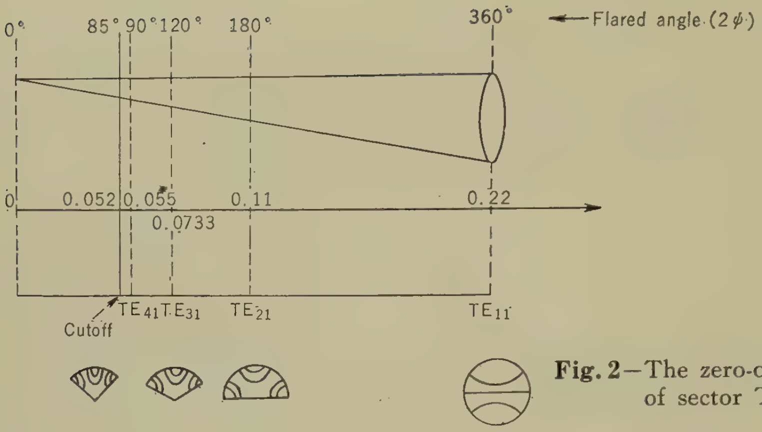

Fig. 2—The zero-order change of shape of sector TE$_{11}$ mode.

24 kMc/s.

Glossary of Symbols

r, ϕ, z	right-handed cylindrical coodinates
$2\,\phi$......	flared angle of sector of metal surface
a........	inner radius of waveguide
$(s), (mn)$	subscripts of sector TM mode
$[s], (mn)$	subscripts of sector TE mode
β_{pm}......	phase constant
$k_{(pn)}$	n-th zero of $J_p(X)$
$k_{[pn]}$	n-th zero of $J_p'(X)$

$$B=\frac{z}{\phi},\quad x_{pn}=\frac{k_{pn}}{a},\quad p=\frac{m\pi B}{z}.$$

1. Coordinate System

The central angle of the sector space surrounded by the metal surface is flared progressively and the edge helix curve of the sector space is expressed by

$$x=a\cos\phi,\quad y=a\sin\phi,\quad\text{and}\quad z=B\phi \qquad (1)$$

where B is determined by the geometrical configuration of the transducer.

The formulas of the inner helix curves are

$$x=r\cos\phi,\quad y=r\sin\phi,\quad\text{and}\quad z=(B\phi/\phi)\phi.$$

2. Normal Mode Functions in Sector Waveguide (See Appendix A)

2.1. TE$_{mn}$ mode

The vector mode function in the sector waveguide is derivable from the scalar function

$$T_{[mn]}=-\sqrt{\epsilon_m}\,\sqrt{\frac{B}{z}}\;\frac{1}{\sqrt{k_{[pn]}^2-p^2}}\;\frac{J_p(x_{[pn]}r)}{J_p(x_{[pn]}a)}\cos p\phi, \qquad (2)$$

where $\epsilon_m=2\,(m\neq0)$, $\epsilon_m=1\,(m=0)$,

and is

$$e_{[mn]}=i_\phi\left(-\frac{\partial T_{[mn]}}{\partial r}\right)+i_r\left(\frac{\partial T_{[mn]}}{r\,\partial\phi}\right) \qquad (3)$$

$$=i_\phi\sqrt{\epsilon_m}\,\sqrt{\frac{B}{z}}\times\frac{k_{[pn]}}{\sqrt{k_{[pn]}^2-p^2}}\;\frac{J_p'(x_{[pn]}r)}{a\,J_p(x_{[pn]}a)}\cos p\phi$$

$$+i_r\sqrt{\epsilon_m}\,\sqrt{\frac{B}{z}}\;\frac{p}{\sqrt{k_{[pn]}^2-p^2}}\times\frac{J_p(x_{[pn]}r)}{rJ_p(x_{[pn]}a)}\sin p\phi.$$

particularly

$$e_{[01]}=i_\phi\left(-\frac{\partial T_{[01]}}{\partial r}\right) \qquad (4)$$

$$=i_\phi\sqrt{\frac{B}{z}}\;\frac{J_0'(x_{[01]}r)}{J_0(x_{[01]}a)}.$$

2.2. TM$_{mn}$ mode

In the same way

$$T_{(mm)} = -\sqrt{\epsilon_m}\sqrt{\frac{B}{z}}\frac{1}{k_{(pn)}} \times \frac{J_p(x_{(pn)}r)}{J_{p+1}(x_{(pn)}a)}\sin p\phi, \tag{5}$$

and

$$\boldsymbol{e}_{(mm)} = \boldsymbol{i}_\phi\left(\frac{\partial T_{(mn)}}{r\partial\phi}\right) + \boldsymbol{i}_r\left(\frac{\partial T_{(mn)}}{\partial r}\right) \tag{6}$$

$$= -\boldsymbol{i}_\phi\sqrt{\epsilon_m}\sqrt{\frac{B}{z}}\frac{p}{k_{(pn)}} \times \frac{J_p(x_{(pn}r)}{r J_{p+1}(x_{(pn)}a)}\cos p\phi - \boldsymbol{i}_r\sqrt{\epsilon_m} \times \sqrt{\frac{B}{z}}\frac{J_p'(x_{(pn)}r)}{a J_{p+1}(x_{(pn)}a)}\sin p\phi.$$

3. Formulas of Magnitudes of Unused Generated Modes

Formulas for determing magnitudes of the unused modes generated from the main mode in a nonuniform waveguide with a straight axis were given by References (2) and (3).

Therefore, the formula for the magnitude of the unused mode generated from sector TE$_{01}$ wave in the TE$_{01}$ mode transducer can be obtained formally:

$$S_{S[01]}(L) = e^{-j\int_0^L \beta_s dz} \times \int_0^L C_{S[01]} e^{j\int_0^z(\beta_s - \beta_{[01]})dz} dz \tag{7}$$

where

$$C_{S[01]} = -\frac{1}{2}\left[\sqrt{\frac{K_{[01]}}{K_S}}\,{}^{V}T_{S[01]} + \sqrt{\frac{K_S}{K_{[01]}}}\,{}^{I}T_{S[01]}\right]. \tag{8}$$

$${}^{V}T_{S[01]} = \iint \frac{\partial \boldsymbol{e}_{[01]}}{\partial z}\boldsymbol{e}_s dS + \int_\sigma \tan\vartheta\, \boldsymbol{e}_{[01]}\boldsymbol{e}_s d\sigma \tag{9}$$

$${}^{I}T_{S[01]} = \iint \frac{\partial \boldsymbol{e}_{[01]}}{\partial z}\boldsymbol{e}_s dS \tag{10}$$

$K_{[01]}$ and K_S are wave impedances of TE$_{01}$ mode and s mode respectively, and ϑ is the angle between the outward normals to the cross section and to the wall surface of the waveguide.

4. Integral Forms of Magnitudes for Unused Generated Modes

Substituting the normal mode functions in Section 2 into the general formulas in Section 3, the following integral forms can be obtained.

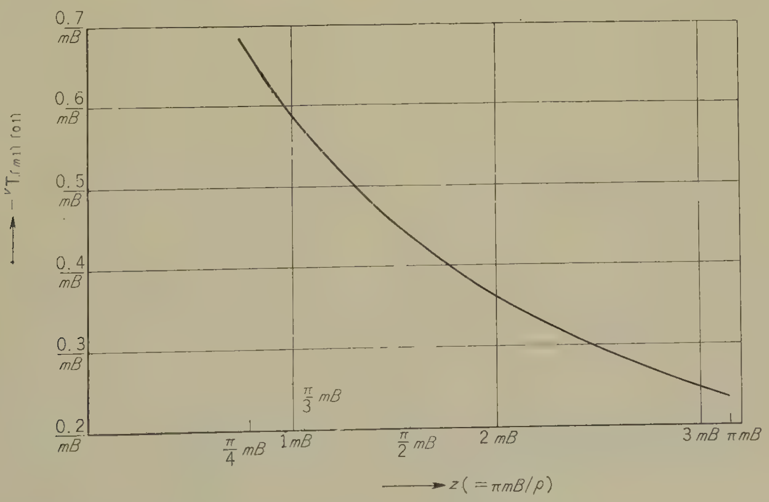

Fig. 3—Universal curve of $^{V}\mathrm{T}_{[m1][01]}$ of TE$_{m1}$ wave (m is the subscript of TE$_{m1}$).

4.1. Magnitudes of Generated TE Mode (See Appendix B)

Substituting Eqs. (3, 4) into (7–10), we obtain

$$S_{[s]}^{[01]}(L) = -e^{-j\int_0^L \beta_{[s]}\,dz}\frac{1}{2\sqrt{\beta_{[01]}}}$$

$$\times\int_0^L \sqrt{\beta_{[s]}}\;{}^{V}T_{[s][01]}\,e^{j\int_0^z(\beta_{[s]}-\beta_{[01]})dz}dz, \tag{11}$$

where

$${}^{V}T_{[s][01]} = \frac{2}{B}\int_0^a\left\{\frac{\partial T_{[s]}}{\partial r}\right\}_\phi\left\{\frac{\partial T_{[01]}}{\partial r}\right\}_\phi rdr. \tag{12}$$

(See Fig. 3 for ${}^{V}T_{[m1][01]}$)

4.2. Magnitude of Generated TM Mode (See Appendix B)

Substituting (4, 6) into (7–10), we obtain

$$S_{(s)}^{[01]}(L) = -e^{-j\int_0^L \beta_{(s)}dz}\frac{\sqrt{\omega^2\mu\epsilon}}{2\sqrt{\beta_{[01]}}}$$

$$\times\int_0^L\frac{1}{\sqrt{\beta_{(s)}}}\;{}^{V}T_{(s)[01]}\,e^{j\int_0^z(\beta_{(s)}-\beta_{[01]})dz}\,dz, \tag{13}$$

where

$${}^{V}T_{(s)[01]} = -\frac{2}{B}\int_0^a\left\{\frac{\partial T_{(s)}}{r\partial\phi}\right\}_\phi\left\{\frac{\partial T_{[01]}}{\partial r}\right\}_\phi rdr. \tag{14}$$

(See Fig. 4 for ${}^{V}T_{(m1)[01]}$)

5. Approximate Formulas of Magnitudes for Unused Generated Modes

In this section the concise formulas of magnitudes for unused generated modes, which are obtained from the integral forms in Section 4 by the use of the principle of stationary phase, are described.

Sector TE_{01} wave has a constant wave number in any axial position, z, in the TE_{01} mode transducer. On the other hand, the wave numbers of the sector TE_{11}, TE_{21}, and TM_{11} waves vary according to the sector angle. Therefore, in certain positions the sector TE_{11}, TE_{21}, and TM_{11} waves degenerate with the sector TE_{01} wave. These spurious waves build up mainly in these positions, respectively. Principle of stationary phase can be applied to these phenomena. (See Appendix C)

5.1. Approximate Formulas of Magnitudes for Unused Modes

The results obtained are the following:

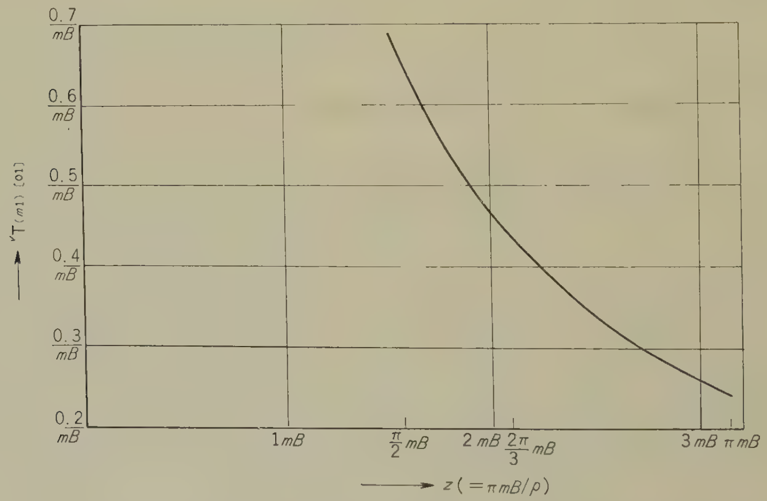

Fig. 4—Universal curve of ${}^{V}T_{(m1)[01]}$ of TM_{m1} wave (m is the subscript of TM_{m1}).

① TE_{11} wave

$$\left|S^{[01]}_{[11]}(L)\right| = 0.418\sqrt{\frac{\lambda_{c[01]}}{\lambda_{g[01]}}}\sqrt{\frac{a}{B}} \tag{15}$$

② TE_{21} wave

$$\left|S^{[01]}_{[21]}(L)\right| = \frac{\left|S^{[01]}_{[11]}(L)\right|}{\sqrt{2}} \tag{16}$$

③ TM_{11} wave

$$\left|S^{[01]}_{(11)}(L)\right| = 0.235\frac{\sqrt{\lambda_{g[01]}\lambda_{c[01]}}}{\lambda_0}\sqrt{\frac{a}{B}} \tag{17}$$

where

λ_0………free space wavelength
$\lambda_{c[01]}$ …cutoff wavelength of TE_{01} wave
$\lambda_{g[01]}$ …guide wavelength of TE_{01} wave
a………inner radius of waveguide
B………see (1)

5.2. Numerical Examples of Magnitudes for Unused Modes

The magnitudes of the unused modes generated in the transducer of 22.2 mm inside diameter and 220 mm length can be calculated numerically from (15, 16, 17) at a frequency of 24 kMc/s. The numerical results are as follows:

① TE_{11} mode : −15.4 dB
② TE_{21} mode : −18.4 dB
③ TM_{11} mode : −17.6 dB

Conclusion

The concise approximate formulas for the magnitudes of the unused modes generated in a taper type TE_{01} mode transducer are obtained from the integral forms which are derived by the telegraphist's equations for a nonuniform waveguide.

Acknowledgement

The author is indebted to I. Someya, Y. Nakamura, and B. Oguchi of the Electrical Communication Laboratory for helpful suggestions relating to this work.

Appendix

A. Normal Mode in Sector Waveguide

§ 1. TE mode : (See Fig. 5)

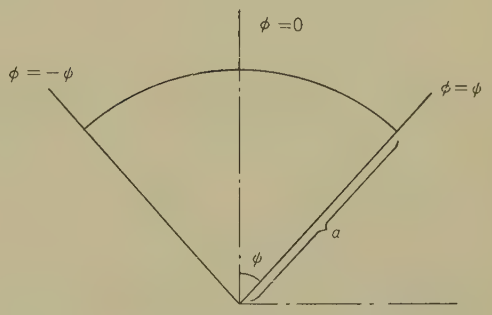

Fig. 5—Cross section of a sector waveguide.

Only the waves coupled with the TE_{01} wave are described here.

$$T = J_p(\chi r)\cos p\phi$$

$$E_r = \frac{\partial T}{r\partial\phi} = -\frac{1}{r}J_p(\chi r)\sin p\phi\cdot p$$

$$E_\phi = -\frac{\partial T}{\partial r} = -\chi J_p'(\chi r)(\cos p\phi)$$

$E_r=0$ in $\phi=\pm\psi$ $\quad\therefore\ \sin p\phi=0.$

Hence $p=m\pi/\psi.$ $(m=0,1,2,\cdots\cdots)$ (A. 1)

Next

$E_\phi=0$ in $r=a,$ $\quad\therefore\ J_p'(\chi a)=0.$

Hence χa is the zero of J_p'. (A. 2)

Here $p=m\pi/\psi=m\pi B/z.$

Normalizing $T_{[mn]}$ by the factor determined from

$$\chi^2_{[pn]}\int_{-\psi}^{\psi}\int_0^a T_{[mn]}{}^2\, r dr d\phi = 1,$$

we obtain (2).

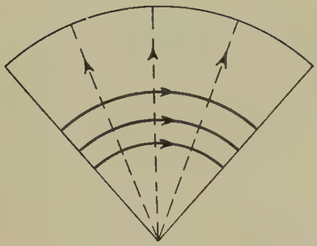

Fig. 6—Transverse field of sector TE$_{01}$.

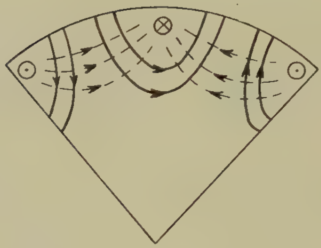

Fig. 7—Transverse field of sector TE$_{11}$.

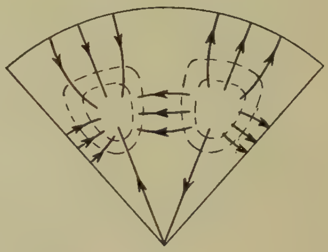

Fig. 8—Transverse field of sector TM$_{11}$.

§2. TM mode:

Only the waves coupled with the TE$_{01}$ wave are described here.

$$T = J_p(\chi_{(pn)} r)\sin p\phi$$

Where $x_{(pn)}a$ is the n-th zero of J_p. In this case, we also obtain the following formulas.

$$p = m\pi/\phi = m\pi B/z.$$

Normalizing $T_{(mn)}$ by the factor determined from

$$\chi_{(pn)}{}^2\int_{-\phi}^{\phi}\int_0^a T_{(mn)}{}^2\ rdrd\phi = 1,$$

we obtain (5).

Figs. 6, 7, and 8 are the patterns of the electric and magnetic fields of sector TE$_{01}$, TE$_{11}$, and TM$_{11}$ waves respectively.

B. Coupling Coefficient $^V T_{S[01]}$ and $^I T_{S[01]}$

From Eq. (3, 4, 6), we obtain

$$\iint \frac{\partial \boldsymbol{e}_{[01]}}{\partial z}\boldsymbol{e}_s\, dS = 0.$$

Therefore form Eqs. (9, 10), we obtain

$$^V T_{s[01]} = \int_\sigma \tan\vartheta\ \boldsymbol{e}_{[01]}\boldsymbol{e}_s\, d\sigma$$

$$^I T_{s[01]} = 0.$$

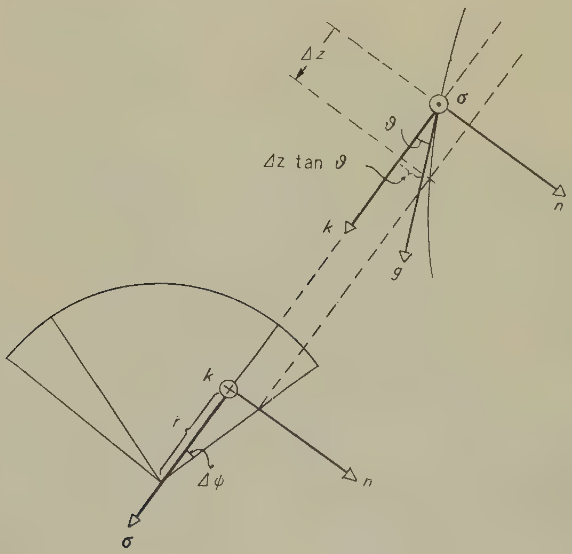

$$\tan\vartheta = \lim \frac{r\tan\Delta\phi}{\Delta z}$$

$$= \frac{rd\phi}{dz}$$

$$= \frac{r}{B}$$

Fig. 9—tan ϑ.

On the arc line of sector cross section,

$$\tan \vartheta = 0.$$

On the radius of sector cross section,

$$\tan \vartheta = \frac{rd\phi}{dz} = \frac{r}{B}. \qquad \text{(See Fig. 9)}$$

Therefore

$$\int_{\sigma} f(r) \tan \vartheta \, d\sigma = \int_{a}^{0} f(r) \frac{r}{B} (-dr)$$

$$+ \int_{0}^{a} f(r) \frac{r}{B} \, qr = 2 \int_{0}^{a} f(r) \frac{r}{B} \, dr$$

(See Fig. 10)

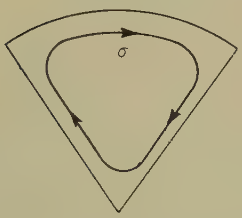

Fig. 10—Direction of integration.

From the above results and Eqs. (3, 4, 6), we obtain

$$^{V}T_{[s][01]} = \frac{2}{B} \int_{0}^{a} \left\{ \frac{\partial T_{[s]}}{\partial r} \right\}_{\psi} \left\{ \frac{\partial T_{[01]}}{\partial r} \right\}_{\psi} rdr$$

$$^{V}T_{(s)[01]} = -\frac{2}{B} \int_{0}^{a} \left\{ \frac{\partial T_{(s)}}{r\partial \phi} \right\}_{\psi} \left\{ \frac{\partial T_{[01]}}{\partial r} \right\}_{\psi} rdr.$$

C. Approximate Calculation of the Magnitude for Unused Modes

Derivation of approximate formulas of the magnitudes for unused generated modes, which have been shown in Section 5, are described in this section. Description will be made only for generated TE_{11} mode in detail but derivation for the other generated modes may be made similarly.

§1. Approximate Formula of Eigen Value

Only the neighbourhood where sector TE_{11} mode degenerates with sector TE_{01} mode comes into the problem.

The Eigen value of circular TE_{01} mode exists between the circular TE_{21} and TE_{31} modes.

The Eigen value $k_{p[1]}$ of TE_{p1} mode in this neighbourhood may be approximately expressed by the first order equation of p.

$$k_{[p1]} = Ap + C \qquad (C.1)$$

where A and C are constant.

Substituting $p = \pi B/z$ into (C. 1) we obtain

$$k_{[p1]} = \frac{A\pi B}{z} + C. \qquad (C.2)$$

Substituting $k_{[p1]} = \chi_{[p1]} a$ into (C. 2), we obtain

$$\chi_{[p1]} = Dz^{-1} + E, \qquad (C.3)$$

where

$$D = \frac{A\pi B}{a}, \quad E = \frac{C}{a}. \qquad (C.4)$$

When $p=2$, $k_{[21]}=3.0542$ and when $p=3$, $k_{[31]}=4.2012$.

From this relation and (C. 1), we get

$$A = 1.1470, \quad C = 0.7602. \qquad (C.5)$$

§2. The Axial Position z_0 where Sector TE_{11} Mode Degenerated with TE_{01} Mode

From (C. 2) we get

$$k_{[01]} = \frac{A\pi B}{z_0} + C,$$

where $k_{[01]} = 3.8317$.

$$\therefore \quad z_0 = \frac{A\pi B}{k_{[01]} - C} \qquad (C.6)$$

§3. Phase angle $\Theta = \int_0^z (\beta_{[s]} - \beta_{[01]}) dz$ in Eq. (11)

First order approximate formula of Tailor expansion of $\beta_{[p1]} = \sqrt{\omega^2 \mu\epsilon - (Dz^{-1} + E)^2}$ in the neighbourhood of z_0 is

$$\beta_{[p1]} \doteqdot \beta_{[01]} + F(z-z_0),$$

where

$$F = \frac{\chi_{[01]}}{\beta_{[01]}} \frac{D}{z_0^2} = \frac{\chi_{[01]}}{\beta_{[01]}} \frac{(k_{[01]}-C)^2}{A\pi Ba}. \tag{C. 7}$$

$$\therefore \quad \Theta = \int_0^z (\beta_{[p1]} - \beta_{[01]})\, dz$$

$$= \frac{1}{2} Fz^2 - Fz_0 z$$

$$\therefore \quad \frac{d\Theta}{dz} = F(z-z_0)$$

Therefore $d\Theta/dz = 0$ in $z = z_0$.

Expanding Θ in Tailor series in the neighbourhood of z_0, we get

$$\Theta = -\frac{1}{2} Fz_0^2 + \frac{F}{2}(z-z_0)^2. \tag{C. 8}$$

§4. Approximate Formula of the Magnitude of Generated TE$_{11}$ Mode

From Eqs. (11) and (C. 8), we obtain

$$\left| S^{[01]}_{[11]}(L) \right| \doteqdot \left| \frac{1}{2} {}^{V}T_{[11][01]} \int_0^L e^{j\int_0^z (\beta_{[11]} - \beta_{[01]}) dz} dz \right|$$

$$\doteqdot \left| \frac{1}{2} {}^{V}T_{[11][01]} \int_0 e^{j(F/2)(z-z_0)^2} dz \right|$$

If $\sqrt{\frac{F}{2}}(z-z_0) = t$, then $dz = \sqrt{\frac{2}{F}}\, dt$.

Therefore

$$\left| \int_0^L e^{j(F/2)(z-z_0)^2} dz \right| \doteqdot \left| \sqrt{\frac{2}{F}} \int_{-\infty}^{\infty} e^{jt^2} dt \right| \tag{C. 9}$$

$$= \sqrt{\frac{2}{F}} \sqrt{\pi}$$

$$\therefore \quad \left| S^{[01]}_{[11]} \right| = \frac{1}{2} \left| {}^{V}T_{[11][01]} \right| \sqrt{\frac{2\pi}{F}} \tag{C. 10}$$

$$= \left| {}^{V}T_{[11][01]} \right| \sqrt{\frac{\pi}{2}} \frac{\sqrt{A\pi Ba}}{k_{[01]}-C} \sqrt{\frac{\beta_{[01]}}{\chi_{[01]}}}$$

$\cdot$ {use (C. 7)}

Substituting (C.5) into above equation, we obtain

$$\left| S^{[01]}_{[11]} \right| = 0.418 \sqrt{\frac{\lambda_{c[01]}}{\lambda_{g[01]}}} \sqrt{\frac{a}{B}}.$$

Approximate calculation for generated TE$_{21}$ mode can be made similarly. Following explanation can be made easily by attaching the subscript corresponding to each mode to each symbol (D, z_0, and F).

$D_{[21]}$ and $z_{0[21]}$ are twice $D_{[11]}$ and $z_{0[11]}$ respectively.

Therefore, from similar formula to (C.7), $F_{[21]}$ is obtained in half of $F_{[11]}$.

And ${}^{V}T_{[21][01]}$ is half the ${}^{V}T_{[11][01]}$ from Fig. 3.

Therefore, from similar formula to (C.10), $\left| S^{[01]}_{[21]} \right|$ is $1/\sqrt{2}$ of $\left| S^{[01]}_{[11]} \right|$.

Calculation for generated TM$_{11}$ mode can be made similarly. But, in this case the neighbourhood where the sector TM$_{11}$ mode degenerates with the TE$_{01}$ mode exists only on one side of z_0. Therefore, it is necessary to notice that the bounds of the integral about t in the similar formula to (C.9) are not $(-\infty, \infty)$ but $(0, \infty)$.

References

1) S. Iiguchi, Mode Conversion in the Excitation of TE$_{01}$ Waves in a TE$_{01}$ Mode Transductor (Rectangular→Sector Portion→Circular), *Rev. Electr. Commun. Labor. NTT*, Japan, 8, 7–8, pp. 324–334, 1960. 7–8.
2) G. Reiter, Generalized Telegraphist's Equation for Waveguides of Varying Cross Section, the Convention on Long-Distance Transmission by Waveguide, 1959-01.
3) L. Solymar, Spurions Mode Generation in Nonuniform Waveguide, *Trans. I. R. E.*, MTT-7, **3**, pp. 379–383, 1959-07.
4) G. N. Watson, A Treatise on the Theory of Bessel Functions, p. 229, 1922.

* * * *

REVIEW OF THE ELECTRICAL COMMUNICATION LABORATORY
VOLUME 9, NUMBERS 11-12, NOVEMBER-DECEMBER 1961

U.D.C. 621.315.2:621.315.616.9]:621.395.73:771.5

Foamed Polyethylene Insulated City Cable*

Mitsuru ROKUNOHE†

This report clarifies the resarch on the development of foamed polyethylene insulated multi pair city cable with fine conductors explaining a series of studies from the design theory of the city cable and the improvement of the manufacturing technique to the trial manufacture of the cable and the field tests of it.

Introduction

The increasing demand for telephones has been getting greater year after year, and this tendency is especially remarkable in and around great cities. In these urban areas, many ducts with accommodation for 0.4 mm 2,400 pair paper insulated cable have been laid. But now nearly all of these ducts have been filled with cables, and so without building new ducts, the accumulated demand cannot be satisfied. In these areas, what is worse; transportation is prosperous and tall buildings are densely massed. As a result, it costs very much to increase the number of ducts, and sometimes it is nearly impossible.

In this case, there is no other way of answering the demand than to replace the existing cables with new ones which enable the duct to provide service to a larger number of subscribers. Even when it is possible to establish new ducts, the replacement method is preferable, because by increasing the number of pairs of cables the cost of the duct per subscriber can be lowered.

A fairly large amount of copper is required for the production of cable lines. Above all more than half of it is used for city cable lines. Therefore, the amount of copper per subscriber is decreased by making the conductor for the city cable finer, then the cost of the cable is significantly lowered, and it is possible to meet a greater demands.

These are the reasons why the city cable with finer conductor and multiple pairs is necessary and desirable.

Moreover, in parallel with this research on the cable, other research on the development of telephone sets and telephone switching equipment was undertaken at the Electrical Communication Laboratory. Owing to the study, new types of telephone set and cross-bar telephone switching system, far more excellent in gain and current sensitivity than those in existence, were developed. As a result, it proved possible to increase the distribution of transmission loss to city cables and to raise the tolerance of line resistance. This did much toward the promotion of the author's researches on the city cable.

Under the above-mentioned demands and circumstances, the researches on the development of this foamed polyethylene insulated cable with fine conductors and multi-pairs, have been carried out for about eight years since 1954. Thanks to the researches, this city cable was newly developed, and is now specified as "PEF city cable." The characteristics of this city cable are as follows.

1) The diameters of conductors are reduced

---

* MS in Japanese received by the Electrical Communication Laboratory on October 9, 1961. Originally published in the *Kenkyû Zituyôka Hôkoku* (*Electrical Communication Laboratory Technical Journal*), N.T.T., Vol. 11, No. 1, pp. 1–95, 1962.

† Outside Plant Section.

by one size, i.e. from the 0.4, 0.5, and 0.65 mm diameter in existence to 0.32, 0.4, and 0.5 mm respectively.

2) The insulation is quite different from that of the existing cable. That is; the conductor of this new cable is covered with thin polyethylene layer with very fine independent bubbles.
3) As a result of reducing the space coefficient of pair conductor compared with the existing cable, a remarkable increase of the number of pairs has been accomplished by the use of finer conductors and thinner insulation. In other words, the maximum number of pairs of existing full size cable for 75 mm dia. duct was 2,400, but it has been raised at a stroke to 4,000.
4) Because the insulation of the cable conductor is made of plastic, there is no

Table 1 COMPARISON OF PROPERTIES OF PEF CITY CABLE AND EXISTING CITY CABLE

		PEE city cable	Existing city cable
Diameter of conductor	mm dia.	0. 32, 0. 4, 0. 5	0. 4, 0. 5, 0. 65
D.C. resistance	Ω/km	216 (0. 32 mm dia.), 139 (0. 4 mm dia.), 88. 7 (0. 5 mm dia.), 52. 5 (0. 65 mm dia.)	
Insulation construction		Foamed polyethylene insulation by coating method	paper-tape wound sideways Paper-pulp insulation
Thickness of insulation	mm	About 1/4 of the conductor diameter	——
Degree of foaming insulation	%	20 - 30	——
Size of foams in insulation	mm	0. 01 - 0. 02	——
Effective specific dielectric constant of insulation		2. 0 - 1. 9	——
Equivalent specific dielectric constant of circuit		1. 6 - 1. 5	1. 8 - 2. 0
Break-down voltage between the twisted strands (0. 4 mm dia. conductor)	kV	about 4 (0. 5 mm dia.)	about 1 (0. 4 mm dia.)
Electrostatic capacity of side-circuit	mμF/km	50±5	
Electrostatic coupling between side-circuit	pF/500 m	Max. below 800 Mean below 150	Max. below 16,00 Mean below 300
Attenuation at 1. 5 kc/s	dB/km	2. 8 (0. 32 mm dia.), 2. 1 (0. 4 mm dia.), 1. 8 (0. 5 mm dia.), 1. 3 (0. 65 mm dia.)	
Space coefficient of conductor pair		2. 60 - 2. 56	3. 0 - 2. 78
Maximum number of pairs that can be laid in a 75mm dia. duct		4000 (0. 32 mm dia.)	1000 (0. 65 mm dia.)
		2400 (0. 4 mm dia.), 1800 (0. 5 mm dia.)	

fear that a failure such as a whole circuit grounding may be caused by flooding over a large area.

5) Concerning near-end cross talk, the new city cable is better than existing cable more than 6 dB.

The circuit electrostatic capacity of the new city cable is the same as that of the old one; therefore, when the conductor diameter is 0.4 or 0.5 mm, the attenuation constant of the new cable is the same as that of the existing paper-insulated cable. Table 1 shows a comparison of characteristics of the two city cables. Fig. 1 shows a comparison between every type of 0.32 mm-conductor-diameter foamed polyethylene insulated city cable with 20 or to 4,000 pairs and the paper-insulated lead-sheathed existing city cable with the finest conductor and the greatest number of pairs, i.e., with 0.4 mm diameter conductor and 2,400 pairs.

The author invented the manufacturing method of the new cable strand and conducted the research on manufacture of the new cable. Of course, at the same time, not only a new theoretical analysis necessary for designing cable but also a study on the methods of cable connection was made by author's team. Furthermore, field trials of methods of laying and connection of cables were made repeatedly by us in order to confirm the practicability of the new cable. The regular observation has been conducted for the past three years on some of these lines but there have been no reports of any line failures.

1. Design of the New City Cable

As mentioned above, the conductors of city cables in existence are covered with absorptive paper; therefore the circuits cannot completely be protected from grounding failures due to flooding. Accordingly, if the present type of insulation is used, an increase in the number of pairs in the cable will never fail to result in the expansion of the range of subscribers who will sustain outages due to grounding failures. Moreover, the space coefficient per pair conductors of existing city cables is apt to increase inverse proportion to the conductor diameter. If the present type of insulation is retained, the use of finer conductor will make the space coefficient larger than in the present cable with 0.4 mm conductors. Therefore, the gain from the increase of pairs owing to the adoption of finer conductors will be decreased.

For these reason, the finer conductors of

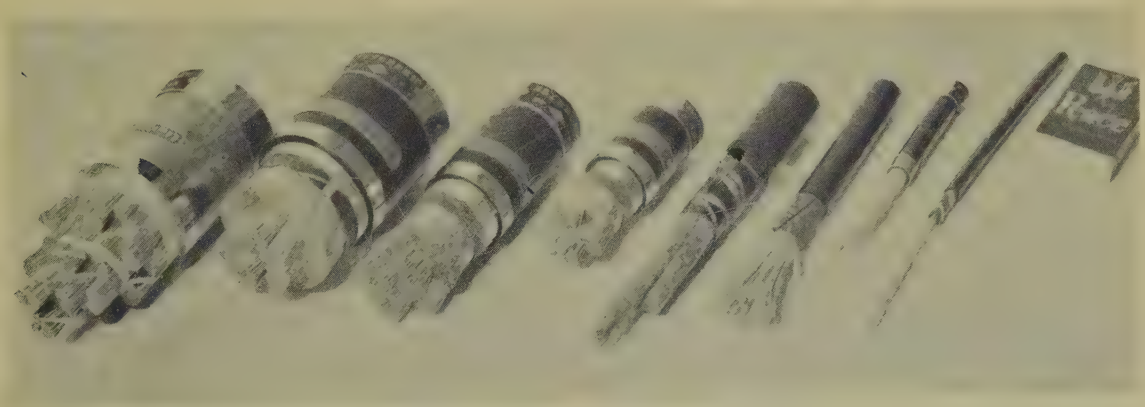

Fig. 1—From left; 0.4 mm 2,400-pair existing paper-insulated lead sheathed cable.
0.32 mm 4,000-pair PEF unit cable. 0.32 mm 1,600-pair PEF unit cable.
0.32 mm 1,000-pair PEF unit cable. 0.32 mm 400-pair PEF unit cable.
0.32 mm 200-pair PEF layer cable. 0.32 mm 100-pair PEF layer cable.
0.32 mm 20-pair PEF layer cable.

the new city cable with multiple pairs to be developed in the future must be insulated by a thin plastic layer whose effective specific dielectric constant is smaller. This is necessary not only in order to present the growth of the space coefficient per pair and raise the benefits of the increase of pairs due to the adoption of finer conductors, but also to protect the subscribers from circuit failures caused by flooding. In addition, if the sensitivity of the telephones is improved, the permissible range of circuit loss will be extended, and the cable conductor can be made still finer. In this case, to keep the transmission quality as it is, the near-end cross talk of the circuit, i.e. the electrostatic coupling between circuits, must be improved as much as the circuit loss is increased. Considering the above-mentioned necessities, a study was carried out on the design theory of the insulating structure of conductors, under the conditions that the circuit electrostatic capacity of the cable is to be kept at the rated value of existing city cable. The purpose of the study is to clarify theoretically the relation between the electrostatic capacity of the circuit, the thickness of its strand insulation, and the effective specific dielectric constant; also the relation between the electrostatic coupling between circuits and the deflection of strand insulation.

First of all, the reason why 0.32 mm copper line was selected as the minimum conductor size for the foamed polyethylene insulated city cable will be outlined.

Because of the modernization of telephone sets, the permissible loss for the city cable and telephone switching equipment was increased by about 10 dB, without changing articulation. And it was clarified that about 6 dB of the increased permissible loss could be distributed among subscriber's cables. That is to say, the distribution of the circuit loss between the subscriber and telephone switching equipment will be increased by about 3 dB, being changed to about 7 to 10 dB. City cable is used only for the transmission of voice frequency band, and so its attenuation is in inverse proportion to the conductor diameter of the cable, when the electrostatic capacity of circuit is fixed. In the existing city cable, three conductor diameters sizes are adopted, i.e. 0.4, 0.5, and 0.65 mm. But regardless of the diameter, the circuit electrostatic capacity of the cable is determined by specification to be 50±5 mμF/km. Accordingly, if under these circumstances the circuit electrostatic capacity of the city cable with finer conductor is presupposed to be decided by the rating of the existing cable, then as shown by the above relation between attenuation and conductor diameter, the diameter of the new cable can be reduced to 70% of that of the existing cable. In other words, under the above conditions of articulation equivalent loss telephone circuits (A.E.N.) increase, the conductor diameter of the new cable can be reduced from the existing 0.65, 0.5, and 0.4 mm sizes to 0.46, 0.35, and 0.28 mm respectively.

Subsequently, as the telephone switching equipment is changed to crossbar type, the current sensitivity of the relays is increased, and so the permissible limit of the d.c. resistance of the circuit between the subscriber and the switching equipment can be raised to 1,500Ω from 1,000Ω. Therefore, if the length of a subscriber's circuit is left unchanged, the conductor of the new city cable can be finer, i.e. about 80% of that of the existing cable. That is to say, due to the adoption of crossbar switching equipment, the conductor diameters of the subscriber's cables can be reduced to 0.52, 0.4, and 0.32 mm from the sizes of cables now in existence.

From the two conditions shown above and JIS rating, when the new type telephone sets and crossbar switching equipment is introduced to the city network, the cable conductor diameters can be reduced by one size, to 0.5, 0.4, and 0.32 mm. That is, the minimum conductor diameter can be reduced to 0.32 mm from the 0.4 mm size now adopted.

Next, a brief description of the design for the insulation construction of the fine conductors chosen will be made.

Figs. 1 to 5, and Table 2 show the results of this research. In Fig. 2 are represented C_s—the electrostatic capacity in side circuits of the star quad city cable with multi-pairs, and

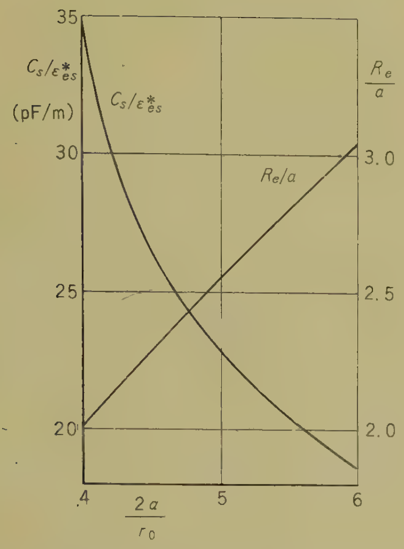

Fig. 2—Electrostatic capacity of side-circuit, diameter of equivalent electrostatic shield.

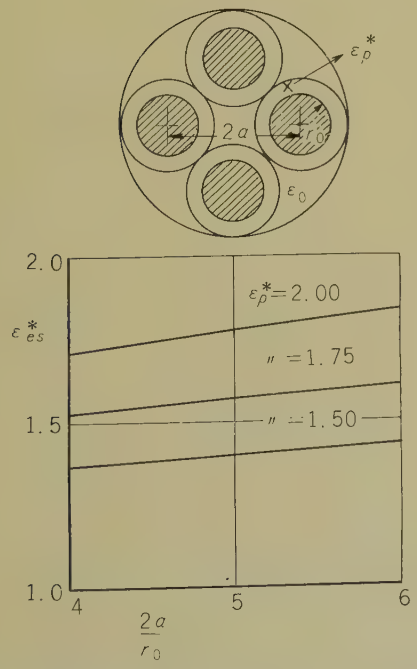

Fig. 3—Equivalent specific dielectric constant of side-circuit.

R_0—the radius of the equivalent electrostatic shield of the same cable, as a function of $(2a)/r_0$, i.e. the ratio of interval between the pair condnctor axes to the conductor radius. In the figure, the electrostatic capacity is show after division by ε_{es}*—specific dielectric constant—and the radius of the equivalent shield is expressed after division by $2a$—the interval between pair conductor axes. In this case, the cable space caused when conductor has been removed from the cable is assumed to be filled with uniform dielectric of specific dielectric constant equal to ε_{es}*—equivalent specific dielectric constant of side-circuit of a single shielded star quad such as shown in cross section in Fig. 3. Besides the cross section, the figure shows the equivalent specific dielectric constant of the quad as a function of ε_p*—effective specific dielectric constant of strand insulation—and the ratio of the interval between pair conductor axes to the conductor radius.

Fig. 4 shows the relation between f—the degree of foaming of strand insulation—and the effective specific dielectric constant, which has been derived from Rayleigh and Wagner's theoretical equation. By using these results, the thickness of strand insulation necessary for equalizing the electrostatic capacity of side

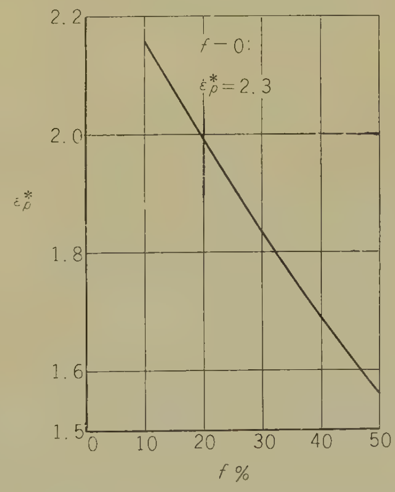

Fig. 4—Degree of foaming and effective specific dielectric constant.

Table 2

THEORETICAL VALUES OF INSULATION THICKNESS NECESSARY TO MAKE SIDE-CIRCUIT ELECTROSTATIC CAPACITY 50 mμF/KM

f% / $2r_0$ mm	20	30
0.32	0.07	0.08
0.4	0.09	0.10
0.5	0.10	0.12

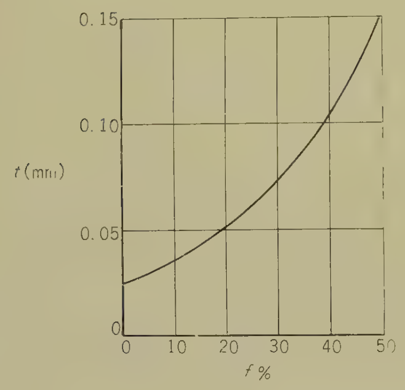

Fig. 5—Thickness of the insulation, necessary to withstand 1,000 V d.c.

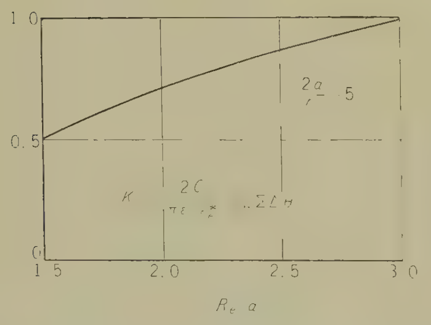

Fig. 6—The theoritical value of the coefficient S_θ to express the relation between the electrostatic coupling of side-circuits and the arrangement of conductors.

circuits of the cable to 50 mμF/km i.e. to the rated value of the capacity of the existing cable, was obtained. The results are illustrated in Table 2.

In Table 2, the degree of foaming is 20 to 30%. If the foaming is greater, the necessary thickness becomes smaller, and its mechanical strength is lowered so much that the insulator becomes too weak to endure such process stages as cable manufacture, laying and connection, or to endure the telephone hook pulse voltage. The thickness of polyethylene insulation which will with stand 1,000 V d.c. was obtained as a result of experiments on test samples with various degrees of foaming, and the results are shown in Fig. 5. It is found, from Fig. 5, that with the thickness in Table 2, the insulation is strong enough to resist voltage breakdown even when the conductor diameter is 0.32 mm.

Concerning the electrostatic coupling between the side-circuits, S_θ—the new coefficient that relates the distortion of conductor arrangement to the electrostatic coupling between side-circuits, which becomes as shown in Fig. 6 when the multi-pair cable quad has been replaced by the single shielded star quad of Fig. 2—was theoretically obtained. Then by using the value, the permissible limit of deflection necessary to keep the coupling below half the rated value of the existing city cable, was obtained. Next, it was expressed in the form of the ratio of minimum thickness to the maximum thickness of the strand on the same section. In this way, the design value of about 0.8 was obtained. As the coupling, in this case, was adopted the maximum value proportional to the cable length. As to the existing city cable, its rated value is 1,600 pF/500 m.

The result of the selection of conductor diameters as above or of the design for insulation construction was used for the study of manufacture of cable treated later. In this way, the new foamed polyethylene insulated multi-pairs city cable with fine conductor has been made. Its conductor diameter is 0.32 mm, electrostatic capacity 50 mμF/km and electrostatic coupling below 500 pF/5000 m.

2. The Method of Manufacturing Cable Strand

As a result of researches described in Section 1, the conditions necessary for the new city cable with fine conductor were brought to light. Then it was examined whether or not some of the insulating constructions of the following existing cables can fulfill the above conditions. That is to say, various studies were made on the ribbon paper insulation and paper pulp insulation of the existing city cable; on the foamed plastic insulation by extruding method, applied now to the new toll cables; on the plastic insulation by extruding process applied to office cable etc. It was found that by any method in existence the manufacturing of a thin insulator with low effective specific dielectric constant for fine condnctor is very difficult. If the insulation construction is left unchanged, the purpose of increasing pairs cannot be fulfilled only by the adoption of finer conductor, and the cost rise due to the decrease in manufacturing speed and the ratio of operation is inevitable. As a result of these researches, instead of the existing method, a new method of manufacturing a thin insulator with low effective dielectric constant on a fine conductor by the coating of plastic solution was developed.

As generally known, the strand of the existing PEF toll cable is manufactured by extruding a compound of polyethylene and blowing agent. By this method, foams are caused when the analyzed gas of the blowing agent, produced and compressed under high temperature and pressure in the extruder, expands on the extrusion of plastic. On the other hand, the foamed insulation of the city cable conductor developed by this study is made by the following process: as coating (the solution of only polyethylene, polyethylene solution dispersed or solved blowing agent) –crystarization–heating. This coating method is essentially far more suitable for the manufucture a thin insulation than the existing method. And as described later, when polyethylene solution without blowing agent is used for coating, the size of foam is much smaller than it is when extrusion is adopted —so small that even in the case of insulation 0.1 mm thick, several independent foams can be piled up. Therefore, the insulation by this method is satisfactory for insulating fine conductors 0.32 mm in diameter.

This research was begun with two stages of fundamental experiments lasting for about two years. Subsequently, on the basis of the result, was trially made the experimental apparatus on a small scale, by which the compound of polyethylene and blowing agent can successively be made into the foamed insulator on the conductor with the help of toluene solution. With this apparatus, further experiment was continued. Next, this apparatus was enlarged to an intermediate scale, and another experiment was made with this apparatus. In this stage, blowing agent was used at first, but in the midst of examination it was found that much better insulation was obtained when no blowing agent was used, and so the method was changed. As a result of the above experiments, a method of manufacturing foamed polyethylene insulation which was unparalleled in thickness and included very fine independent foams was developed. Like this, the strand of fine conductor cable that can satisfy the necessary conditions has become obtainable. Now it can be said confidently that application of fine conductor and multi-pairs to the city cable will be accomplished to the full.

This technique was removed at once to the three wire corporations—Furukawa, Sumitomo, and Fujikura. These factories have already been equipped with plants for foamed polyethylene insulated cable conductor on a scale large enough for mass production, which are to be operated before long.

Figs. 7 to 9 show how the above plant was developed. That is to say, Fig. 7 represents the plant used for the fundamental experiment, and Fig. 8 the plant on an intermediate scale used for regular experiments. Fig. 9 shows an example of the plants equipped in wire factories at present. This plant can produce foamed polyethylene insulation on ten conductors 0.32–0.65 mm in diameter simultaneously at the speed of 30–60 m/min.

Fig. 7—The plant of polyethylene insulated cable conductors used for the fundamental experiments.

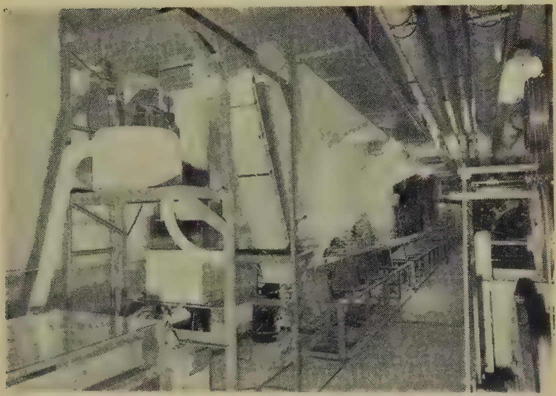

Fig. 8—The plant of the conductors used for the factor experiments.

On the basis of Fig. 10, the construction and facility of the coating will be described. As shown in the figure, the hard copper wire is softened by annealing at part ②; after washing—drying—preliminary heating at ③ and ④, it is led to the coating tank at ⑤. Different from the ordinary soak-in style, this tank is an intermediate type between the soaking and the extruding, where the core is put out and the outer diameter is adjusted with a nipple and dice. This tank is heated and kept warm by over-heated steam, and filled with polyethylene solution of toluene or xylene for coating use. This solution is painted over the surface of bare annealed copper wire. Then at the part ⑦, the solvent in the coating is excluded by evaporation, and the polyethylene is crystallized. This is passed through the short electric furnace ⑧ warmed to a high temperature, and as a result polyethylene insulation with fine independent bubbles is obtained. In order to make foamless insulation by this plant, the solvent has only to be excluded by degrees by heat drying lest the spherulite should be caused. In this way, without using blowing agent, polyethylene insulation whose thickness is 0.06–0.18 mm and degree of foaming 0–50%, is obtained.

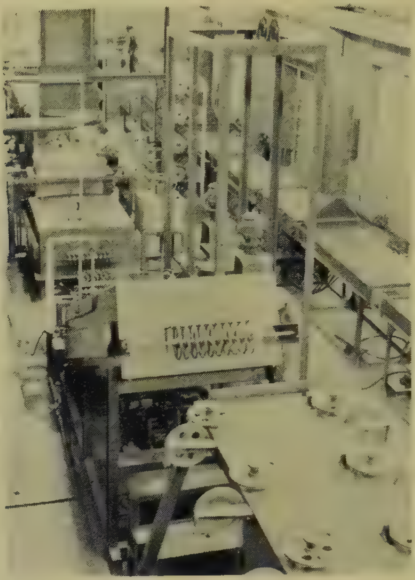

Fig. 9—The plant of PEF city cable conductor on a large scale, equipped in a wire corporation.

This technique for manufacturing foamed polyethylene insulation was discovered and improved through the following processes. During the experiment in which blowing agent was used, it was found that if the drying temperature of the solvent in the coating is lowered, fine independent foams (0.01–0.03 mm in diameter) were caused among larger foams (over 0.05 mm in diameter), and that even if the blowing agent was decreased

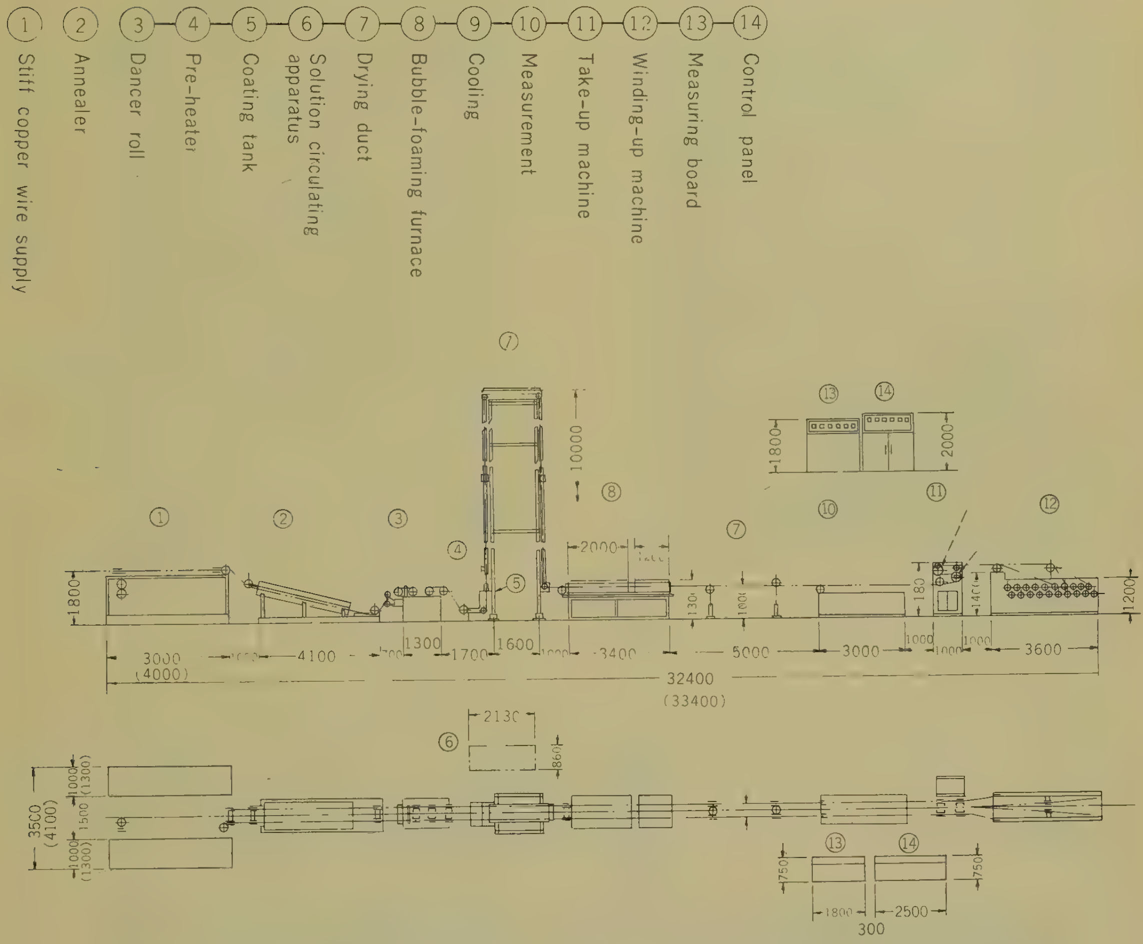

Fig. 10—The construction of the plant of PEF city cable conductor.

to lower the degree of foaming, the degree was not lowered in proportion to the decrease, but many fine foams were scattered as before.

On the basis of these experiences, experiment was repeated by normal temperature drying method, without using blowing agent, and as a result it was clarified that blowing agent is not necessary for the manufacture of foamed polyethylene insulation. Besides, the insulation obtained by this method is much better in every way than that produced when blowing agent was used.

From these observations, the process through which foams are produced is considered as follows. According to the results of our observation, when toluene solution of Alathon

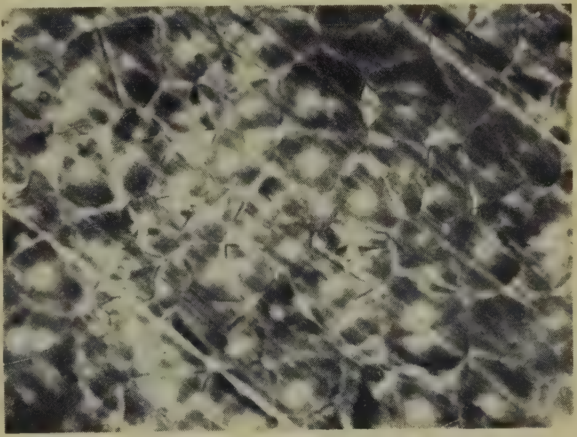

Fig. 11—An instance of polyethylene spherulites.

10 polyethylene (Du Pont Chemical Co., U.S.A.) is used for coating, the spherulites of polyethylene, i.e. the crowded crystals of polyethylene, are regular polyhedrons of several microns in diameter, as shown in Photo 5. In it, some stripes are clearly found. When such spherulites are produced, toluene is put out to the surfaces and some of it is evaporated away. On the other hand, air is absorbed to the boundaries. For instance, the spherulites are piled up like a stone wall (Fig. 11). Next, in this state when they are suddenly heated and melted, the air and toluene vapour which have failed to get away at that time, are enclosed in the melted polyethylene. It is thought that, foamed polyethylene insulation is produced in this manner. This reasoning is proved by the following facts.

1) The density of foams is low near the conductor, i.e. where gas pressure is high, or near the boundary, i.e. where the resistance is lower against the gas leaving away.
2) The size of spherulite is directly related to that of the foam.
3) When the boiling point of the solvent is lower than the melting temperature of the plastic, the foams do not become spherical but varied in shape.

Thus, without using any blowing agent, foamed insulation can be made on an industrial scale by using the growth of spherulites. This success is matchless in the world, to say nothing of Japan.

3. Characteristics of the Strand

The size of foams: In foamed polyethylene insulation, even when the thickness and the degree of foaming are fixed, the smaller the foam becomes, the higher its mechanical strength and break-down voltage grow, and the density of pinhole generation is lowered. For this reason, in the course of study of the new manufacturing method of strands, every attention was paid to decreasing the size of the foams.

In relation to the method by the use of blowing agent, nearly all the manufacturing factors were studied, i.e., the minimization of the particle of blowing agent. the selection of solvent and plastic, the viscosity of paint, the method of drying solvent, the temperature

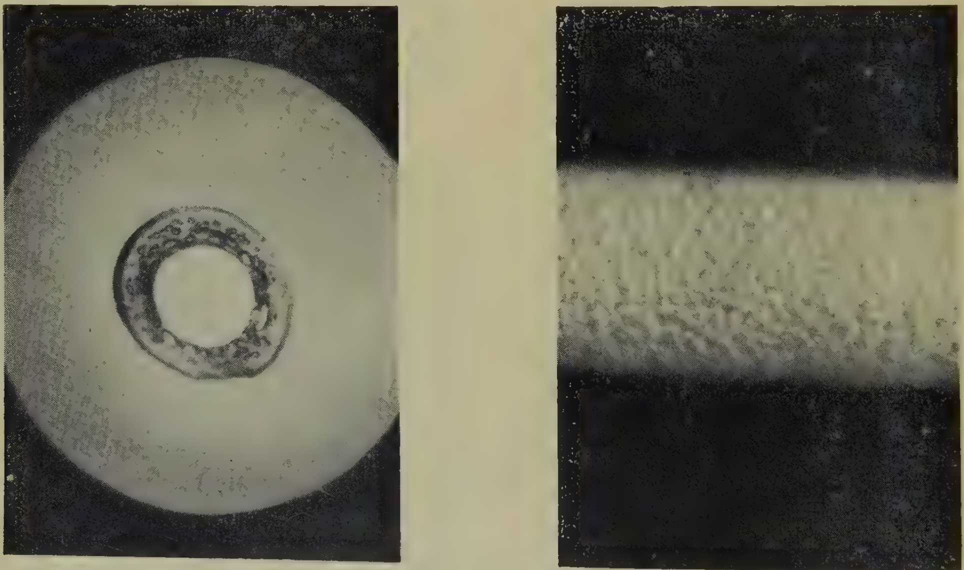

Fig. 12-A—The cross section (left) and side-view (right) of foamed polyethylene insulation by coating method without using blowing agent; conductor diameter is 0.32 mm.

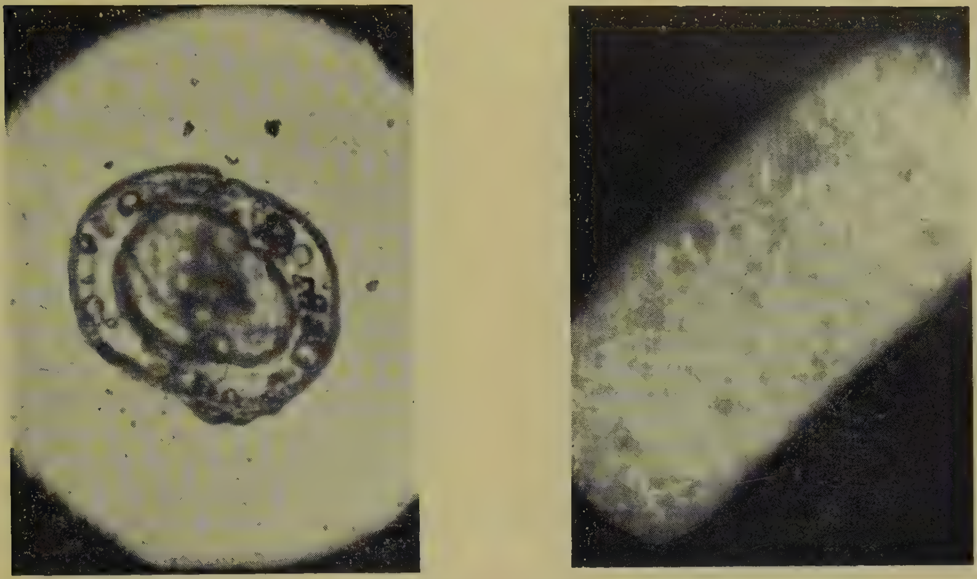

Fig. 12-B—The foamed polyethylene insulation by coating method with the use of blowing agent (cross section—left, and side-view—right) conductor diameter is 0.32 mm.

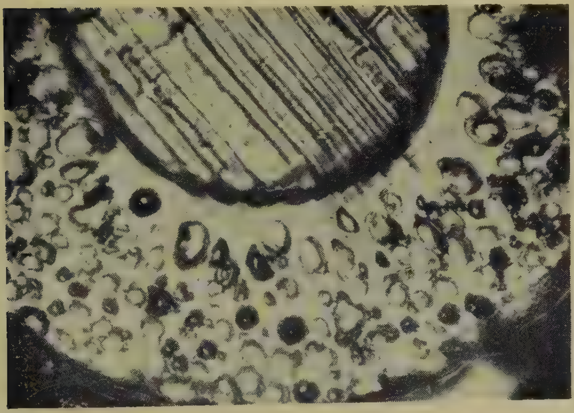

Fig. 12-C—The cross section of foamed polyethylene insulation by the existing extruding method; conductor diameter is 0.9 mm.

and length of the electric furnace, and the taking-up speed of strands. For all this, the size of independent foam in the insulation could not be reduced below 0.05 mm diameter. But during this study, it was found that much smaller foams of the same size were easily obtained if blowing agent was not used, and by adoption of this method, the study was continued further. As a result, a method of manufacturing strands insulated by the coating of very warm solution of polyethylene was developed as mentioned before. Fig. 12-A shows the cross section of the 0.32 mm strand insulation produced by this method. As compared with the insulation in Fig. 12-B made by using blowing agent, this fact shows that the new method is far more suitable for the manufacture of insulator whose thickness is thinner and whose effective specific dielectric constant is lower. For convenience is comparison, the foamed polyethylene insulation due to the extruding method in existence is shown in the photo of Fig. 12-C.

Foaming degree and effective specific die-

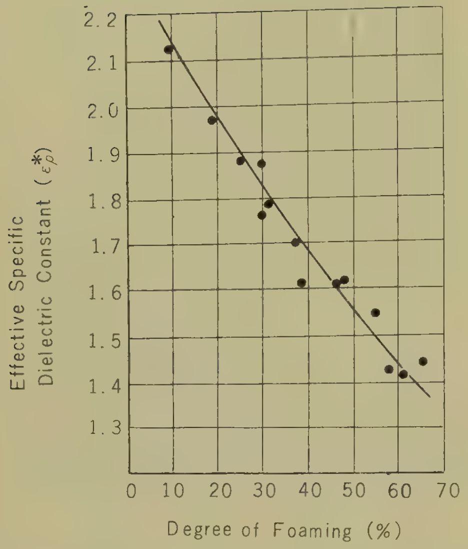

Fig. 13—The degree of foaming and effective specific dielectric constant of foamed polyethylene insulation by the coating method.

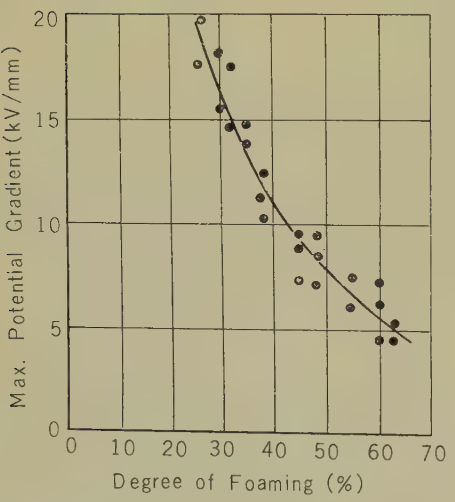

Fig. 14—The degree of foaming and max. potential gradient of foamed polyethylene insulation by coating method.

lectric constant: Fig. 13 shows the effective specific dielectric constant of test piece of every degree of foaming. The test pieces are foamed polyethylene insulation made by using no blowing agent. The curve in the figure shows the dielectric constants of insulation with spherical foams uniformly scattered, which were calculated through Rayleigh and Wagner's equation. Owing to the unevenness of the insulation surface, the different sizes and uneven distribution of foams, and to the uneven thickness, the experimental values vary, but correspond comparatively well to the theoretical values. So it can be said reasonable to have used this theoretical equation of Rayleigh and Wagner.

Breakdown voltage: Fig. 14 shows the experimental values of maximum potential gradient of the above-mentioned test pieces due to submerged load method. This maximum potential gradient becomes lower in proportion to the size of foams. The values for test pieces made by using blowing agent are less than half the values of those in the figure.

In these strands, so-called pinholes are produced owing to the undesired mixture into the paint and to some mechanical cause in the manufacturing process. And in the cases of accidents, e.g. when water has rushed into the cable, grounding trouble occurs to the strand with pinholes. As a result of every effort to decrease pinholes, there is now no strand that has more than one pinhole per 1,000 m length at 300 V d.c. test voltage, even when considered together with insulator breakdown due to striking deflection.

Concerning the strand of 0.32 mm conductor diameter, coating thickness of 0.08 mm, and foaming degree of 30%, the breakdown voltage of the twice-twisted strand was found about 3.6–4.0 kV.

Mechanical strength: As a property important in every manufacturing process from strand to cable, in the laying of cable or in the joint process, the mechanical strength of strand insulation must be given.

Fig. 15 shows some results of the tensile strength test upon the same test pieces as above. The degree of elongation is represented by the ratio of the elongated length to the original length; and the tensile strength by the load per unit section when the test piece was torn off. In the case of the PEF city cable insulation with conductors of 0.32, 0.4, 0.5, and 0.65 mm, the tensile loads of the test pieces with degree of foaming of about 25%, were about 60, 90, 130, and 230 gm respectively.

4. The Construction of Cable

The method of insulating fine conductor with a thin polyethylene layer containing ex-

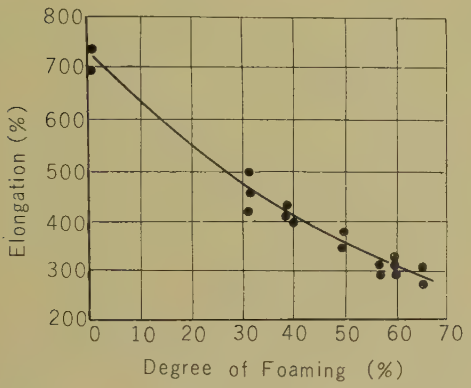

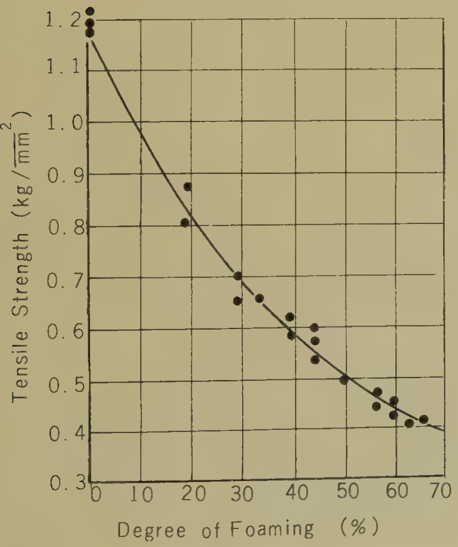

Fig. 15—The degree of foaming, elongation and tensile strength of foamed polyethylene insulation by coating method.

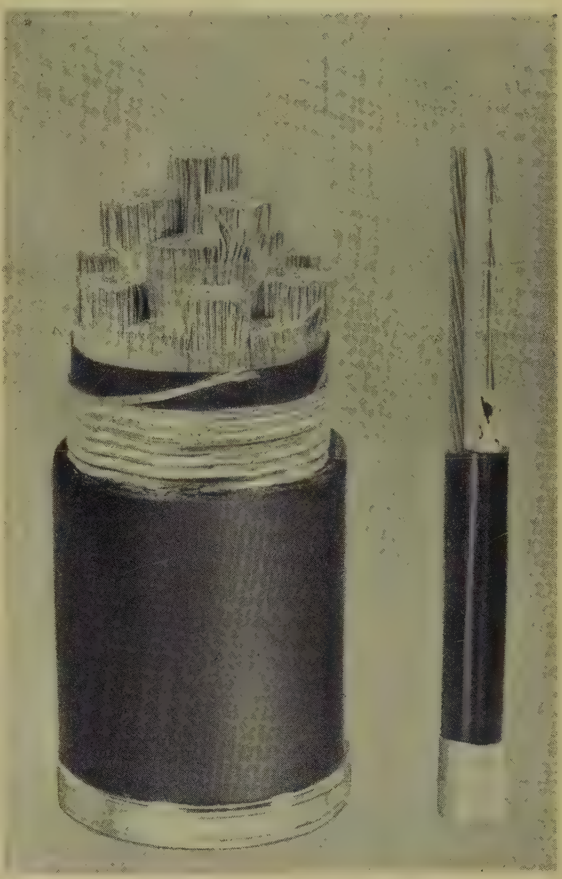

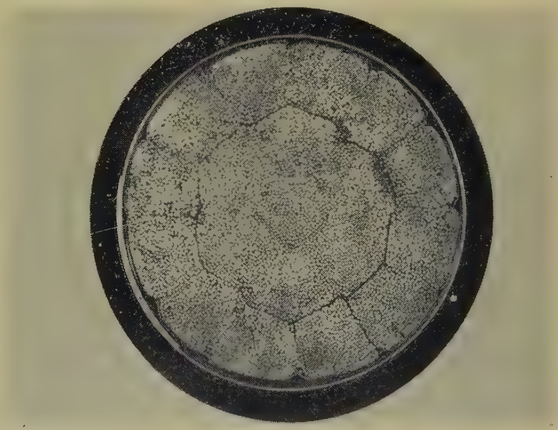

Fig. 16—Construction of the PEF city cable. Unit types, upper left and bottom; layer type, upper right.

tremely fine independent foams by using heated polyethylene solution mentioned previously was developed enough for us to expect the possibility of the industrial production of satisfactory strands of fine-conductor multi-pair cables. As a result, for the purpose of technique guidance of strand manufacture and joint research on the method of manufacturing cable, a circle was organized with the assistance of the three wire corporations mentioned before. Like this, the cables were experimentally produced and study was carried out on them. It was a success.

As already described, the new multi-pairs city cable with fine conductor was specified by the Nippon Telegraph and Telephone Public Corporation, and is now named "PEF city cable". Like the existing city cables, the new city cables are divided into two kinds, i.e. layer type cables to be used as aerial cable and unit type cables mainly to be used as underground cable. As shown in Fig. 16, the

Table 3 ARRANGEMENT OF QUADS AND UNITS

	Nominal number of pairs	Number of quads of each layer						Actual number of pairs
		Center	1st layer	2nd layer	3rd layer	4th layer	5th layer	
Layer cable	20	2	8					20
	30	4	11					30
	50	3	8	14				50
	100	4	10	16	21			102
	200	2	8	14	20	26	32	204

	Nominal number of pairs	Number of units of each layer				Actual number of pairs
		Center	1st layer	2nd layer		
Unit cable	400	4			102	408
	600	1	5		//	612
	1000	2	8		//	1020
	1400	4	10		//	1428
	1800	1	6	11	//	1836
	2400	3	9		204	2448
	3200	1	5	10	//	3264
	4000	1	7	12	//	4080

layer type cable is constructed as follows. The core of this type is made of a necessary number of quads twisted together, and mylar tape with which the quads are covered. This core is wrapped in two-fold vinylchloride-covered cotton tape which is to serve as the adiabatic layer of the cable core in extruding process. And then the core, to which aerial stay is attached, is covered, by an extruding process with black polyethylene. This type of cable, is a self-supporting type.

The unit type cable is constructed as follows. 51 or 102 quads are twisted together into a nominal 100 or 200 pair unit. Then the necessary number of units collected together are wrapped in mylar tape. To the cable core made in the above-described manner, rubber tape is longitudinally attached for adiabatic purposes. Next corrugated Al protector is wrapped for the purposes of electrostatic shielding and of shaping. And then it is covered by an extruding process with black polyethylene. This type is the so-called alpeth type cable.

Concerning both the types, the range of the number of pairs, and the arrangement of quads and units are shown in Table 3. As to the strand insulators of the new city cable, they are, as in the case of existing paper-covered cable, colored red, blue, and white. Strands of the same color are made into a pair; three kinds of quads are made by changing the combination of the pair colors; by the combination of these quads, and the ordinary quads of every layer in the cable or in the unit are made distinguishable from the tracer quads. Besides, in the same way, the ordinary units of every layer in the unit cable are made distinguishable from the tracer units.

The conductor diameters of the PEF city cables are classified into four kinds, i.e. 0.32, 0.4, 0.5, and 0.65 mm. The thicknesses of their foamed polyethylene insulation is respectively about 1/4 of the conductor diameters, and their degree of foaming is about

Table 4 LIST OF PEF CITY CABLES

Conductor diameter (mm)	Type	Nominal number of pairs	Cable core diameter (mm)	Outer diameter of cable (mm)	Weight (kg/m)	Existing paper-insulated lead city cable	
						Outer diameter (mm)	Weight (kg/m)
0.32	Layer type	20	about 7	about 10	about 0.09		
		30	8	11	0.11		
		50	10	13	0.15		
		100	13	16	0.25		
		200	17	20	0.45		
	Unit type	400	21	25	0.80		
		600	26	30	1.16		
		1000	32	38	1.8		
		1400	37	44	2.6		
		1800	42	49	3.3		
		2400	49	56	4.3		
		3200	56	64	5.8		
		4000	62	70	7.0		

Table 4

Conductor diameter (mm)	Type	Nominal number of pairs	Cable core diameter (mm)	Outer diameter of cable (mm)	Weight (kg/m)	Existing paper-insulated lead city cable	
						Outer diameter (mm)	Weight (kg/m)
0. 4	Layer type	20	8	11	0. 12	about 8	about 0. 36
		30	10	13	0. 16	9	0. 44
		50	11	14	0. 20	11	0. 57
		100	15	18	0. 35	15	0. 86
		200	20	23	0. 65	19	1. 42
	Unit type	400	26	30	1. 2	27	2. 78
		600	30	36	1. 8	32	3. 78
		1000	39	46	2. 8	41	5. 75
		1400	46	53	3. 8	47	7. 56
		1800	52	59	5. 0	53	9. 55
		2400	60	68	6. 7	62	12. 73
0. 5	Layer type	20	9	12	0. 16	10	0. 45
		30	11	13	0. 21	11	0. 56
		50	13	16	0. 30	13	0. 74
		100	17	20	0. 55	17	1. 14
		200	23	27	1. 02	24	2. 00
	Unit type	400	32	36	1. 9	33	3. 88
		600	37	44	2. 8	40	5. 46
		1000	48	55	4. 3	50	8. 33
		1400	57	65	5. 9	59	11. 58
		1800	62	70	7. 8	67	14. 73
0. 65	Layer type	20	12	15	0. 25	12	0. 60
		30	13	16	0. 31	14	0. 75
		50	16	19	0. 55	16	1. 02
		100	22	25	1. 10	22	1. 80
		200	30	34	1. 7	30	3. 00
	Unit type	400	42	47	3. 0	42	5. 94
		600	50	57	4. 5	51	8. 40
		1000	62	70	7. 2	65	13. 80

20–30%. The list of these city cables is shown by Table 4. In Photo 1, for comparison with every type of 0.32 mm PEF city cable with 4,000–20 pairs, is shown the existing paper-insulated city cable with the finest conductor, i.e. 0.4 mm in diameter, and with the greatest number of pairs, i.e. 2,400 pairs.

The space coefficients of pair conductors were calculated from the measured values of the outer diameters of experimental cable cores, and are shown in Table 5 and Fig. 17. For the convenience of comparison, the values of existing paper-insulated city cables, are given. As shown by these values, the space coefficient of pair conductors is much smaller than that of any existing cable. From this fact, it is understood what an important part the foamed polyethylene insulator made by the coating method played for the increase of pairs. As shown in Table 4, by the decrease of this space coefficient, city cables with 4,000 pairs—so many pairs as to be unprecedented—have been obtained.

Table 5

SPACE COEFFICIENT PER PAIR DUE TO MEASURED VALUES

Cable / Conductor diameter (mmφ)	PEF city cable	Paper-insulated lead-sheathed city cable
0.32	2.87	
0.4	2.85	3.0
0.5	2.85	2.78

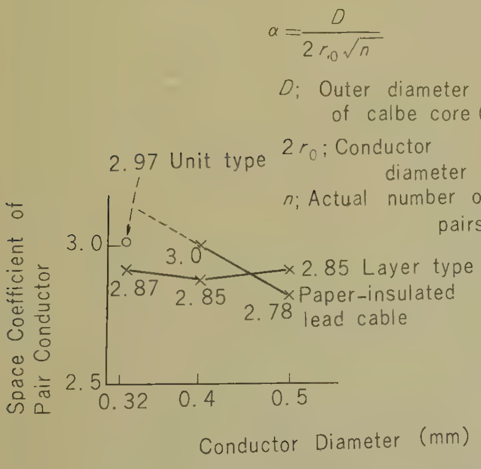

Fig. 17—Space coefficient per pair of PEF City Cable obtained from measured values.

5. Characteristics of Cable

The PEF city cables with 0.32–0.65 mm conductor diameters and with 20–4,000 pairs were experimentally made several times in accordance with the following design:

Thickness of strand insulation;
about 1/4 of conductor diameter
Degree of foaming; about 20–30%
Permissible deflection in thickness;
below 4/5

As a result, the electrostatic capacity of the side-circuit of the cable has been equalized to that of existing city cable, and by decreasing the electrostatic coupling between side-circuits to less than half the rated value in existence, the near-end cross-talk of the cable has been improved by over 6 dB. What is better, it has been proved that this strand satisfies the conditions as to the electrostatic capacity and electrostatic coupling, and that it has voltage durability strong enough to endure the hook-pulse of telephone and mechanical strength enough to endure the manufacturing processes after quad twisting.

Conductor resistance and insulation resistance: The whole span of the coating plant from the unit supplying of bare copper wires to the unit which winds up cable strands was so long, and the manufacturing speed was so high, that elongation of the copper wire was feared. But the variation of the diameter was kept, as shown in Table 6, far below the allowable error of JIS rating —i.e. far bellow ±0.01 mm—by decreasing the friction of every part of the plant in order to smooth the operation. The elongation of the copper wire in the cable manufacturing process after coating, was very small, as seen from the resistance values in Table 6. Eeah of the maximum values of the conductor resistance of the completed cable was below the maxi-

Table 6

THE CONDUCTOR DIAMETER OF EXPERIMENTAL PEF CITY CABLE STRAND AND THE CONDUCTOR RESISTANCE OF THE CABLE

Nominal conductor diameter (mm)		Strand daimeter (mm)	Conductor resistance of cable (Ω/km)				Max. value of D.C. resistance of JIS normal diameter (Ω/km)
			20 pairs	200 pairs	1000 pairs	4000 pairs	
0. 32	Mean	0. 321	212. 3	213. 8	213. 0	224. 2	221
	Max.	0. 325	214. 1	217. 2	221. 4	242. 0	
	Min.	0. 318	210. 2	212. 0			
0. 40	Mean	0. 401	137. 6	139. 0	Note: The cables were made at three corporations in November, 1960.		141. 4
	Max.	0. 403	138. 1	141. 2			
	Min.	0. 398	136. 8	137. 0			
0. 50	Mean	0. 500	87. 1	88. 4			89. 6
	Max.	0. 503	87. 5	89. 5			
	Min.	0. 499	86. 9	87. 8			

mum value of each normal conductor diameter of JIS rating. For the cable with 4,000 pairs, only the maximum value seemed above that of the rating, but it has proved due to the twisting process of units, and now this has been corrected.

The minimum value of insulation resistance of all cables charged with d.c. current at 500 V over 1 minute, was 300—2,000 KMΩ/Km, and there was no insulation break-down during this test. Thus, this cable has proved to have enough dielectric strength for practical use.

Table 7

DESIGN VALUES OF PEF CITY CABLE STRAND

Nominal conducter diameter (mm)	Thickness of insulation (mm)	Degree of foaming of insulatior (%)
0. 32	0. 080	20
0. 40	0. 100	20
0. 50	0. 125	20

Note: Design value of side-circuit electrostatic capacity of the cable

Electrostatic capacity of side circuit: As shown in Table 8, in the case of manufacturing the city cables with conductor diameters of 0.4 mm and 0.5 mm, the thickness of strand insulation and the degree of foaming were decided as shown by Table 7. As a result, nearly all the measured values of electrostatic capacity became almost equal to the standard value of existing city cable rating —i.e. 50 mμF/Km, as expected. For the 0.32 mm cable, however, the insulation thickness became a little larger than the design value, and so the measured value became a little below design value. From this result, it is understood how useful the new theoretical analysis in Section 1 was, to design the city cable with fine conductor.

Electrostatic coupling between side-circuits: Fig. 18 shows the relation between the cable length, and the electrostatic coupling among side-circuits which we measured cutting the cable, concerning the 0.32 mm 200 pairs PEF city cable in Table 6. From this relation, it has been clarified that the maximum value of the coupling in the new cable is approximately proportional to the cable length, and

Table 8

INSULATION THICKNESS DEGREE OF FOAMING AND CABLE SIDE-CIRCUIT ELECTROSTATIC CAPACITY OF THE STRAND OF PEF CITY CABLE MADE FOR TRIAL

Nominal conductor diameter (mm)		Thickness of insulation (mm)	Degree of foaming of insulation (mm)	Side-circuit electrostatic capacity of cable (mμ/km)			
				20 pairs	200 pairs	1000 pairs	2000 pairs
0. 32	Mean	0. 090	20. 8	50. 7	48. 2	45. 7	45. 8
	Max.	0. 100	29. 4				
	Min.	0. 085	16. 6				
0. 40	Mean	0. 100	21. 5	50. 8	49. 4	Note: The cable is the same as in the tabe.	
	Max.	0. 110	30. 0				
	Min.	0. 095	16. 5				
0. 50	Mean	0. 125	23. 5	51. 6	49. 3		
	Max.	0. 135	30. 1				
	Min.	0. 120	15. 7				

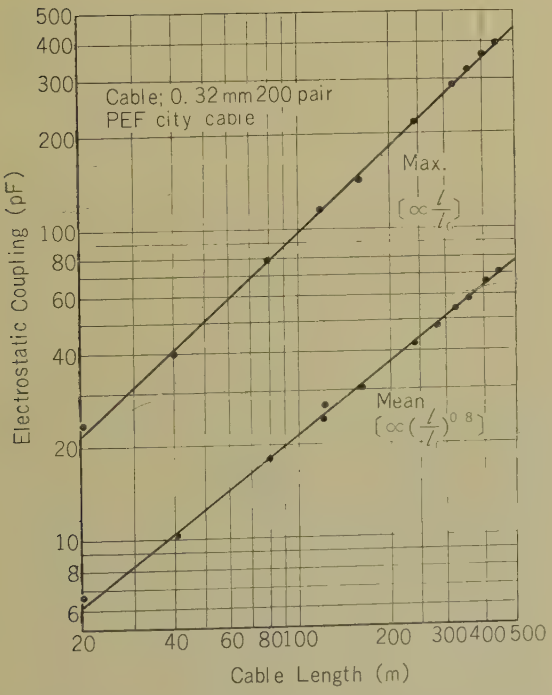

Fig. 18—Relation between the cable length and side-circuit electrostatic coupling of PEF city cable experimentally made.

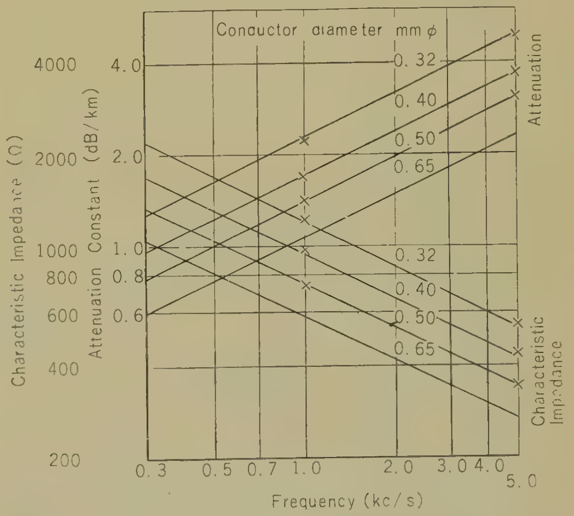

Fig. 19—The calculated values of attenuation and characteristic impedance of the city cable, and the measured values of those of experimental PEF city cable.

Table 9 ELECTROSTATIC COUPLING BETWEEN SIDE-CIRCUITS OF PEF CITY CABLE MADE FOR TRIAL

Nominal conductor diameter (mm)		Electrostatic coupling between side circuits (pF)			
		20 pairs	200 pairs	1, 000 pairs	4, 000 pairs
0. 32	Max.	325	440	95	80
	Mean	99	75	17	15
0. 40	Max.	360	650	Note: Cable is the same as in the table.	
	Mean	120	96		
0. 50	Max.	130	330		
	Mean	70	51		

Note : Length of 20-pair cable : 510 m, Length of 200-pair cable : 510 m
〃 1000-pair cable : 112 m, 〃 4000-pair cable : 110 m.

that the mean value is approximately proportional to the 0.8 th power of it.

Table 9 shows the measured values of the electrostatic coupling between the circuit of quad of the PEF city cable in Table 6. The design of quad and measured values of strand insulation thickness and degree of foaming of these cables are shown in Tables 7 and 8. In the case of manufacturing this strand, the ratio of the minimum insulator thickness to the maximum thickness on the same section was kept below 4/5, in order to make the mean coupling below half the rated value now in existence (the mean value in the range: 300 pF/500 m, the maximum value in the range: 1,600 pF/500 m).

On the basis of the results shown in Fig. 18, if the above values of the 0.32 mm 1000 pair and 4000 pair cable piece of short length are changed into the values of the same cables 510 m long, then the following results are obtained:

1) 1,000 pair cable
   Max. value: 432 PH
   Mean value: 57 PF
2) 4,000 pair cable
   Max. value: 371 PF
   Mean value: 51 PF

From this, the max. value of the trial cable ranges from 650 to 130 PF, and the mean value from 120 to 51 PF; but the coupling could be kept below half the coupling of the existing cable rating, as expected at first.

Attenuation and characteristic impedance: In the city cable specification of the Nippon Telegraph and Telephone Public Corporation, there is no provision related to such transmission characteristics as attenuation and characteristic impedance, but these are shown indirecly in the form of d.c. current resistance and electrostatic capacity. Fig. 19 shows the values of the attenuation and characteristic impedance calculated from the specification, in relation to the 0.32, 0.4 and 0.5 mm city cables. The PEF city cable in Table 8 also was designed and manufactured so that the electrostatic capacity might be equal to that of the existing city cable rating, and so concerning the 0.4 and 0.5 mm city cables made for trial, the attenuation and characteristic impedance should correspond to those in the figure. Table 10 shows the measured values of attenuation and characteristic impedance of the PEF city cable for trial at the frepuences of 1 kc/s and 5 kc/s. As shown by the mark × in Fig. 10, each of them

Table 10 SIDE-CIRCUIT ATTENUATION AND CHARACTERISTICS IMPEDANCE OF PEF CITY CABLE MADE FOR TRIAL

Nominal conductor diameter (mm)	Measured frequency (kc/s)	Side-circuit attenuation (dB/km)					Side-circuit characteristic impedance (Ω)				
		20 pairs	200 pairs	1000 pairs	4000 pairs	Overall mean	20 pairs	200 pairs	1000 pairs	4000 pairs	Overall mean
0. 32	1	2. 27	2. 12	2. 30	2. 18	2. 22	1152	1285	1226	1238	1225
	5	4. 94	4. 65	4. 75	4. 97	4. 83	518	558	549	559	546
0. 40	1	1. 72	1. 70			1. 71	999	987			993
	5	3. 65	3. 67			3. 66	450	444			447
0. 50	1	1. 45	1. 42			1. 44	716	753			735
	5	3. 07	3. 00			3. 04	324	350			337

Table 11 FIELD TEST OF PEF CITY CABLE

	Date of the test	Place	Cable	Note	
1st	June '59	Electrical Communication Laboratory	0. 32 mm 200 p City PEF-P 1200 m 0. 32 mm 100 p City PEF-P 500 m	Aerial and underground combined	Connected to experimental crossbar and semi-electric switching equipment 100 circuits now in operation. Without line failure.
2nd	June '60	Within the jurisdiction of Kamakura Telephone Exchange Office	0. 32 mm, 0. 4 mm, 0. 5 mm } 200 p City PEF-CP, V 840 m 0. 32 mm 1600 p City PEF-P 260 m	Aerial and underground	No subscribers
3rd	July '60	Within the jurisdiction of Choshi Telephone Exchange Office	0. 32 mm 100 p, 0. 32 mm 800 p } City PEF-VSS 480 m	Aerial	No subscribers
4th	Aug. '60	Within the jurisdiction of Shirogane Telephone Exchange Office	0. 32 mm 3800 p City PEF-P 190 m	Underground	No subscribers

agrees well with the calculated values.

6. Installing and Joining Method, Field Tests of Cable

As a result of the trial manufacture of the cable, it was clarified that the new PEF city cable achieves the purpose of using finer conductors and increasing pairs, and that the near-end cross-talk can be made less than half that of the existing cable. But in order to complete the study of developing the city cable, further study must be made by using the cables practically, to confirm the following items:

1) Whether the aierial installation and the lead in duct of the new cable and its conductor splice and sheath join is practically accomplished.
2) Whether the contact resistance at joints of this new cable increases in use because of vibration and temperature change after installation.
3) Whether the cable is reliable enough for commercial use or not.

From this point of view, such field tests as shown in Table 11, were carried out four times by using the above trial city cables, with the assistance of members in active service of the Nippon Telegraph and Telephone Public Corporation. As a result, the following points have come to light.

1) The new city cable is so light (about half as heavy as the existing paper-insulated lead-sheathed cable with the same number of pairs), that the installation is carried out very efficiently. For instance, in the fourth test, a 3,800-pair cable 60 m in length was installed by 5 workers, in only 10 minutes or so.
2) Before the test, the adoption of the existing splicing method was felt somewhat easy, because the conductor diameter was reduced from 0.4 mm to 0.32 mm and the conductor cross-section area had become only 6/10 of that of the existing cable. So various studies were made on the engineering method for about one year. As a result, concerning the short test piece, it was confirmed that the method was good enough to serve the purpose. This was still more assured by several more field testes. The time required for splicing was the same as that for the existing conductor 0.4 mm in diameter. These field testing plants are left as they were, and by using them the contact resistance at joints has been observed for two years, but nothing out of order has been found.
3) As to the sheath joint, the fusing method has proved proper for the cable sheathed with vinyl chloride, and the auxiliary lead-sleeve method for the cable sheathed with poly-ethylene. As in the case of cable-core joint, the plants of the 2nd, 3rd, and 4th test have been observed for two years, no insulation resistance drop due to deterioration of joints has been found.

These several fiield tests on the aerial installation and the lead-in of the cable, and on the joint method of its conductor and sheath; the tests on the cable in commercial use for about 3 years. As a result of these, this new cable has been confirmed worthy of commercial use. Thereupon, 5,000 subscribers were admitted (to be increased to 12,000 in all) into the Showa Telephone Office in Tokyo, which opened to service in

Fig. 20—Men at work on the conductor joint of the 0.32 mm, 3,800-pair PEF city cable during the 4th field test.

1961, and the commercial use test of the cables were carried out on a large scale; more in detail, the tests on the changes of telephone set and cable of the whole office into No. 600 type and PEF city cables respectively. The tests are proceeding now. Fig. 20 shows how the cable core joint of 0.32 mm, 3,800 pair PEF cable was carried out in a manhole, in the case of the of the 4th field test.

Conclusion

On the basis of the above-mentioned design theory, a consistent study of the development of the new city cable—from the method of manufacture to field test—was carried out. As a result, the foamed polyethylene insulated multi-pair city cable with fine conductor which is manufactured by the coating method with the characteristics shown by Table 1, is specified as the PEF city cable. According to the specification, the cables about 240 km long (by 50 pairs conversion) have already been ordered from the three wire corporations—Furukawa, Sumitomo Denkō KK., and Fujikura Densen KK.—for the purpose of the tests of commercial use to be held in the Showa Telephone Office. If the result of the test on a large scale is satisfactory, this PEF cable will be put into wide commercial use in the year 1963.

The effects of the development of this PEF city cable are as follows:

1) Price reduction of the cable: The conductor diameter of the new city cable is 0.32 mm, 0.08 mm less than that of the existing one; the manufacturing method of the foamed polyethylene insulated strand at the speed of 1,000 m/min. was developed. On account of this, the new city cable will be 20% cheaper per pair than the existing paper-insulated cable with 0.4 mm diameter conductor in the near future. In the case of 0.4 or 0.5 mm conductor diameter, it will be about the same in price as the existing cable.
2) Reduction of cost for installation: Owing to the introduction of the fine conductor and of the foamed polyethylene insulation by coating method, the maximum number of pairs per 75 mm dia. duct has been increased from 2,400 to 4,000. Accordingly, the duct cost is decreased by 40% at most, and the number of the circuits can be increased without increasing ducts by about 70%.
3) Improvement of cross-talk characteristics and the unification of cables: Thanks to the development of the new city cable, the electrostatic coupling has become less than half as large as that of the existing cable. The transmission quality is not lowered, in spite of the change of telephone sets to the No. 600 type. Besides, by the unification of city trunk cables and subscribers' cables to the PEF city cables, the cost of cables can be reduced.
4) Improvement of service to the subscribers: The city cables so far used have been only paper-insulated cables. But by the development of this cable, plastic is now applicable to the insulator and sheath of city cables so that the grounding troubles of submerged circuits may be avoided. In this way, the service to subscribers can be improved.

As a result of the development of the PEF city cables, the city subscribers' net work is expected to be made better in quality, and more economical by the combination of cross-bar type switching equipment and No. 600 type telephone sets.

In parallel to the tests of the commercial use at the Showa Office, engineering guidance of the manufacturing method of the PEF city cables is now being conducted by members of the Electrical Communication Laboratory at four wire corporations—Dainichi, Nippon, Hitachi, and Showa, in preparation for the year 1963, when the city cables will be put into commercial use.

* * * *

Papers Contributed to Scientific and Technical Journals by the Members of the Laboratory*

Papers Published in Other Publications of the Electrical Communication Laboratory

U.D.C. 546.289 : 539.27 : 621.382.333.001.2

Observation of Antimony-Diffused Germanium Surfaces by Electron Diffraction Method
Kazumasa ONO, *Osamu MIKAMI*, and *Joichi SUZUKI*
Kenkyû Zituyôka Hôkoku (Electr. Comm. Labor. Techn. Journ.), NTT, **10**, 10, pp. 2147–2158 Oct. 1961

The structure of diffused germanium surfaces was studied in relation to the surface impurity concentration by varying the germanium and the impurity source temperatures.

U.D.C. 311.68 : 621.382.3

Low-Capacity No-Break Power System
Isamu YAMAGISI and *Sozi HARAGUTI*
Kenkyû Zituyôka Hôkoku (Electr. Comm. Labor. Techn. Journ.), NTT, **10**, 10, pp. 2129–2145, Oct. 1961

Description of design and characteristics of power supply system for communication equipment using primary cell and series-regulated transistor voltage regulator.

U.D.C. 621.382.333 : 621.318.57 : 62

Characteristics and Applications of Three-Terminal pnpn Speech-Path Switches
Kingo YAMAGISHI and *Ichiro ENDO*
Kenkyû Zituyôka Hôkoku (Electr. Comm. Labor. Techn. Journ.), NTT, **10**, 10, pp. 2173–2183, Oct. 1961

Static and switching characteristics of experimentally made pnpn switches are discussed. Several applications are also described.

U.D.C. 621.395.38 : 621.373.431.1 : 621.375.52

Small Capacity Ringers for Telephone Exchanges
Hideyosi NAKAZAWA
Kenkyû Zituyôka Hôkoku (Electr. Comm. Labor. Techn Jour.), NTT, **10**, 10, pp. 2185–2198, Oct. 1961

Small capacity ringers for telephone exchangers are described.

---

[*] Translations of many of these papers will appear in a future addition of the Review of Electrical Communication Laboratory.
Please address requests for copies of these papers, which are in Japanese, directly to the authors to whom credited at: The Electrical Communication Laboratory, 1551 Kitizyôzi, Musasino-si, Tokyo.

U.D.C. 678.632.049 : 678.643 : 621.315.619 : 539.5

Curing Mechanism in Phenolic Resin with Internal Plasticization Epoxy Resin Added
Masaaki KATAGIRI and *Moritaka TAJIMA*
Kenkyû Zituyôka Hôkoku (Electr. Comm. Labor. Techn. Jour.), NTT, **10**, 10, pp. 2199–2215, Oct. 1961

Curing processes in phenolic resin and phenolic resin with epoxy resin added were studied by means of infra-red spectrometry and differential thermal analysis. Considerations on internal plasticization mechanism are presented from these experimental results.

U.D.C. 681.18 : 621.318.1 : 621.374.3

Automatic Selector of Magnetic Cores for the Double-Frequency Memory System
Tsuneori KOSHIBA
Kenkyû Zituyôka Hôkoku (Electr. Comm. Labor. Techn. Jour.), NTT, **10**, 10, pp. 2159–2171, Oct. 1961

Description of construction and function of automatic selector for magnetic cores, to be used in the double frequency memory system.

U.D.C. 666.97.03 : 678.674 : 621.315.65/66

Thermosetting Plastics Filled with Large Volume of Iron Sand etc.
Nobuo MURAI and *Susumu MIZUNO*
Kenkû Zituyôka Hôkoku (Electr. Comm. Labor. Techn. Jour.), NTT, **10**, 10, pp. 2107–2127, Oct. 1961

Experiments in which polyester resin were mixed with large volumes of iron sand, stone, etc. were conducted. The cured mixture has good electrical insulating properties, and can be used in compression as a structural material.

Papers Published in Publications of Scientific and Technical Societies

U.D.C. 537.56 : 538.569

Plasma Oscillations in External Fields
Masao SUMI
Jour. Phys. Soc. Japan, **16**, 9, pp. 1718–1728, 1961

Plasma oscillations are considered under uniformly applied electric and magnetic fields. The dispersion relation describes characteristics of temporal change of excited waves.

U.D.C. 541.64 : 538.569 : 678.012

Stereo Regularity of Linear Polymer and Nuclear Magnetic Resonance
Atsuo NISHIOKA
The Society of Polymer Science Japan, **10**, 114, pp. 788–793, 1961

Stereo regularity of linear polymethylmethacrylate was determined by high-resolution nuclear magnetic resonance method.

U.D.C. 621.317.74 : 621.372.812

A Smith Diagram Display Unit for Small Reflection Cofficients Using "Vibration Dummy Method"
Shoji TSUCHIYA
Jour. Inst. Electr. Engineers, Japan, **44,** 10, pp. 1504–1511, 1961

A new method of obtaining a perfect reflectionless termination, the vibration dummy method, was invented. Display unit for small reflection coefficients using this method was developed.

U.D.C. 621.375.9 : 621.382.2

Traveling-Wave Parametric Amplifier
Yasuhiro ISII
Jour. Inst. Electr. Engineers, Japan, **44,** 10, pp. 1480–1488, 1961

Theoretical consideration of the design of a periodically loaded traveling-wave parametric amplifier is described.

U.D.C. 621.391.82.621.395.61 : 621.395.62

Some Considerations on Antisidetone Circuits
Hiroyasu MIURA
Jour. Inst. Electr. Engineers, Japan, **44,** 9, pp. 1328–1336, 1961

The analysis of antisidetone circuits whose elements are complex impedances is described.

U.D.C. 621.391.832. : 538.566 : 535.4

Propagation Distortion on VHF Mountain Diffraction Paths
Yoshihisa OKUMURA and *Masami HARA*
Jour. Inst. Electr. Engineers, Japan, **44,** 9, pp. 1354–1362, 1961

This paper describes the variation of characteristics, mechanism of origin, and distortion on mountain diffraction paths.

U.D.C. 621.395.3

Optimum Design of Switching Systems
Haruo AKIMARU
Jour. Inst. Electr. Engineers, Japan, **44,** 10, pp. 1496–1504, 1961

Optimization of switching systems consisting of switching equipment and trunks by introducing the concept of trunk function is described.

U.D.C. 621.395.616 : 534.64

Capacitor Vibrometer
Minji SUZUKI, Takashi IWASE
Jour. Inst. Electr. Engineers, Japan, **44,** 9, pp. 1337–1341, 1961

A new method of measuring an accoustical driving point impedance using a capacitor transducer as vibrometer is described.

U.D.C. 621.9.01 : 534.321.9

Some Considerations on the Mechanism in Ultrasonic Machining Particularly on Chip Removal, Trace Penetration, and Residual Strains

Masahiro OHIRA, *Harumichi KAGEYAMA*, and *Osamu AKUTSU*

Jour. Soc. Precision Mechamics. Japan, **27**, 9, pp. 625–630, 1961

Our observations and measurements are used to discuss the mechining machanism; particularly work surface roughness, chip removal, traces left, and residual strains.

* * * *

R E V I E W
of
THE ELECTRICAL COMMUNICATION LABORATORY
NIPPON TELEGRAPH AND TELEPHONE PUBLIC CORPORATION

Published Bimonthy by
The Electrical Communication Laboratory, 1551, Kitizyôzi, Musasino-si, Tôkyo, Japan
Satoshi Kojima, *Director*

Index to Volume 9—1961

Contents of Issues

page

NOS. 1-2 JANUARY-FEBRUARY

On Fundamental Qualities of Vowel Sounds in Speech Communication (III) 1
Toshiyuki OCHIAI and *Teruo FUKUMURA*

Staggered Operation of Doubly Resonant Parametric Amplifiers 20
Shigetaka HAMADA and *Hisakazu MUKAI*

Construction and Characteristics of Silver-Bonded Dioded 26
Shoichi KITA

Determination of Molecular Distribution of High Polymers by Fractionation 31
Hiroshi OKAMOTO

Core Matrix Driver Employing Magnetic Amplifiers 43
Junji YAMAMOTO and *Yasunobu SUZUKI*

A Consideration on Relation between Mechanical Behavior of Glass and Their Internal Structure 50
Muneo WATANABE and *Taro MORIYA*

Effects of the Force Factor and the Eddy Current on the Operate and Release Time of the Ordinary Relays 72
Yasuo TOMITA

A New Type of Vestigial-Sideband Facsimile System 85
Keijiro KUBOTA and *Kazuo KOBAYASHI*

A Study of Internally Plasticized Melamine Laminates 91
Masaaki KATAGIRI

Papers Contributed to Scientific and Technical Journals by the Members of the Laboratory 97 page

NOS. 3-4, MARCH-APRIL

Chatter Vibration of Switching Relay 99
Masao TAKAMURA, Yuichi SHIMIZU, and Yuji OTSUKA

Feedback Type Distributed Amplifier Tube 150
Takuya KOJIMA

Recent Development of Quartz Crystals Units for Telecommunication 165
Kiyoshi TAKAHARA

Studies of Magnetization Processes of Magnetic Cores by Supersonic Methods 207
Katsumi NISHIGUCHI and *Hiroshi SAWABE*

A High-Speed Facsimile System with Electronic Scanning 214
Keijiro KUBOTA, Kazuo KOBAYASHI, Yositaro OKAJIMA, and *Shogo NANBO*

The Dimensional Accuracy of Molded Spur Gears of 610-Nylon 220
Tetsuo KUDO and *Takashi YAMANARI*

Triple Balanced Modulator Binocular Type Cores 233
Takashi ITO

Papers Contributed to Scientific and Technical Journals by the Members of the Laboratory 248

NOS. 5-6, MAY-JUNE

Majority Decision Functions of Six Variables 253
Iwao TODA, Mamoru KONDO, and *Saburo MUROGA*

Ferroelectric Polarization Reversal by Linear Fields 279
Hiroyuki SHIBATA, Hiroo TOYODA, and *Sigeru WAKU*

Formation of Cesium Antimonide. II. Formation of Cs_3Sb at Temperatures below 130°C 287
Kiyoshi MIYAKE

Formation of Ceisum Antimonide. III. Logarithmic Growth of Cesium Antimonide Films on Antimony 295
Kiyoshi MIYAKE

A Method of Quantifying Fe^{2+} and Mn^{3+} in Sintered Mn-Zn Ferrites 300
Hideo NAGATO

An Input Admittance Meter for Electron Tubes 309
Takuya KOJIMA and *Hiroshi HARA*

Characteristics of Fading due to Ducts and Quantitative Estimation of Fading 319
Shigetaka UGAI

page

Interference Waves in Waveguide Transmission and Intermodulation Noise in FM System for Waveguide Communication 361
Kazuhiro MIYAUCHI

The C 8 Crossbar Toll Switching System 394
Toshiichi MASUDA

Papers Contributed to Scientific and Technical Journals by the Members of the Laboratory 400

NOS. 7-8, JULY-AUGUST

Radioactivation Analysis of Oxygen and Boron in Transistor-Grade Silicon 403
Tadashi NOZAKI, and *Junichi SHIMADA*

Observations of Uniaxial Anisotropy in Ferromagnetic Thin Films by Means of Bitter Technique 408
Yuzo ODANI and *Yuzi GOMI*

A 48 Gc Center-Excited Type Channel Branching Filter for Circular Electric Waves 421
Shin-ichi IIGUCHI, Bun-ichi OGUCHI, and *Kazuo YAGUCHI*

The Design of Germanium Diodes used for Junction Capacitance Parametrons 429
Yasuhiro HIYAMA

Binary Data Transmission on Private Telephone Line 437
Toshi MINAMI, Hiroshi SUNAGAWA, and *Shun'itsu HAMAO*

Growth and Electrical Properties of Ferroelectric Glysine Sulfate Single Crystals 485
Hiroo TOYODA, Yoichi TANAKA, and *Wataru SHIOKAWA*

A Study of M-type Tube Electron Guns 497
Tomoyuki UNOTORO

Inclusive Telegraphist's Equations for Waveguides 526
Shin-ichi IIGUCHI

Papers Contributed to Scientific and Technical Journals by the Members of the Laboratory 536

NOS. 9-10, SEPTEMBER-OCTOBER

Compound pnpnp Switches for Bidirectional-bistable Electronic Switches 545
Kingo YAMAGISHI

Circuit Interruption and Circuit Interruption Measuring Set 552
Toshi MINAMI and *Masamichi ONO*

A Study on the Efficiency of Graded Multiple Delay System Through Artificial Traffic Trials 564
Eiichi GAMBE

page

Thermosetting Plastic Swelled with Grainy Fillers (Plastic Concrete) 581
Nobuo MURAI and *Susumu MIZUNO*

An Electronic System for Translating Japanese into Braille 589
KIYASU Zen'iti and *SEKIGUTI Sigeru*

Study of Active Circuits 600
Shunitsu HAMAO

Microwave Amplitude Characteristics Measuring Equiqment 606
Masamitu OTA and *Ituo SUGIURA*

Binomial Probabilistic Sequential Circuit 627
Makoto SUGIMORI

Papers Contributed to Scientific and Technical Journals by the Members of the Laboratory 653

NOS. 11-12, NOVEMBER-DECEMBER

Equiavlent Circuit and Four-Terminal Parameters of High Frequency Transistor 661
Seiichi KAWAGUCHI and *Minoru HIRAI*

Microwave Propagation Test in Mirage District 687
Shigetaka UGAI, Yoshiie KANEDA,
and *Tadashi AMAKURA*

Characteristics and Application of Three-Terminal pnpn Transistors for Speechpath Switches 718
Kingo YAMAGISHI and *Ichiro ENDO*

Mode Conversion in the Excitation of TE_{01} Waves in a TE_{01} Taper Type mode Transducer 725
Shin'ichi IIGUCHI

Foamed Polyethylene Insulated City Cable 733
Mitsuru ROKUNOHE

Papers Contributed to Scientific and Technical Journals by the Members of the Laboratory 756

Index to Subjects

U.D.C. 003.24 Braille

An Electronic System for Translating Japanese into Braille
KIYASU Zen'iti and SEKIGUTI Sigeru
9–10, pp. 589–599, Sept.–Oct.

U.D.C. 517 Analysis

Study of Active Circuit
Shun'itsu HAMAO
9–10, pp. 600–605, Sept.–Oct.

U.D.C. 519.2 Calculas of probabilities: Statistical mathematics

Majority Decision Functions of Six Variables
Iwao TODA, Mamoru KONDO,
and Saburo MUROGA
5–6, pp. 253–278, May–June

Binomial Probabilistic Sequential Circuit
Makoto SUGIMORI
9–10, pp. 627–654, Sept.–Oct.

U.D.C. 531.66 Mechanics: Collisions. Impact

Chatter Vibration of Switching Relay
Masao TAKAMURA, Yuiti SHIMIZU,
and Yuji OTUKA
3–4, pp. 99–149, Mar.–Apr.

U.D.C. 534.321.9 Acoustics vibrations.: Ultra-sonic vibrations

Studies of Magnetization Processes of Magnetic Cores by Supersonic Methods
Katsumi NISHIGUCHI and Hiroshi SAWABE
3–4, pp. 207–213, Mar.–Apr.

U.D.C. 537.226 Electrostatics: Dielectrics

Ferroelectric Polarization Reversal by Linear-Field
Hiroyuki SHIBATA, Hiroo TOYODA
and Shigeru WAKU
5–6, pp. 279–286, May–June

Growth and Electrical Properties of Ferroelectric Glycine Sulfate Single Crystals
Hiroo TOYODA, Yoichi TANAKA
and Wataru TANAKA
7–8, pp. 485–496, July–Aug.

U.D.C. 537.312.5 Electrical conductivity: Photoconductivity

Formation of Cesium Antimonide II, Formation of Cs_2Sb at Temepratures below 130°C
Kiyoshi MIYAKE
5–6, pp. 287–294, May–June

Formation of Cesium Antimonide. III. Logaithmic Growth of Cesium Antimonide Films on Antimany
Kiyoshi MIYAKE
5–6, pp. 295–299, May–June

U.D.C. 537.533.3 Geometrical electron optics

A Study of M–type Tube Electron Guns
Tomoyuki UNOTORO
7–8, pp. 497–524, July–Aug.

U.D.C. 538.2 Electromagnetism: Magnetic process

Studies of Magnetization Processes of Magnetic Cores by Supersonic Methods
Katsumi NISHIGUCHI and Hiroshi SAWABE
3–4, pp. 207–213, Mar–Apr.

U.D.C. 538.566 Propagation electromagnetic oscillations

Characteristics of Fading due to Ducts and Quantitative Estimation of Fading
Shigetaka UGAI
5–6, pp. 319–360, May–June

U.D.C. 539.1 Molecules: Atoms

Observations of Uniaxial Anisotropy in Ferromagnetic Thin Films by Means of Bitter Technique
Yuzo ODANI and Yuzi GOMI
7–8, pp. 408–420, July–Aug.

U.D.C. 539.23 Structure of molecular system: Thin films

Formation of Cesium Antimonide. III. Logarithmic Growth of Cesium Antimonide Films on Antimony
Kiyoshi MIYAKE
5–6, pp. 295–299, May–June

Observations Uniaxial Anisotropy in Ferromagnetic Thin Films by Means of Bitter Technique
7–8, pp. 408–420, July–Aug.

U.D.C. 539.6 Intermolecular forces

A Consideration on Relation between Mechanical Behavior of Glasses and Their Structure
Muneo WATANABE and Taro MORIYA
1–2, pp. 50–71, Jan.–Feb.

U.D.C. 541.127 Physical chemistry: Velocity of reaction. Reaction velocity coefficients. Guldbery and Weage's law

Formation of Cesium Antimonide. II. Formation of Cs_3Sb at Temperatures below 130° C
Kiyoshi MIYAKE
5–6, pp. 287–294, May–June

U.D.C. 542.65 Chemical strucure: Relation between structure and optical properties

Determination of Molecular Distribution of High Polymers by Fractionation
Hiroshi OKAMOTO
1–2, pp. 31–42, Jan.–Feb.

U.D.C. 543.062 Analytical chemistry: Quantitative analysis. Estimation

A Method of Quantifying Fe^{2+} and Mn^{3+} in Sintered Mn–Zn Ferrites
Hideo NAGATO
5–6, pp. 300–308, May–June

U.D.C. 543.43 Optical methods analysis: Colorimetric and nephelometric analysis

A Method of Quantifying Fe^{2+} and Mn^{3+} in Sintered Mn–Zn Ferrites
Hideo NAGATO
5–6, pp. 300–308, May–June

U.D.C. 543.53 Physicochemical methods of analysis: Radio chemical methods of analysis, activation analysis

Radioactivation Analysis of Oxygen and Boron in Transistor-Grade Silicon
Tadashi NOZAKI and Junichi SIMADA
7–8, pp. 403–407, July–Aug.

U.D.C. 546.1/.2 Inorganic chemistry: Nonmetals and metalloids in general

Radioactivation Analysis of Oxygen and Boron in Transistor–Grade Silicon
Tadashi NOZAKI and Juichi SIMADA
7–8, pp. 403–407, July–Aug.

Equivalent Circuits and Four-Terminal Parametrons High Frequency Transistor
Seiichi KAWAGUCHI and Minoru HIRAI
11–12, pp. 661–686, Nov.–Dec.

U.D.C. 546.3 Inorganic chemistry: Metals in general

Formation of Cesium Antimonide. II. Formation Formation of Cs_3Sb at Temperatures below 130° C
Kiyoshi MIYAKE
5–6, pp. 287–294, May–June

Formation of Cesium Antimonide. III. Logarithmic Growth of Cesium Antimonide Films on Antimony
Kiyoshi MIYAKE
5–6, pp. 295–299, May-June

U.D.C. 546.7 Metals of the sixth, seventh, and eighth groups. Iron and manganese groups

A Method of Quantifying Fe^{2+} and Mn^{3+} in Sintered Mn-Zn Ferrites
Hideo NAGATO
5–6, pp. 300–308, May–June

Observations of Uniaxial Anisotropy in Ferromagnetic Thin Films by Means of Bitter Technique
Yuzo ODANI and Yuzi GOMI
7–8, pp. 408–420, July–Aug.

Ferroelectric Polarization Reversal by Linear-Field
Hiroyuki SHIBATA, Hiroo TOYODA, and Shigeru WAKU
5–6, pp. 279–286, May–June

U.D.C. 547 Organic chemistry

Ferroelectric Polarization Reversal by Linear-Field
Hiroyuki SHIBATA, Hiroo TOYODA, and Shigeru WAKU
5–6, pp. 279–286, May–June

Growth and Electrical Properties of Ferroelectric Glycine Sulfate Single Crystals
Hiroo TOYODA, Yoichi TANAKA, and Wataru SHIOKAWA
7–8, pp. 485–496, July–Aug.

U.D.C. 548 Crystallography

Growth and Electrical Properties of Ferroelectric Glycine Sulfate Single Crystals
Hiroo TOYODA, Yoichi TANAKA, and Wataru SHIOKAWA
7–8, pp. 485–496, July-Aug.

U.D.C. 551.51/.59 Meteorology: Theoretical meteorology, phenomena

Microwave propagation Test in Mirage District

Shigetaka UGAI, Yoshiie KANEDA,
and Tadashi AMEKURA
11–12, pp. 687–717, Nov.–Dec.

U.D.C. 620 Test materials. Faults in materials

The Dimensional Accuracy of Molded Spur Gears of 610-Nylon
Tetsuo KUDO and Takashi YAMANARI
3–4, pp. 220–232, Mar.–Apr.

U.D.C. 621-272 Springs

Chatter Vibration of Switching Relay
Masao TAKAMURA, Yuiti SHIMIZU,
and Yuji OTUKA
3–4, pp. 99–149, Mar.–Apr.

U.D.C. 621.314.6 Rectifiers

Compound pnpn Switches for Bidirectional-bistable Electronic Switches
Kingo YAMAGISHI
9–10, pp. 545–551, Sept.–Oct.

U.D.C. 621.315.2 Cables

Foamed Polyethylene Insulated City Cable
Mitsuru ROKUNOHE
11–12, pp. 733–755, Nov.–Dec.

U.D.C. 621.315.6 Insulating materials

Formed Polyethylene Insulated City Cable
Mitsuru ROKUNOHE
11–12, pp. 733–755, Nov.–Dec.

A Study of Internally Plasticized Melamine Laminates
Masaaki KATAGIRI
1–2, pp. 91–96, Jan.–Feb.

U.D.C. 621.315.65 Supports fixing the insulators

Thermosetting Plastics Swelled with Grainy Fillers (Plastic Concrete)
Nobuo MURAI and Susumu MIZUNO
9–10, pp. 581–588, Sep.–Oct.

U.D.C. 621.317.3 Measurement of electric quantities

An Input Admittance Meter for Electron Tube
Takuya KOJIMA and Hiroshi HARA
5–6, pp. 309–318, May–June

Microwave Amplitude Characteristics Measuring Equipment
Masamitu OTA and Ituo SUGIURA
9–10, pp. 606–611, Sept.–Oct.

U.D.C. 621.317.6 Determination of the relation between various quantities characteristics

Equivalent Circuits and Four-Terminal Parametrons High Frequency Transistor
Seiichi KAWAGUCHI and Minoru HIRAI
11–12, pp. 661–686, Nov.–Dec.

U.D.C. 621.317.7 Electrical measuring apparatus. Meters. Oscillograph

An Input Admittance Meter for Electron Tubes
Takuya KOJIMA and Hiroshi HARA
5–6, pp. 309–318, May–June

Microwave Amplitude Characteristics Measuring Equipment
Masamitu OTA and Ituo SUGIURA
9–10, pp. 606–611, Sept.–Oct.

Circuit Interruption and Circuit Interruption Measuring Set
Toshi MINAMI and Masamichi ONO
9–10, pp. 552–563, Sept.–Oct.

U.D.C. 621.318.1 Magnetic materials

Studies of Magnetization Processes of Magnetic Cores by Supersonic Methods
Katsumi NISHIGUCHI and Hiroshi SAWABE
3–4, pp. 207–213, Mar.–Apr.

U.D.C. 621.318.5 Relays, electronic switches

Effects of the Force Factor and the Eddy Current on the Operate and Release Time of the Ordinary Relay
Yasuo TOMITA
1–2, pp. 72–84, Jan.–Feb.

Chatter Vibration of Switching Relay
Masao TAKAMURA and Yuiti SHIMIZU
3–4, pp. 99–149, Mar.–Apr.

Compound pnpnp Switches for Bidirectional-bistable Electronic Switches
Kingo YAMAGISHI
9–10, pp. 545–551, Sept.–Oct.

Binomial Probabilistic Sequential Circuit
Makoto SUGIMORI
9–10, pp. 627–654, Sept.–Oct.

Characteristics and Application of Three-Terminal pnpn Transistors for Speech Path Switches
Kingo YAMAGISHI and Ichiro ENDO
11–12, pp. 718–724, Nov.–Dec.

U.C.C. 621.371 Radiation and propagation of electromagnetic waves in free space

Characteristics of Fading due to Ducts and Quantitative Estimation of Fading
Shigetaka UGAI
5–6, pp. 319–360, May–June

Microwave Propagation Test in Mirage District
Shigetaka UGAI, Yoshiie KANEDA,
and Tadashi AMAKURA
11–12, pp. 687–717, Nov.–Dec.

U.D.C. 621.372 Guided propagation of electric oscillations in general. Theory of transmission lines

Interference Waves in Intermodulation Noise in FM System for Waveguide Communication
Kazuhiro MIYAUCHI
5–6, pp. 361–393, May–June

Study of Active Circuits
Shunitsu HAMAO
9–10, pp. 600–605, Sept.–Oct.

U.D.C. 621.372.8 Waveguides

Interference Waves in Waveguide Transmission Intermodulation Noise in FM System for Waveguide Communication
Kazuhiro MIYAUCHI
5–6, pp. 361–393, May–June

Inclusive Telegraphist's Equations for Waveguides
Sen-ichi IIGUCHI
7–8, pp. 525–534, July–Aug.

A 48 Gc Center-Excited Type Channel Branching Filters for Circular Electric Waves
Shin-ichi IIGUCHI Bun-ichi OGUCHI
and Kazuo YAMAGUCHI
7–8, pp. 421–428, July–Aug.

Mode Conversion in the Excitation of TE_{01} Waves in a TE_{01} Taper Type Mode Transducer
Shin-ichi IIGUCHI
11–12, pp. 725–732, Nov.–Dec.

U.D.C. 621.373 Generators of electric oscillation and pulses

Recent Development of Quartz Crystal Units for Telecommunication
Kiyoshi TAKAHARA
3–4, pp. 165–206, Mar.–Apr.

U.D.C. 621.374 Pulse process. Frequency multipliers and dividers

Core Matrix Driver Employing Magnetic Amplifiers
Junji YAMATO and Yasunobu SUZUKI
1–2, pp. 43–49, Jan.–Feb.

Triple Balanced Modulator Using Binocular Type Cores
Takashi ITO
3–4, pp. 233–248, Mar.–Apr.

An Electronic System for Translating Japanese into Braille
KIYASU Zen'iti and SEKIGUCHI Shigeru
9–10, pp. 589–599, Sept.–Oct.

The Design of Germanium Diodes used for Junction Capacitance Parametrons
Yasuhiro HIYAMA
7–8, pp. 429–436, July–Aug.

Binomial Probabilistic Sequential Circuit
Makoto SUGIMORI
9–10, pp. 627–654, Sept.–Oct.

U.D.C. 621.375 Amplifiers

Feedback Type Distributed Amplifier Tube
Takuya KOJIMA
3–4, pp. 150–164, Mar.–Apr.

Core Matrix Driver Employing Magnetic Amplifiers
Junji YAMATO and Yasunobu SUZUKI
1–2, pp. 43–49, Jan.–Feb.

Staggered Operation of Doubly Resonant Parametric Amplifiers
Shigetaka HAMADA and Hisakazu MUKAI
1–2, pp. 22–25, Jan.–Feb.

U.D.C. 621.376 Modulation and demodulation. Process and apparatus.

Triple Balanced Modulator Using Binocular Type Cores
Takashi ITO
3–4, pp. 233–248, Mar.–Apr.

U.D.C. 621.382.2 Semiconductor devices: Crystal diodes

Construction and Characteristics of Silver-Bonded Diodes
Shoichi KITA
1–2, pp. 26–30, Jan.–Feb.

The Design of Germanium Diodes used for Junction Capacitance Parametrons
Yasuhiro HIYAMA
7–8, pp. 429–436, July–Aug.

Compound pnpn Switches for Bidirectional-bistable Electronic Switches
Kingo YAMAGISHI
9–10, pp. 545–551, Sept.–Oct.

U.D.C. 621.382.3 Semiconductor devices: Transistors

Equivalent Circuits and Four-Terminal Parameters High Frequency Transistor
Seiichi KAWAGUCHI and Minoru HIRAI
11–12, pp. 661–686, Nov.–Dec.

Characteristics and Application of Three-Terminal pnpn Transistors for Speech Path Switches
Kingo YAMAGISHI and Ichiro ENDO
11–12, pp. 718–724, Nov.–Dec.

U.D.C. 621.385 Discharge tubes. Velocity control tubes

An Input Admittance Meter for Electron Tube
Takuya KOJIMA and Hiroshi HARA
5–6, pp. 309–318, May–June

Feedback Type Distributed Amplifier Tube
Takuya KOJIMA
3–4, pp. 150–164, Mar.–Apr.

A Study of M-type Tube Electron Guns
Tomoyuki UNOTORO
7–8, pp. 497–524, July–Aug.

U.D.C. 621.391 Telecommunication. Information theory

Binary Data Transmission on Private Telephone Line
Toshi MINAMI, Hiroshi SUNAGAWA and Shun'itsi HAMAO
7–8, pp. 437–484, July–Aug.

U.D.C. 621.39.8 Quality of the received single. Signal strength. Interference.

Microwave Propagation Test in Mirage District
Shigetaka UGAI, Yoshiie KANEDA, and Tadashi AMAKURA
11–12, pp. 687–717, Nov.–Dec.

Characteristics of Fading due to Ducts and Quantitative Estimation of Fading
Shigetaka UGAI
5–6, pp. 319–360, May–June

Interference Waves in Waveguide Transmission and Intermodulation Noise in FM System for Waveguide Communication
Kazuhiro MIYAUGHI
5–6, pp. 361–393, May–June

Binary Data Transmission on Private Telephone Line
Toshi MINAMI, Hiroshi SUNAGAWA, and Shun'itsu HAMAO
7–8, pp. 437–484, July–Aug.

Circuit Interruption and Circuit Interruption Measuring Set
Toshi MINAMI and Masamichi ONO
9–10, pp. 552–563, Sept.–Oct.

U.D.C. 621.394 Telegraphy

Binary Data Transmission on Private Telephone Line
Toshi MINAMI, Hiroshi SUNAGAWA, and Shun'itsu HAMAO
7–8, pp. 437–484, July–Aug.

Circuit Interruption and Circuit Interruption Measuring Set
Toshi MINAMI and Masamichi
9–10, pp. 552–563, Sept.–Oct.

U.D.C. 621.395 Telephony

A Study on the Efficiency of Graded Multiple Delay Systems Through Artificial Traffic Trials
Eiichi GAMBE
9–10, pp. 564–580, Sept.–Oct.

The C8 Crossbar Toll Switching System
Toshiichi MASUDA
5–6, pp. 394–399, May–June

Characteristics and Application of Three-Terminal pnpn Transistors for Speech Path Switches
Kingo YAMAGISHI and Ichiro ENDO
11–12, pp. 718–724, Nov.–Dec.

Binary Data Transmission on Private Telephone Line
Toshi MINAMI, Hiroshi SUNAGAWA, and Shun'itsu HAMAO
7–8, pp. 437–484, July–Aug.

Foamed Polyethylene Insulated City Cable
Mitsuru ROKUNOHE
11–12, pp. 733–755, Nov.–Dec.

U.D.C. 621.396.6 Radiocommunication: Apparatus and circuits

Microwave Amplitude Characteristics Measuring Equipment
Masamitu OTA and Ituo SUGIURA
9–10, pp. 606–611, Sept.–Oct.

U.D.C. 621.397 Television. Electrical picture transmission

A High-Speed Facsimile System with Electronic Scanning
Keijiro KUBOTA, Kazuo KOBAYASHI, Yoshitaro OKAJIMA, and Shogo NANBO
3–4, pp. 214–219, Mar.–Apr.

A New Type of Vestigial-Sideband Facsimile System
Keijiro KUBOTA and Kazuo KOBAYASHI
1–2, pp. 85–90, Jan.–Feb.

U.D.C. 621.928.5 Sifting and sorting devices

Determination of Molecular Distribution of High Polymers by Fractionation
Hiroshi OKAMOTO
1–2, pp. 31–42, Jan.–Feb.

U.D.C. 658.5 Production control. Shop management: Quality control

The Dimensional Accuracy of Molded Spur Gears of 610-Nylon
Tetsuo KUDO and Takashi YAMANARI
3–4, pp. 220–232, Mar.–Apr.

U.D.C. 666 Glass and ceramic industry. Concrete

A consideration on Relation between Mechanical Behavior of Glasses and Their Internal Structure
Muneo WATANABE and Taro MORITA
1–2, pp. 50–71, Jan.–Feb.

Thermosetting Plastic Swelled with Grainy Fillers (Plastic Concrete)
Nobuo MURAI and Susumu MIZUNO
9–10, pp. 581–588, Sept.–Oct.

U.D.C. 669.15 Iron and steel alloys

A Method of Quantifying Fe^{2+} and Mn^{3+} in Sintered Mn-Zn Ferrites
Hideo NAGATO
5–6, pp. 300–308, May–June

U.D.C. 678 Rubber and plastic industries

Determination of Molecular Distribution of High Polymers by Fractionation
Hiroshi OKAMOTO
1–2, pp. 31–42, Jan.–Feb.

The Dimensional Accuracy of Molded Spur Gears of 610-Nylon
Tetsuo KUDO and Takashi YAMANARI
3–4, pp. 220–232, Mar.–Apr.

A Study of Internally Plasticized Melamine Laminates
Masaaki KATAGIRI
1–2, pp. 91–96. Jan.–Feb.

Thermosetting Plastic Swelled with Grainy Fillers (Plastic Concrete)
Nobuo MURAI and Susumu MIZUNO
9–10, pp. 581–588, Sep.–Oct.

U.D.C. 681 Fine mechanisms: Statistical mechanisms

An Electronic System for Translating Japanese into Braille
KIYASU Zen'iti and SEKIGUTI Sigeru
9–10, pp. 589–599, Sept.–Oct.

* * * *

Vol. 9 Nos. 11-12 NOVEMBER-DECEMBER

CONTENTS

Equivalent Circuits and Four-Terminal Parameters of High Frequency Transistor 661
Seiichi KAWAGUCHI and *Minoru HIRAI*

Microwave Propagation Test in Mirage District 687
Shigetaka UGAI, Yoshiie KANEDA, and *Tadashi AMEKURA*

Characteristics and Application of Three-Terminal pnpn Transistors for Speech-Path Switches 718
Kingo YAMAGISHI and *Ichiro ENDO*

Mode Conversion in the Excitation of TE_{01} Waves in a TE_{01} Taper Type Mode Transducer 725
Shin-ichi IIGUCHI

Foamed Polyethylene Insulated City Cable 733
Mitsuru ROKUNOHE

Papers Contributed to Scientific and Technical Journals by the Members of the Laboratory 756

Copyright 1961 by the Electrical Communication Laboratory, NTT